

CFD Simulation of Downhole Thruster Performance Evaluation

by © Bashir Mohamed

A Thesis submitted

to the School of Graduate Studies in partial fulfillment of the

requirements for the degree of

Master of Engineering

Faculty of Engineering and Applied Science

Memorial University of Newfoundland

October 2018

St. John's

Newfoundland and Labrador

Abstract

The present study investigates the role that the downhole Thruster could contribute towards enhancing drilling performance of oil and gas wells. The core study was numerical simulation implemented ANSYS Software using different fluids of various viscosities. As a main part of the numerical study, an evaluation of the variation of fluid velocities and their resultant pressures at several planes within the Thruster geometry was included. The evaluation methodology included a comparative study of “With-Thruster” versus “Without-Thruster”, which represent two drilling modes involving drilling with axially induced oscillations and drilling without axially induced oscillations; respectively. This was performed to simulate different drilling modes of unconventional (i.e. with controlled and desirable axial oscillations) and conventional (i.e. rigid drilling system); respectively. By implementing the downhole Thruster, the conventional drilling can be shifted to the unconventional drilling mode that produces controlled axial vibrations empowered hydraulically through generating pressure pulses. At first, the drilling performance was simulated by implementing Maurer model, which showed significant increase in the rate of penetration (ROP) when using the Thruster for all fluid velocities. The improvement in ROP was noticed to increase from quarter unit to a one unit induced by a generated force of at as low as 6000 (N) to as high as 10000 (N); respectively. The clear increase in ROP in the simulation work was then carried out for further simulation of the Thruster for comprehensive evaluation under various conditions, including applying back pressures as well as using various fluid viscosities, which also showed improvement in ROP with Thruster implementation.

Acknowledgements

I gratefully give thanks to Allah for the guidance and good health which helped me carry out this study. As well, I thank my supervisors, Prof. Stephen D. Butt and Dr. Mohammed Azizur Rahman, for their invaluable guidance and constant support throughout this research. Their knowledge and input greatly improved my research and writing processes, and I am thankful for their warm and enduring friendship. I also wish to extend thanks to my colleagues and friends, and to all of my acquaintances who in some way contributed to this work; especially, Abdelsalam Abugharara for his valuable assistance and suggestions provided during this investigation. My profound gratitude also goes to the government of Libya, whose generous provision of a scholarship made it possible for me to pursue my Master degree. At last but not the least, I thank my parents, my wife, and my family for their continues love, support, and encouragement. I could not have completed this work without you all.

Table of Contents

Abstract.....	II
Acknowledgements.....	III
List of Tables.....	VIII
List of Figures.....	IX
Abbreviations.....	XII
Symbols.....	XIV
Chapter 1.....	1
1.1 Introduction.....	1
1.2 Objectives of the Research.....	3
1.3 Outline of thesis.....	3
Chapter 2.....	5
2.1 Literature Review.....	5
2.1.1 Consideration of down-hole dynamic load in drilling.....	5
2.1.2 Drilling Hydraulics.....	13
2.1.2.1 Current Rheological Fluid Models.....	13
2.1.2.2 Bit Hydraulics.....	15
2.1.2.3 Bit Pressure Drop.....	15
2.1.2.4 Nozzle Velocity.....	16
2.1.2.5 Drilling Hydraulics and Hole Cleaning.....	16

2.1.2.6	Mud Flow Rate	18
2.1.2.7	Hydraulic Impact Force (HIF)	19
2.1.2.8	Friction Pressure Drop Calculations and Flow Regimes	19
2.1.2.9	Pipe Flow.....	20
2.1.2.10	Annular Flow	21
2.1.3	Properties of Mud.....	23
2.1.4	Drillstring Vibrations	25
2.1.4.1	Vibrations.....	25
2.1.4.2	Problems Caused by Drillstring Vibrations	26
2.1.4.3	Drillstring Vibration Causes and Models	29
2.1.4.4	Drillstring Vibration Measurement.....	31
2.1.4.5	Vibration Reduction Tools	33
2.1.4.6	Computational Fluid Dynamics (CFD)	34
Chapter 3	35
3.1	Thruster Design and Simulation	35
3.1.1	Purpose of Hydraulic Thruster	35
3.1.2	Basic Design Parameters for Downhole Thruster BHA.....	35
3.1.3	Design of Thrusters.....	36
3.1.3.1	Choke Spear and Sleeve Configuration	39
3.1.3.2	CFD Simulations	39

3.1.3.3	CFD Simulation Cases.....	40
3.1.3.4	Geometries	40
3.1.3.5	Meshing	41
3.1.3.6	Thruster Fluid Flow Simulation.....	42
Chapter 4	45
4.1	CFD Numerical Simulation for Downhole Thruster Performance Evaluation	45
4.2	Abstract.....	45
4.3	Introduction	46
4.4	Description of the Thruster	48
4.4.1	Mechanical Design.....	48
4.4.2	Thruster Geometry	50
4.4.3	Thruster Meshing.....	51
4.4.4	Thruster Fluid Flow Simulation.....	53
4.4.5	Data Analysis.....	53
4.5	Results.....	54
4.5.1	Thruster Downhole Force Generation.....	54
4.5.2	Thruster Velocity and Pressure Analysis.....	57
4.5.3	Thruster Positional Velocity and Pressure Drop Analysis.....	62
4.6	Discussions.....	68
4.7	Summary	69

4.8	Future work.....	70
4.9	Acknowledgement	71
4.10	Nomenclature	72
4.11	References	73
Chapter 5	76
5.1	Conclusion.....	76
References	78
Appendix. A	83

List of Tables

Table 2.1: Types of vibrations (Krepp and Mims, 2003).....	26
Table 2.2: Reductions in drilling performance due to drillstring vibration (Al Dushaishi, 2012)	27
Table 2.3: Occurrence of the three vibration models (Al Dushaishi, 2012)	29
Table 2.4: Drillstring vibration mode identity (Al Dushaishi, 2012).....	33
Table 3.1: Summary of the numerical values of the Thruster meshing.....	42
Table 4.1: Summary of the numerical values of the Thruster meshing.....	52
Table 4.2: Summary of the Pressure effect, forces, and ROP for with/without Thruster	55
Table 4.3: Numerical data plotted in Figure 9	58
Table 4.4: Various inlet fluid velocities and the resultant pressure effect	58
Table A.1: Summary of the pressure effect, generated forces and ROP for both applications of with Thruster and without Thruster.....	84
Table A.2: Back pressure.....	89
Table A.3: Percentage back pressure of the pressure effect.....	90

List of Figures

Figure 2.1: Classifications of fluids from Newtonian and non-Newtonian (Irgens, F., & SpringerLink, 2014)	14
Figure 2.2: Drilling path and vibration types (Dunlop et al., 2011)	28
Figure 2.3: Drillstring vibration models (Zamani, 2016)	28
Figure 3.1: Free body diagram of a floating thruster as a part of the BHA	36
Figure 3.2: 2D drawing of the Thruster	37
Figure 3.3: 3D Sectional view of the downhole Thruster	38
Figure 3.4: Geometry setup fluent	40
Figure 3.5: Meshing of the Thruster	41
Figure 3.6: Number of elements and the represented pressure for best Thruster meshing	42
Figure 3.7: ANSYS fluent R 17.2 fluid flow simulation of the Thruster	43
Figure 4.1: Drawing of the Thruster	48
Figure 4.2: Thruster mechanical design	49
Figure 4.3: Thruster geometry simulated by ANSYS	50
Figure 4.4: Thruster meshing	51
Figure 4.5: Number of elements and the representative pressure for best Thruster meshing	52
Figure 4.6: ANSYS Fluent 17.2 fluid flow simulation of the Thruster	53
Figure 4.7: The generated force due to the measured mean pressure effects in both applications of with and without Thruster	56
Figure 4.8: The resultant ROP in both applications based on Maurer Model for with and with no Thruster	56
Figure 4.9: Thruster generated pressure as percentage back pressure of the pressure affect	57
Figure 4.10: Generated Thruster pressure pulse at the input velocity 1	59

Figure 4.11: Input velocity 1 corresponding to pressure pulse in Figure 10	60
Figure 4.12: Combined pressure pulse at the input velocity 1 as a result of the Thruster operation under this condition	60
Figure 4.13: Thruster pressure pulse at velocity 10 with Choked and unchoked regions	61
Figure 4.14: The relationship between various inlet fluid velocities and the resultant pressure effect	61
Figure 4. 15: Planes at various locations throughout the Thruster for velocity and pressure drop analysis	63
Figure 4.16: Relationships between fluid (water) velocities and pressure drops at plane # 1at back pressure = 0 psi	64
Figure 4. 17: Relationships between fluid (water) velocities and pressure drops at plane #1, which is located at the entrance of the Thruster at 2 different back pressures including 0 psi and 110 psi, as the lowest and the highest, respectively	64
Figure 4.18: Relationships between fluid velocities and pressure drops at plane # 8, which is located at the chocking region of the Thruster at 2 different back pressures including 0 psi and 110 psi	65
Figure 4. 19: Relationships between fluid velocities and pressure drops at plane #10, which is located prior to fluid exit from the Thruster at 2 different back pressures including 0 psi and 110 psi	65
Figure 4. 20: Velocity and pressure drop relationship at back pressure 0 psi at plane #1 using water vs. Power Law	66
Figure 4.21: Velocity and pressure drop relationship at back pressure 0 psi at plane #8 using water vs. Power Law fluids	66
Figure 4. 22: Velocity and pressure drop relationship at back pressure 0 psi at plane #10 using water vs. Power Law fluids	67
Figure A.1: AutoCAD drawing of the Thruster	83
Figure A.2: Pressure vs First Velocity Value	84
Figure A. 3: Pressure vs Second Velocity Value	85
Figure A.4: Pressure vs Third Velocity Value	85

Figure A.5: Pressure vs Forth Velocity Value	86
Figure A.6: Pressure vs Fifth Velocity Value	86
Figure A.7: Pressure vs Sixth Velocity Value	87
Figure A.8: Pressure vs Seventh Velocity Value.....	87
Figure A.9: Pressure vs Eighth Velocity Value	88
Figure A.10: Pressure vs Ninth Velocity Value	88
Figure A. 11: Pressure vs Tenth Velocity Value	89
Figure A. 12: Percentage back pressure of the pressure effect	90
Figure A. 13: Back pressure 10%	91
Figure A.14: Back pressure 25%	91
Figure A. 15: Back pressure 50%	92
Figure A. 16: Back pressure 75%	92
FigureA.17: Back pressure 100%.....	923
Figure A.18: Combined pressure and velocity profiles for full length of Thruster. Green: Pre and Post chokedregions, Red: Unchoked region.....	923
Figure A.19: Pressure and velocity fluctuation inducing axial motion of the Thruster. After the drop, the pressure ains some increase compared to the pre-drop stage pressure.....	924
Figure A.20: Relationship between 10 pressure profiles and 10 corresponding flow rates.....	924
Figure A.21: Full 10 velocities profiles of ANSYS evaluating Thruster performance induced by 10 inlet flowrates	925
Figure A.22: Relationships between fluid velocities and pressure drops at back pressure = 0 psi	925
Figure A.23: Relationships between fluid velocities and pressure drops at plane #1.....	926
Figure A.24: Relationships between fluid velocities and pressure drops at plane #8.....	926
Figure A.25: Relationships between fluid velocities and pressure drops at plane #10.....	927

Abbreviations

A	Area (mm ²)
B.C.	Boundary Condition
BHA	Bottom Hole Assembly
BHP	Bottom-Hole Pressure (psi)
CFD	Computational Fluid Dynamics
Db	Bit Diameter (in)
E	Total Mechanical Energy
ECD	Equivalent Circulating Density
ERD	Extended Reach Drilling
HIF	Hydraulic Impact Force
m	Mass (kg)
MSE	Mechanical Specific Energy (psi)
OBD	Over Balanced Drilling
P ₁	Inlet Pressure (psi)
P ₂	Outlet Pressure (psi)
ROP	Rate of Penetration (m/hr)
RPM, N,	Revolution Per Minute, Rotary Speed
T	Torque (N-m)
TFA	Total Flow Area
TVD	True Vertical Depth (m)
UBD	Under Balanced Drilling

UCS	Unconfined Compressive Strength
USGPM	U.S. Gallons Per Minute
WOB	Weight On Bit (kg)

Symbols

a	Constant
b	Constant
D1	ID of annulus (in)
D2	OD of annulus (in)
Dh	hydraulic diameter for annulus (in)
Dn	bit nozzle diameter (in)
N	Newton
ρ	Density (kg/m^3)
g	Gravity
k	consistency index ($\text{lb}f \text{ sec}^n / 100 \text{ ft}^2$)
V	Fluid Velocity
Q	Flow Rate (m^3/sec)
Re	Reynolds Number
Re _L	laminar boundary (dimensionless)
Re _T	turbulent boundary (dimensionless)
y	Height (m)
V _n	nozzle velocity (ft/s)
V _p	fluid velocity in pipe (ft/s)
Δt	Time (sec)
Db	Bit Diameter (mm)

P_{bp}	Back Pressure (psi)
μ	Viscosity (cP)
μ_a	plastic viscosity (cp)
Δp_b	pressure loss across bit (psi)
Δp_t	total pressure loss in drilling system (psi)
F_{thr}	Thruster Force
A_{thr}	Thruster area
F_w	Assembly Weight
m_{BHA}	Mass of Bottom Hole Assembly

Chapter 1

1.1 Introduction

Over the past several decades, oil and gas companies have strived to improve the equipment and tools used in drilling, with the ultimate goal of increasing efficiency while reducing costs. The most effective way to achieve this goal is to drill the wells quickly, accurately and safely. However, most offshore wells are negatively affected by shock and vibration during the drilling process. Drillstring vibrations are the main issue preventing greater footage and rates of penetration (ROP). Despite being an industry goal, quick drilling tends to lead to downhole vibrations, which cause early deterioration of downhole components. This results in higher overall costs for drilling projects. Costs related to issues such as the repair of drilling components, lost-in-hole occurrences and construction phases that run into overtime are the main reasons to mitigate drillstring vibrations in the most economical way possible. Vibrations also cause excess power consumption by preventing optimal transfer of power to the bit. The aim is to decrease or eliminate vibrations and shock so that power losses could be reduced and drilling rates increased.

Performance levels for drilling, which to a large extent are affected by the rate of drilling, the quality of the tools used and the overall drilling dynamics can be a significant challenge to those working in the field as well as those in charge of planning and implementing drilling projects. Compounding these issues are the expenses associated with drilling and the ever-increasing complexity and sensitivity of the equipment used. The most effective way to deal with all of these challenges that are endemic to the industry is to investigate and mitigate the core issue in drilling, which is drillstring vibration. A number of innovative approaches have been applied to deal with this core issue, but there is still no single piece of equipment or operational approach that

consistently overcomes the vibration problem. However, the tool known as the thruster shows enormous potential for enhancing ROP efficiently by reducing vibrations, while at the same time reducing drill time and associated costs.

In general terms, the higher the ROP, the lower the drilling cost per depth unit (i.e. meter). A number of approaches can be employed to enhance ROP, including increasing the flow rate (FR), rotary speed in revolution per minute (RPM), and weight-on-bit (WOB). Unfortunately, however, these approaches can also bring with them unwanted consequences. For instance, a higher flow rate could lead to well deformations, while a higher rate of WOB could cause the drillstring to buckle. To offset these potential problems while still increasing the ROP, the thruster can be applied as a means to enhance the dynamic WOB (Dyn-WOB) at the bit. The thruster is able to alter pressure pulses caused by drill mud moving through it, thereby creating higher Dyn-WOB and ROP.

The primary aim of the oil and gas industry is to maximize profits through quick and efficient drilling, but this can only be accomplished by keeping operations safe and efficient while increasing drilling speeds. Nowadays, as most contracts favour both efficiency and failure-free operations, suppliers can purchase and use whatever equipment they think will result in the fastest, most accurate and safest drill performance. In choosing equipment, both suppliers and operators look to capitalize on equipment that mitigates vibration.

The present study will investigate a range of relevant technologies that decreasing harmful vibration, such as stick/slip and generate desirable vibration, such as controlled axial oscillation leading to increasing drilling rate of penetration.

1.2 Objectives of the Research

Increased resistance of drill pipe rotation, increased of downhole torque, fluctuating rotary speed, and existence of harmful and undesirable vibrations are some of the main drilling challenges that result in decreasing the drilling rate of penetration (ROP) and increasing the drilling cost. The aim of this research investigates the advantages of incorporating a downhole Thruster tool into a steerable drilling assembly as a main portion of the bottom hole assembly (BHA) to (i) overcome drilling problems, such as releasing stuck pipes and minimizing friction forces, (ii) reduce overall drilling costs by protecting BHA equipment and avoiding premature change of pipes and bits, and (iii) enhance drilling rate of penetration.

1.3 Outline of thesis

Chapter 1:

In this chapter, an overview of main factors and parameters (i.e. WOB, FR, RPM, etc.) that are influencing drilling performance were reviewed, previous attempts by oil and gas companies and research centres to enhance drilling performance by applying various techniques , among which applying DWOB were analyzed, as well as research objectives were included.

Chapter 2:

Detailed examination of the main factors affecting drilling performance, a review of the drillstring vibration problems, potential resolutions to eliminate harmful vibrations and induce desirable vibrations, a summary of related literature review of the existing technologies and the chronological order of them, various driving mechanisms of the downhole advancement of the

drill bit that attempt to provide an increase in WOB, including mechanically or hydraulically were included.

Chapter 3:

This chapter includes detailed 2D and 3D mechanical design of the downhole Thruster. It, also includes numerical simulation of the Thruster performance using various fluid types, applying different back-pressures, implementing several fluid velocities, and simulating all at various planes throughout the devise.

Chapter 4:

This chapter includes the conference paper entitled: CFD Numerical Simulation for Downhole Thruster Performance Evaluation. This paper was accepted and prepared to be presented for ASME 2018, the 37th International Conference on Ocean, Offshore and Arctic Engineering on June 17-22, 2018, Madrid, Spain. The Paper Number is OMAE2018-78101. Authors: Bashir Mohamed¹, Abdelsalam Aabugarara¹, M.A. Rahman², and Stephen D. Butt¹.

¹ Department of Process Engineering, Faculty of Engineering and Applied Sciences, Memorial University of Newfoundland, St. John's, Newfoundland and Labrador, Canada.

² Petroleum Engineering, Texas A and M University at Qatar, Doha, Qatar.

Chapter 5:

This chapter includes the conclusion, some recommendations, and to follow up work proposed by the author as future work.

Chapter 6: References

Chapter 7: Appendix.

Chapter 2

2.1 Literature Review

2.1.1 Consideration of down-hole dynamic load in drilling

In the section, the studies reported on the effect of the down-hole dynamic load magnifier (Thruster) on drilling performance enhancement is addressed.

In 1995, Reich, et al. explained the function and principle of thrusters. Their work provides details on field data from four wells and outlines the potential and limitations of a thruster's use. They also included criteria for peak-level performance thrusters in specific applications and designed and tested various devices for improving the use of downhole thrusters. In general, thrusters generate weight-on-bit (WOB) by using drilling fluid hydraulics. The thrusters' pump-open behaviour serves to decouple the lower portion of the bottom-hole assembly from the rest of the drillstring. This then gives a steady and controllable WOB that helps to absorb any shocks or axial vibrations. Across dozens of job sites, thrusters have shown their worth by boosting drilling performance in holes that experience vibrations and shock-related issues. The approach has been applied to enhance penetration rates, lengthen bit lives, increase steerability, and decrease downhole failures in holes ranging in diameter from 12 1/4" to 3 7/8". This includes both horizontal and vertical wells at depths of around 17716.54 feet (approx. 5,400 meters).

While this system is primarily used on fixed rigs today, it can be applied to floating rigs as well, in which case it significantly lowers costs on a per-foot basis. However, because the thruster has an impact on other hydraulic components, such as the mud motor, bit, MWD pulser, etc., the drillstring must be correctly tuned in order to obtain maximum performance levels. Schmalhorst

(1999) indicated that using a thruster in the bottomhole assembly of a drillstring is advantageous because it significantly enhanced the rate of penetration and optimized (e.g., smooth) drilling conditions. Even a simple thruster can improve the axial and torsional vibrations of a drillstring, as the device acts as an anti-vibration tool. With an aim to quantify the forces, accelerations and dynamic pressures, some lab measurements were done on a full-scale assembly, which included a thruster, bit, and downhole mud motor. The measurements were taken at a sampling rate of 6 kHz as well as at other typical operating conditions. After taking the measurements, the researchers analyzed the signals using digital signal processing techniques in order to gauge the dynamic characteristics of the thrusting. These characteristics were then described in terms of transfer functions. The measured vibration responses in the various tests were later used to calibrate the unknown parameters of a bit-motor-thruster dynamics time domain model. The model also included the effects of mud flow forcing. From the data, the computer application was able to predict the dynamic behaviour of a complete drillstring under both normal and abnormal drilling conditions (Schmalhorst, 1999).

Corles, et al. (2001) review the benefits provided by the use of thrusting devices in well bores that are categorized as medium to high-angle and horizontal, all utilized within a steerable drilling assembly format. The outcome of the evaluation tests considers performance-related issues such as depth and rate of penetration as well as downhole tool failure rates. In the study, 85 bottomhole assembly (BHA) runs for three BP Trinidad projects were reviewed. The study began in November 1997 and proceeded until more than 160,000 feet were drilled, comprising over 3,500 tool circulating hours. The data used in the study were derived from drilling ASCII as well as daily drilling reports, measurement-while-drilling (MWD) reports, mud logging final well reports, and directional well reports. An in-depth review of the study indicated that in instances where an

appropriately placed thrusting device was used in the BHAs, rates of penetration drastically increased. Improvements were particularly noted when the thrusters encountered problems related to high hole angles. Overall, the use of thrusting devices led to a significant reduction in failure rates for downhole components, especially with logging-while-drilling (LWD) and MWD devices (Corles, et al. 2001).

Equally important, in Buslaev and Belkin (2015) studied a downhole multi-purpose thrusting device is tested in deep vertical and directional wells. The study is based on five years of research on a hydraulic thruster that was used to create a constant WOB and impact load in order to free stuck pipe in deep and directional wells, including horizontal wells. The device's chief characteristic is its multi-functionalism, enabled by its unique structural design and sliding shaft stroke length overriding both resonance and axial vibrations in the drill string. The article provides details on the importance of using hydraulic thrusters to achieve extended reach. It also cites a number of equations and research results related to the dynamic impact of load change under various accelerations, both during pull-out and when utilizing the thruster to free a stuck pipe. The strength of material and testing requirements are specified and development and field testing methodology and results are described (Buslaev and Belkin, 2015).

Schmalhorst, et al. (2000) proposed a new drillstring dynamics model that takes into account the interaction between the drill string and stationary mud flow circulation. Most previous research has not included the impact of fluid-structure coupling forces or fluid flow excitation forces on drillstring dynamics. The drill string studied includes a BHA made up of a mud-driven positive displacement motor, a PDC bit and an optional measurement-while-drilling pulser (MWD). In a typical setup, the assembly is excited by mud flow and axial bit vibration due in large part to

friction effects between the borehole wall and the string as well as to a profiled bottomhole and motor imbalance. The researchers measured coupled axial, torsional, lateral and pressure vibrations, while simulation results took into account the whirl effects of the assembly as well as bit bouncing and self-excited stick slip. As mentioned, the optional MWD pulser was measured for its vibration response to positive pressure. The proposed approach prevents advancement to critical operating conditions by helping to choose the most appropriate system parameters. This ensures a sizeable reduction in operational costs (Schmalhorst, et al. 2000).

In the study done by Geldof et al. (1999), the researchers applied a multiple viewpoint method, such as the world record horizontal bit runs in Oman. There, continuous performance improvements led to two consecutive world-record horizontal drilling bit runs for Petroleum Development Oman (PDO) along with the company's well engineering partners in the Saih Rawl field of North Oman. The study explains the main success factors behind the technology and management that made this achievement a reality. It also discusses related future improvements that could be made in well time as well as project costs (Geldof et al. 1999). In the article written by Dupriest et al. (2005), it outlined the importance of maximizing ROP with real-time analysis of digital data and MSE. The research provides details on the RasGas Company Ltd Drilling Task Force in North Field, which implemented a novel work process provided by ExxonMobil Development Company. The process aims to increase the rate of penetration (ROP) for every foot of drilled hole. Over the course of the drill design, ROP limiters are identified and eliminated in the drilling design phase as well as during real-time well site operations. A core feature of this process is the real-time display and analysis of Mechanical Specific Energy (MSE), which is the work necessary to destroy a certain volume of rock. If the device is functioning at optimal efficiency, the energy-to-rock-volume ratio stays more or less constant. This relationship is applied

during operations by gauging whether the MSE changes during drilling parameter adjustments (e.g., WOB or RPM). The bit is considered efficient if it stays constant throughout WOB increases. However, if the MSE ratio sees a notable rise during regular drilling procedures or parameter adjustments, the bit is considered to have failed (foundered). After the reason for the foundering has been determined, the parameters can be adjusted and readjusted until the value of the MSE drops to acceptable levels. This procedure of parameter adjustment is called MSE testing. The recorded results from these tests are also analyzed to assist in redesigns of the drilling system in cases where the ROP limiters are beyond the driller's control. In the North Field site, data related to downhole vibrations were added to MSE curves to augment and deepen the interpretation of the cause of the founder and to determine future drilling parameters.

The study provides examples from Qatar operations that indicate how vibrational data and MSE were applied at the rig site to assist in operations, as well as in post-drill analyses towards the redesign of the system, when needed. The performance data clearly showed the effects of the new system on the operations, with performance improvements ranging from 60% all the way up to 380%, depending on a hole size (Dupriest et al. 2005).

In this work, the main parameters are RPM & ROP. Directional drilling is a critical necessity in many of today's wells. Therefore, it is important to ensure accurate prediction and awareness of feasible build rates in order to decrease both drilling and overall operational expenses. The science that underlies controlled wellbore deviation has moved beyond BHA geometry-dependent predictions. While BHA configuration remains a critical element, how the four primary components (i.e., bit, BHA, operating parameters and formation) work together should also be investigated.

Earlier work by Ernst, Pastusek, and Lutes, (2007) showed how alterations among BHA configuration, bit characteristics, and different formations can affect build rates. Furthermore, adjusting the operating parameters of WOB is known to be beneficial when increasing the build rate but does not necessarily provide benefits in other situations. The researchers indicated that the majority of WOB effects are caused by its effects on bit tilt and ROP. The problem here is that the impact of operating parameters has not yet been fully explored. Moreover, RPM has also not been fully explored as a prime influence on steerability. In response to this gap, their paper investigates how RPM and ROP impact build rate, thus showing the significance of these parameters. The work also provides guidelines to understand the effects of operating parameters on steerable systems.

In one such case, Li et al. (2010) described the important factors of bit vibration on rotary drilling penetration rate. This investigation concerned the impact of bit vibration on ROP in laboratory rotary core drilling. Their approach was modified and instrumented to function under constant WOB conditions that included different levels of axial vibration amplitudes. The experiments were carried out for cases of 300 RPM and 600 RPM (no vibration) and 60 Hz vibration, at increasing amplitudes measuring 0.09, 0.29 and 0.44mm. The study results indicated that for WOB at levels below the founder point, the ROP rose in tandem with the vibration amplitude, with some results pointing to the ROP increase being greater near the ROP-WOB curve peak. Additional lab tests and numerical simulations have been planned by the researchers to delve deeper into vibration-assisted rotary drilling technology (Li, et al. 2010).

In this work, the researchers show how tool manufacturers have made notable progress in advancing downhole drilling technologies. However, the researchers also point out that little to no effort has been made to optimize the drilling process. Instead, most drill operations adopt a “set-

it-and-forget-it” approach that brings with it inherent inefficiencies of the automatic driller. This is proving to be an inefficient and even dangerous method for matching bit parameters to lithology and wellbore conditions. Therefore, as the researchers indicate, the industry urgently requires a novel approach that aims to assist rig-site personnel assist in making better-informed decisions about drilling parameters. Such decisions should be based on real-time offset data analysis, as this would enhance operating efficiency and ultimately lower drilling and overall project expenses.

In addressing the issue, researchers relay on how the service provider can develop an artificial neural network (ANN) drilling parameter optimization system (DBOS OnTime). This system aims to provide real-time data to rig-site personnel in order to inform them about maximum run length of all bits and downhole tools at the highest possible ROPs. The main perceived advantages of the DBOS OnTime system are longer tool life and the ability to manage dull bit conditions. The overall objective in developing the system is to get rid of the ‘human factor’ involved in estimating operating parameters, such as WOB and RPM. Thus, by utilizing an ANN-based software system, parameters can be chosen according to the physical rock characteristics and then fine-tuned to suit the bit’s specific wear rate and cutting structure. By adhering to the real-time ANN suggestions, site personnel can enact changes that would enhance ROP and maximize bit life (Gidh, et al. 2011).

In their study, Clausen, et al. (2014) show that drilling with induced vibrations improves ROP and mitigates stick/slip in vertical and directional wells. Over the years, drillers have usually attempted to reduce vibrations in the drillstring during drilling procedures in order to maximize ROP while keeping bit damage at a minimum to extend bit life. They found that mitigating lateral vibrations and stick/slip can improve drill performance and maintain directional control, but the results were not optimal. Then, more recently, the industry discovered that by inducing axial

agitation with specialized downhole tools, lateral reach can be enhanced. However, the advantages of downhole oscillation tools have not been investigated for other related performance gains (e.g., ROP in non-directional wells).

A research study involving both laboratory and field testing discovered that low-frequency axial vibration can substantially increase ROP across all well types. Early lab tests were done to induce axial vibrations in the drilling process, but only on a small-scale drill bit and into hard rock. Despite the limitations of these tests, notable improvements in ROP and drilling efficiency were observed. There were also the additional advantages of longer bit life and decreased stick/slip (Clausen, et al. 2014).

These lab tests were later expanded to field testing, using a downhole oscillation tool in an active BHA. Fortunately, the field tests reflected lab test results, and notable performance gains were again observed. As well, the novel downhole oscillation tool gave improved directional control when operated above a Rotary Steerable System (RSS) tool, and stick/slip was more or less eliminated with no adverse impacts either on the BHA reliability or bit life.

The proposed method's validity was further underlined by high-speed sensor data gathered at the bit during both the lab and field tests. Trials for hard-rock applications using roller cone bits have been planned, as the data points to clear potential performance gains in that aspect as well. The researchers demonstrated that the study provided many benefits, including substantial decreases in Non-Productive Time (NPT) and Time to Total Depth (TD). This was achieved by avoiding damage to BHA components through beneficial axial vibrations from the downhole oscillation tool, which can significantly improve overall drilling performance (Clausen et al. 2014).

2.1.2 Drilling Hydraulics

The main focus of this section is drilling hydraulics, with an aim to establish an academic basis for future calculations, analysis and investigation. The topics covered here are bit hydraulics, ECD, problems around hole-cleaning, and pressure drop calculations. The latter measurements are made based on a preferred model, even though the use of readily available rheological fluid models might bring better results.

2.1.2.1 Current Rheological Fluid Models

A wide range of rheological fluid models are typically applied in fluid hydrodynamics. Some of these models are applied while characterizing drilling fluids, whereas others are simply not suitable for drilling fluid environments. Over the course of the investigations, it was discovered that eight rheological models are suitable for drilling purposes. These eight models, in alphabetical order, are:

- API Model (RP 13D)
- Bingham Plastic Model
- Casson Model
- Herschel-Buckley Model
- Newtonian Model
- Power Law Model
- Robertson-Stiff Model
- Unified Model

All eight models have specific applications. However, under certain conditions and operational parameters, they can still be compared to one another.

The drilling industry has, at one time or another and under varying conditions, used all of these listed approaches except for the Newtonian and Casson models to characterize drilling fluids. Although available data indicate that the power law model more closely reflects the characteristics and behaviour of drilling fluid utilized in the field case in this study, this on its own does not mean that the power law model is the best choice for drilling fluid. Nonetheless, because this model is a good fit for the field data, the pressure loss calculations are based on it. Figure 2.1 shows the classifications of main fluids, among which are the two main fluid used for testing the Thruster as Newtonian and Non Newtonian fluids.

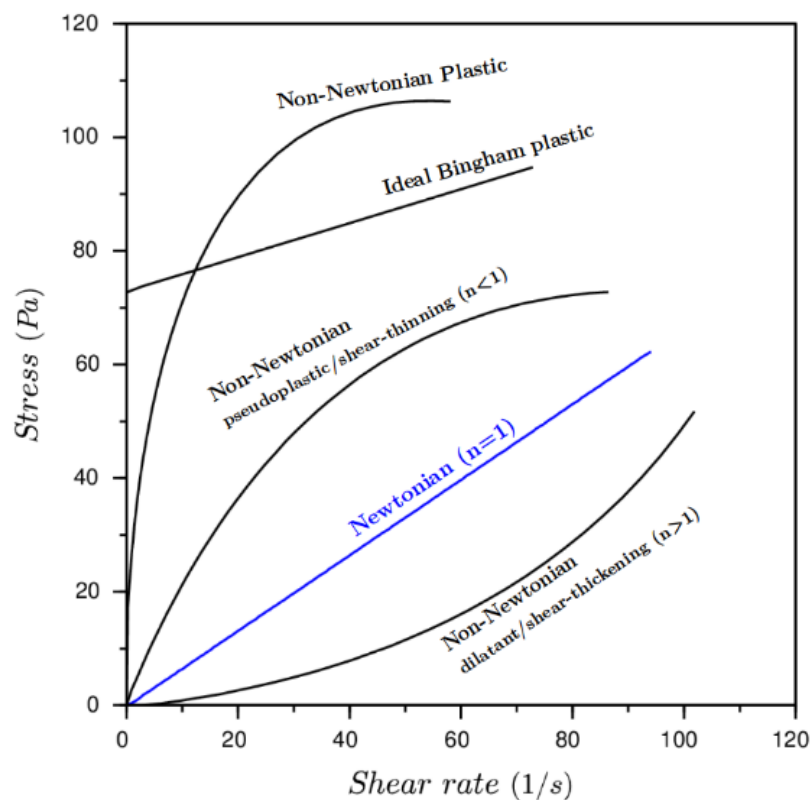


Figure 2.1: Classifications of fluids from Newtonian and non-Newtonian (Irgens, F., & SpringerLink, 2014)

2.1.2.2 Bit Hydraulics

The following subsections will focus on the relevant bit hydraulics for the work, briefly examining key elements, such as hydraulic impact force, pressure loss and nozzle velocity.

2.1.2.3 Bit Pressure Drop

The primary aim of every hydraulics program is to optimize the pressure drop across the bit in order to maximize bottomhole cleaning. Research shows that pressure drop on the bit is significantly affected by the size of the bit nozzles. Specifically, smaller bit nozzles cause higher pressure drops Rahimov, E. (2009). To calculate the pressure drop on a drill bit, the following equation is used:

$$\Delta P_b = \frac{156.5 \rho f Q^2}{(D_{n1}^2 + D_{n2}^2 + D_{n3}^2 + \dots)^2} \quad (2.1)$$

Where:

ΔP_b = pressure drop across a bit, psi

Q = flow rate, gpm

D = Diameter mm

W = mud weight, ppg

A = total flow area, square inch

However, if coring or diamond bits are being utilized, the above equation must be adjusted to include the total flow area (TFA) and fitting conversion factor. Thus, the pressure drop equation for diamond and coring bits is:

$$\Delta P_b = \frac{\rho_f Q^2}{10858 (TFA)^2} \quad (2.2)$$

Furthermore, the percentage of pressure loss across the bit can be calculated as:

$$\Delta P_b = (\%) = \frac{\Delta P_b}{\Delta P_t} 100 \quad (2.3)$$

Along with bit pressure loss, many other hydraulics computations can be performed to maximize drilling performance, such as impact force, hydraulic horsepower and nozzle velocity. In the following section, nozzle velocity and hydraulic impact force are investigated.

2.1.2.4 Nozzle Velocity

The flow velocity through a bit nozzle (or nozzles) is called nozzle velocity. Although a bit can contain more than one nozzle, the nozzle velocity will be the same for all of the nozzles unless the sizes differ. In most drilling operations, nozzle velocity can be anywhere between 76 and 137 m/sec, but those higher than 137 m/sec are considered too aggressive for bit cutting structures Rahimov, E. (2009). Nozzle velocity can be formulated as:

$$V_n = \frac{417.2 Q}{D_{n1}^2 + D_{n2}^2 + D_{n3}^2 + \dots} \quad (2.4)$$

2.1.2.5 Drilling Hydraulics and Hole Cleaning

Calculations of drilling hydraulics are usually conducted to estimate the desired capacity of rig pumps to drill the well. Generally, the drilling hydraulic system is a component of the drilling fluid characteristics; it either supports or reduces the ability of drilling fluids to deliver efficient

drilling and ensure wellbore integrity and stability. To that end, the pump pressure should be able to provide the necessary flow rate that enables transportation of the cuttings up through the annulus and out of the wellbore to the surface through the mud return line. The pressure should also be sufficient to overcome any accumulated pressure losses on the bit, drill string, surface equipment and annulus. In fact, the drilling fluid behaviour determines hydraulics applications and analyses. The behaviour is informed by interrelated rheology and hydraulics studies. Rheology is defined as the way in which matter (substance) deforms and flows, while hydraulics is defined as the way in which pressures are formed by various fluid flows.

In addition to ECD Management, some other elements that contribute to drilling fluid success in the planning and construction of extended reach wells are:

- Lubricity
- Hole Cleaning
- Borehole Stabilization
- In choosing ERD drilling fluids, the following factors should be taken into consideration. For optimal results, the fluid should:
 - Significantly reduce potential issues such as circulation losses and differential sticking
 - Enable the establishing of a stable wellbore for drilling long open hole intervals at high angles
 - Create the appropriate rheology for ease of cuttings transport
 - Optimize lubricity to reduce torque and drag
 - Decrease any formation damage of production intervals.

2.1.2.6 Mud Flow Rate

In drill sites, the mud flow rate is often considered the most crucial factor for hole cleaning in deviated wells. The motto is: “The faster you pump, the faster you move cuttings out of the hole.” Therefore, mud pumps and liner sizes are usually chosen with an eye to optimizing flow rate when drilling ERD wells.

The main limiting factor for achieving the required flow rate is usually pump pressure. For this reason, the design and selection of the BHA and bit nozzle need to be done carefully in order to reduce pump pressure. In an ideal setting, maximum available flowrates on surface pressure and downhole tool limits would be applied to each and every section of an ERD well. However, when a hole angle diverges from the vertical, the transport of cuttings becomes more of a potential issue. This is because the flow rate for removing cuttings from the hole rises rapidly from 0° to 60°, at which point the rate of the flow rate increase levels off.

Generally speaking, hole angles situated at between 45° and 60° usually cause the most issues, as the cuttings removed at these angles often slide back down the annulus. A few commercially available drilling hydraulics computer programs can be utilized to calculate achievable drilling circulation rates according to drilling fluid rheology, rig pump capacity and drillstring /wellbore configuration. These rates are easily evaluated by using hole cleaning models for high angle wellbores, which are able to predict the efficiency of the overall hole cleaning.

Both real-life experience and industry simulations have provided expertise and data to devise a list of recommended practices and flow rates for ERD wells. Table 2 shows the industry-recommended minimum and maximum flow rates according to hole size Rahimov, E. (2009).

2.1.2.7 Hydraulic Impact Force (HIF)

Hydraulic impact force (HIF) can be defined as the per unit of time momentum rate change in fluid moving through bit nozzles. More specifically, the hydraulic impact is a force created by the passing of liquid through a nozzle. The formula for impact force can be derived from Isaac Newton's second law, which, roughly, is the following: velocity change per unit of time multiplied by mass results in force. Then, if mass is substituted with density and multiplied by volume, the hydraulic impact force is calculated as:

$$\text{HIF} = \frac{Q \rho_f v_n}{1930} \quad (2.5)$$

Then, if expressed as per square inch of bit area impact force, the expression is:

$$(\text{HIF} / \text{in}^2) = \frac{1.27 \text{ HIF}}{D_b^2} \quad (2.6)$$

2.1.2.8 Friction Pressure Drop Calculations and Flow

Regimes

As part of the drilling industry's ongoing attempts to devise workable pressure loss calculations, a slew of equations and procedures have been proposed and implemented, mostly by service companies that offer software packages to the oil industry. However, there is as yet no single solution or agreed-upon process or model for dealing with pressure drop in drilling. Some companies and institutions have nonetheless moved forward by developing equations for various issues, such as computing apparent viscosity, power law constants (k and n), and the Reynolds number. In the next section, a procedure that uses the fundamental power law fluid model is presented.

The power law constants applied in the following equations are computed by:

$$n = 3.32 \log \left(\frac{R_{600}}{R_{300}} \right) \quad (2.7a)$$

$$k = \frac{510 R_{300}}{511^n} \quad (2.7b)$$

2.1.2.9 Pipe Flow

For all known rheological models, the velocity of liquids moving through a pipe can be expressed as:

$$V_p = \frac{Q}{2.448 D_p^2} \quad (2.8)$$

The Reynolds number for Newtonian fluids is given as

$$Re = 928 \frac{D_p \rho_f V_p}{\mu_a} \quad (2.9)$$

When calculating non-Newtonian drilling fluids, apparent viscosity for a power law fluid is given as:

$$\mu_a = \frac{k}{96} \left(\frac{D_p}{V_p} \right)^{1-n} \left(\frac{3+1/n}{0.0416} \right)^n \quad (2.10)$$

Substituting of appearing viscosity given by Equation (2.10) in the place of Equation (2.9) leads to the Reynolds number for power law fluid flow through a pipe that is given by:

$$Re = \frac{89100 \rho_f V_p^{2-n}}{k} \left(\frac{0.0416 D_p}{3+1/n} \right)^n \quad (2.11)$$

Moreover, if the liquid is Newtonian (e.g., if it is water), n is 1.0 and k is equal to the viscosity of the water, in which case Eq. (2.11) can change to the original Eq. (2.9). The power law model sets forth the following conditions to determine flow regime, based on the Reynolds number:

$$\text{Laminar: } Re \leq Re_L = 3470 - 1370 n \quad (2.12a)$$

$$\text{Transition: } 3470-1370 n < \text{Re} < 4270-1370 n \quad (2.12b)$$

$$\text{Turbulent: } \text{Re} \geq \text{Re}_T = 4270-1370 n \quad (2.12c)$$

Then, after the flow regime and the Reynolds number are determined, the friction factor can be calculated as follows:

$$\text{Laminar: } f = \frac{16}{\text{Re}} \quad (2.13a)$$

$$\text{Transition: } f = \frac{16}{\text{Re}_L} + \left[\frac{\text{Re} - \text{Re}_L}{800} \right] \left[\frac{a}{\text{Re}_T^b} - \frac{16}{\text{Re}_L} \right] \quad (2.13b)$$

$$\text{Turbulent } f = \frac{a}{\text{Re}^b} \quad (2.13c)$$

Hence, parameters a and b can be determined by:

$$a = \frac{\log n + 3.93}{50} \quad (2.14a)$$

$$b = \frac{1.75 - \log n}{7} \quad (2.14b)$$

For calculating frictional pressure drop in a drill pipe the following equation is used:

$$\left(\frac{dp}{dL} \right)_p = \frac{f_p V_p^2 \rho_f}{25.81 D_p} \quad (2.15a)$$

$$\Delta P_p = \left(\frac{dp}{dL} \right)_p L \quad (2.15b)$$

2.1.2.10 Annular Flow

For liquid moving through the annulus, the velocity of the liquid (or annular velocity) can be determined by expressing Equation (2.8) for annulus, as follows:

$$V_a = \frac{Q}{2.448 (D_2^2 - D_1^2)} \quad (2.16)$$

Next, in expressing the Reynolds number for the annulus flow, the Reynolds number for the pipe flow is extended to annular geometry by including the hydraulic diameter measurement. Hence, four expressions for calculating the hydraulic diameter are devised.

$$D_h = D_2 - D_1 \quad (2.17a)$$

$$D_h = \sqrt{D_2^2 + D_1^2} - \frac{D_2^2 - D_1^2}{\ln(D_2/D_1)} \quad (2.17b)$$

$$D_h = 0.816 (D_2 - D_1) \quad (2.17c)$$

$$D_h = \frac{\sqrt[4]{D_2^4 + D_1^4 - \frac{(D_2^2 - D_1^2)^2}{\ln(D_2/D_1)}} + \sqrt{D_2^2 - D_1^2}}{2} \quad (2.17d)$$

All of the above calculations have been applied in the petroleum industry to determine annular flow, but the most commonly applied are Equations (2.17a) and (2.17c). The popularity of these equations is due more to their ease of computation than to their precision. Equation (2.17c) is used here as well. Thus, the pipe diameter in Equation (2.9) is substituted with the hydraulic diameter expressed by Equation (2.17c). The Reynolds number can be determined by:

$$Re = 757 \frac{(D_2 - D_1) \rho_f V_a}{\mu_a} \quad (2.18)$$

Similarly, the apparent viscosity of power law fluid moving through the annulus can be formulated as:

$$\mu_a = \frac{K}{144} \left(\frac{D_2 - D_1}{V_a} \right)^{1-n} \left(\frac{2+1/n}{0.0208} \right)^n \quad (2.19)$$

Furthermore, if Eq. (2.19) is substituted for Eq. (2.18), the results as expressed in a Reynolds number are:

$$Re = \frac{109000 \rho_f V_a^{2-n}}{k} \left(\frac{0.0208 (D_2 - D_1)}{2+1/n} \right)^n \quad (2.20)$$

Therefore, having an annular flow regime formulated based on the Reynolds number results in the following:

$$\text{Laminar: } Re \leq Re_L = 3470-1370 n \quad (2.21a)$$

$$\text{Transition: } 3470-1370 n < Re < 4270-1370 n \quad (2.21b)$$

$$\text{Turbulent: } Re \geq Re_T = 4270-1370 n \quad (2.21c)$$

As shown, the constants a and b can be calculated using the same expressions given by Equation. (2.14). Hence, the annular frictional pressure loss is formulated and expressed as:

$$\text{Laminar: } f = \frac{24}{Re} \quad (2.22a)$$

$$\text{Transition: } f = \frac{24}{Re_L} + \left[\frac{Re - Re_L}{800} \right] \left[\frac{a}{Re_T^b} - \frac{24}{Re_L} \right] \quad (2.22b)$$

$$\text{Turbulent } f = \frac{a}{Re^b} \quad (2.22c)$$

One of the most critical parameters to manage and control during drilling is annular frictional pressure loss. This is because any possible rise in annular pressure loss can lead to a rise in the bottom-hole pressure Rahimov, E. (2009).

2.1.3 Properties of Mud

In general terms, there are three main categories of drilling fluids: water-based muds, oil-based muds and gaseous drilling fluids. A wide range of gases can coexist in these fluids, so the main functions of drilling fluids are to:

- Suspend drill cuttings in the annulus region when circulation is stopped.
- Clean the bottom hole under the bit
- Stabilize the wellbore
- Remove cuttings to the surface

- Support the wellbore wall
- Manage subsurface pressure
- Lubricate and cool down the drillstring parts and joints

Several different types of liquids can provide the same or similar transportation of cuttings as long as their down-hole properties are more or less the same. Choosing the best properties requires careful consideration of the varieties of the parameters. The most significant parameters particularly in hole-cleaning are mud viscosity, carrying capacity, gel strength and mud weight. In the next section, mud viscosity and mud weight are reviewed.

The benefits of Mud Viscosity are the following: In hole-cleaning, viscosity not only serves an important role but also helps in defining the carrying capacity. Rotational viscometer readings at 600 and 300 rpm are typically employed to gauge the mud's plastic viscosity and yield point. The viscosity of drilling fluid can be significantly affected by down-hole conditions, particularly in high temperature and high-pressure environments. Generally, the viscosity is reduced with increasing temperature.

Mud Weight: In the hole-cleaning process, the main purpose of the mud weight of the drilling fluid is to buoy the drill cuttings and thus slow down their settling velocity. This process conformed to Stokes' law. Moreover, rather than to improving the hole-cleaning, the mud weight's main purpose is to exert hydrostatic pressure, so it should be adjusted according to changes in pore pressure, fracture gradient and wellbore stability. Wellbore instability in particular demonstrates how the mud weight focuses on the cause rather than the symptoms of hole-cleaning issues (Rahimov, E. (2009)).

2.1.4 Drillstring Vibrations

2.1.4.1 Vibrations

When compared to low angle and vertical wells, downhole vibrations are usually less problematic in ERD wells. However, they can still cause concerns because of their direct and indirect effects on the drilling operation. A few of these potential impacts are listed below:

- Decreased ROP
- BHA failures
- Decreased bit life
- Lengthy drilling time and increased costs
- Hole conditions that are less than optimal
- Decreased drill string life and twist-offs

By adopting a series of implementations, vibrations may be reduced or even eliminated. These implementations include adjusting drilling parameters and related practices and downhole monitoring. Simply monitoring any surface vibrations that emerge is not sufficient, as what is occurring downhole might not be visible at the surface. Therefore, in order to deal with vibrations, it is useful to be aware of the various types of vibrations and their causes. Table 2.1 provides a description of the most common vibrations.

Table 2.1: Types of vibrations (Krepp and Mims, 2003)

Type of Vibration	Description and Symptoms
Bit Bounce (Axial)	<ul style="list-style-type: none">• Occurs mainly in large surface vibrations in vertical or short wells• Can occur as the result of drilling hard formations• Damage to bits
Bit and BHA Whirl (Lateral)	<ul style="list-style-type: none">• Highly destructive and complex• Was a significant issue for early PDC bits• Can inflict damage on bit gauge pads• Mostly localized tool joint wear• Can cause irregular surface torque and fluctuations
Stick-Slip (Torsional)	<ul style="list-style-type: none">• Can cause cyclic surface torque fluctuations as well as top drive stalling• MWD sensors show fluctuations of 0 - 300 rpm in downhole regions• Hyper-torqued tool joints

2.1.4.2 Problems Caused by Drillstring Vibrations

One of the primary causes of drill bit and drillstring component failure can be traced to drillstring vibration. This is because vibrations at any point along the drillstring can interfere with measurements while drilling (MWD), which can then cause incorrect measurement of crucial and sensitive parameters. As well, drillstring vibration can cause wellbore instability, damage the bit, waste energy and thus increase costs. According to research, the most harmful vibrations occur in the area of the drill collars and adjacent drill pipes. Every vibration model affects the drilling operation in a different way (Al Dushaishi,2012). Drillstring vibration problems for each mode are shown in Table 2.2.

Table 2.2: Reductions in drilling performance due to drillstring vibration (Al Dushaishi, 2012)

Vibration Mode	Type	Impact
Axial	Bit Bounce	Bits break or wear out quickly; ROP impact is reduced by BHA failures, which subsequently negatively affects other vibration modes
Torsional	Stick/Slip	Early failure of drillstring BHA and downhole tools; connection fatigue Decreased ROP Bit-cutting components endure fatigue failure or other damage through variable RPM and cutter load Washouts and twist-offs Overall cost increases Fishing trips and replacements Easily generated with PDC bits
Lateral	Whirl	Enlargements of boreholes Lower ROP BHA washouts and twist offs Early bit wear Unbalanced wear on string stabilizer Lateral effects causing further vibrations

There are three vibrational modes that express the following issues: torsional vibration oscillations caused by non-linear frictional torques between the drill-bit and the rock surface (or torsional "slip-stick"); axial vibrations that make the drill-bit occasionally lose contact with the rock surface (or "bit-bounce"); and the whirling motion of the drillstring and bit in the borehole (or bit and BHA-whirl). Figure 2.2 shows the "slip-stick" clearly. Also, the three of these modes are illustrated in Figure 2.3 and in Table 2.3.

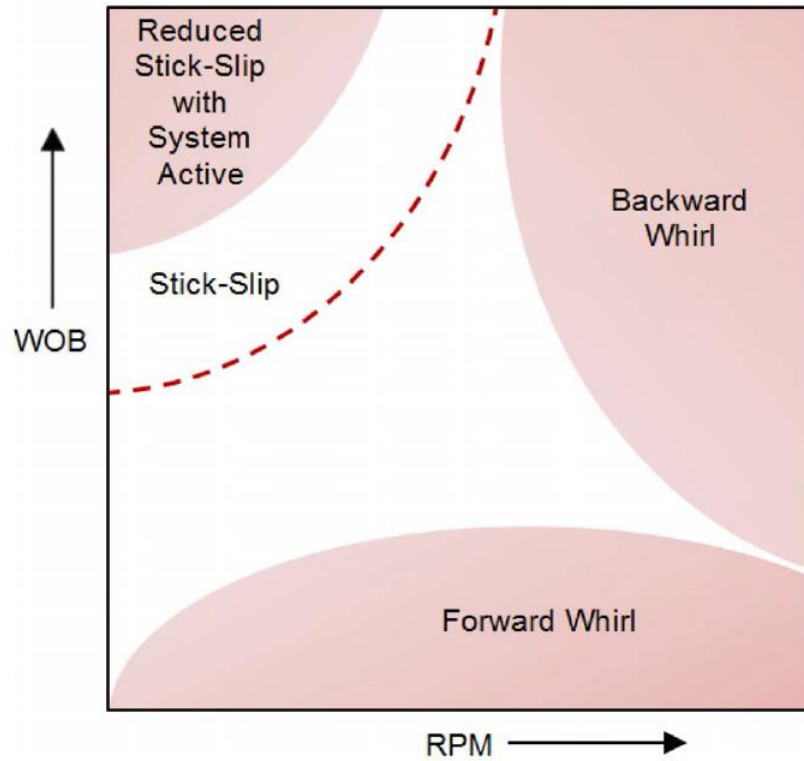


Figure 2.2: Drilling path and vibration types (Dunlop et al., 2011)

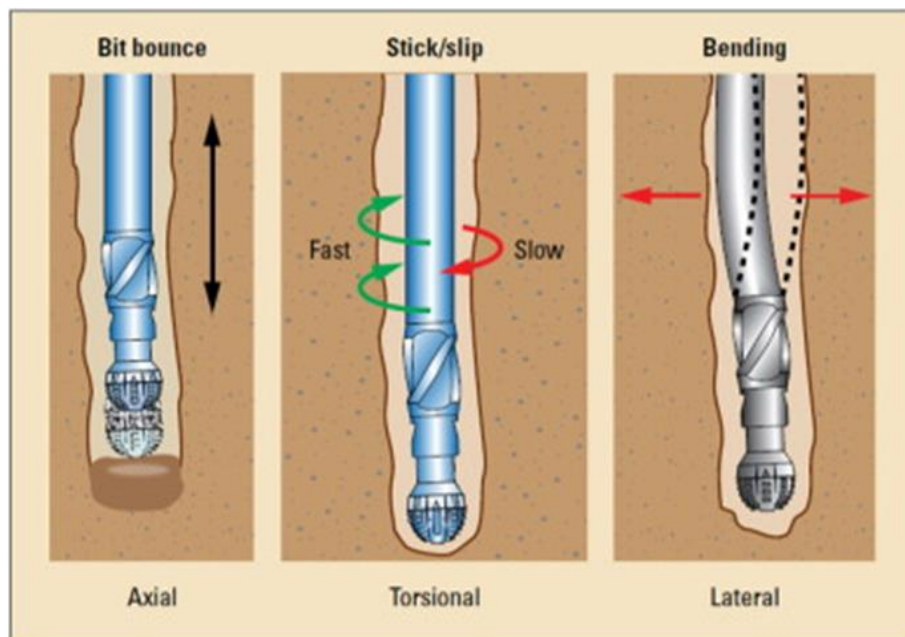


Figure 2.3: Drillstring vibration models (Zamani, 2016)

2.1.4.3 Drillstring Vibration Causes and Models

At the initial point when the bit touches the formation to begin penetration, drillstring vibration can occur. As mentioned previously, drillstring vibration is a somewhat complex function of the bit, BHA, formation conditions, along with a few other factors. The areas in which the three different vibration modes (detailed above) typically occur are shown in Table 2.3.

Table 2.3: Occurrence of the three vibration models (Al Dushaishi, 2012)

Vibration Mode	Common Situations
Axial	Drilling with roller-cone bits Hard drilling regions Vertical wells
Torsional	High angle, deviated wells Hard drilling regions Hard and abrasive lithologies
Lateral	Vertical wells Alternating lithologies

While major excitations can cause rapid failure of drilling operations, smaller vibrations can also cause fatigue and crack growth, wearing down the components in small but steady increments. This involves the transfer of energy between axial, lateral and torsional motion caused by the drillstring and BHA interacting with their surroundings. This type of inter-mode coupling can be strongly affected by different drilling strategies and conditions. For example, the axial vibration mode occurs in two forms:

- Bit bounce: This type occurs when a continuous contact between the bit and the formation is lost and becomes an intermittent and the bit bounces on and off the bottom

- Vertical vibration: This type occurs when the bit is still in contact with the formation.

A number of factors could lead to a decrease or increase in axial vibration. A few are listed below:

- BHA length
- Fluid viscosity
- Lithology hardness
- Bit type
- Hole angle

These and other types of vibrations can occur during any stage of the drilling operation. When the bit first hits the formation on the bottom, a degree of axial vibration is produced along the drillstring. The first bit bounce is caused by excessive speed during the lowering of the bit to the bottom. This model has enjoyed widespread use in the industry because the vibrations can travel from the bottom of the well to the surface, whereas the lateral vibration model is typically positioned beneath the neutral point. Excessive axial vibration can occur when roller-cone bits are being used.

Despite the focus here on the negative, axial vibrations can be useful to drilling operations because they have an effect on WOB, which subsequently has an impact on ROP. Axial vibrations occur most frequently in hard drilling areas, in vertical wells where energy propagation is easier, or when roller-cone bits are being utilized.

Torsional vibration occurs when the rotation of the drillstring is reduced or halted at the bottom and then released when the torque overwhelms the friction-resisting string rotation. Several factors can either decrease or increase torsional vibration, depending on their impact. The three main factors are listed below:

- BHA weight and stability

- Hole angle (from enhanced oscillations at higher hole angles) and
- Bit type (when PDC creates high levels of friction to start the stick phase).

2.1.4.4 Drillstring Vibration Measurement

Dubinsky et al. (1992) made the first attempt to record and process surface and downhole vibrations. These vibrations can be detected at the surface via torque and standpipe pressure oscillations. More recently, downhole vibrations have been recorded utilizing MWD and LWD tools. Real-time vibration modes have also been introduced. The latest models can warn about rotary speeds that will lead to lateral vibration. The main reason for real-time vibration modeling is to help BHA develop and establish operating parameters (Heisig and Neubert, 2000). Downhole data, however, indicate that these models usually have varying degrees of limitations in application.

Surface vibration measurement is used to gauge vibration level. At the same time, surface torque and related oscillations can provide useful data regarding downhole vibration (Dubinsky et al., 1992 and Macpherson et al., 1993). Each vibration mechanism displays unique symptoms that aid in identifying the type of vibration. Table 2.4 presents an array of drillstring vibration mode identifiers (Bernt et al., 2009). As can be seen, downhole vibration measurements can be divided into two categories. The first category is a memory measurement device that measures and records vibrations for subsequent lateral analysis. The second category of downhole vibration measurements is real-time vibration measurement.

A prime example of a memory measurement device is the BlackBox™. It is a memory mode vibration logging tool that is suitable for use throughout the BHA (see Figure 2.2). The BlackBox™ device operates on lithium batteries, giving it a 220-hour life, and records three types

of vibration: maximum lateral acceleration, RMS acceleration and stick/slip indicator. This device can be placed anywhere in the BHA. Furthermore, the device can analyze the dynamic behaviour of the entire system. So, to get a better understanding of the dynamic behaviour of the entire drillstring, a few or even several of these devices could be installed in the BHA.

Along the same lines, the Downhole Dynamic Recorder (DDR) is an MWD tool. It is comprised of an accelerometer that measures lateral acceleration (Lesso et al. 2011). Like the BlackBox™, the DDR uses batteries. Moreover, it can sample lateral acceleration at 400Hz and record data every 2.6 seconds. The DDR is typically installed with MWD and LWD tools.

A real-time vibration measurement is the Multi-Axis Vibration Chassis (MVC), which is a 4-axis shock measurement tool. The first of the four axes consist of the strain gauges used in torsional measurement. The other three are systems made up of the vibration acquisition board and three board accelerometers. This system is mounted on a special chassis in the MWD tool. The vib_x sensor measures axial shocks, vib_y and vib_z sensors measure lateral shocks. As well, the vibration acquisition system calculates the root mean square (RMS) value of the tool acceleration.

Table 2.4: Drillstring vibration mode identity (Al Dushaishi, 2012)

Vibration Mode	Surface	Downhole	Tool Damage
Stick/Slip	Reduction in ROP Surface torque RPM fluctuations Top drive stalling	Low frequency Torsional vibration	PDC cutter damaged Drillstring twist-off or washout
BHA Whirl	Reduction in ROP	High frequency of lateral and torsional vibration	Cutter and/or stabilizers Increased torque
Bit Bounce	Reduction of ROP Large surface RPM Large WOB fluctuations	Large axial vibration	Bit damage BHA washout
Coupling	Reduction in ROP Significant WOB fluctuations	Significant lateral, torsional and axial vibrations	Drilling twist- off/washout

2.1.4.5 Vibration Reduction Tools

In order to avoid the development of wellbore instability, the planning process needs to address it right from the start (i.e., when the formation type is evaluated). In this approach, the operational phase of wellbore instability prevention involves ongoing real-time monitoring of drill events. This is done to enable early detection as well as to identify possible trouble spots during drilling. Models based on mathematical computations and monitoring systems that keep watch on surface and downhole areas can be used to stop the development of drillstring and bit damage. These methods can also prevent failures in downhole tools as well as reduced rates of penetration. Specifically, the mathematical models are able to identify critical rotary speed ranges that might cause vibrations. However, the best and most effective way to find problems before they occur

when drilling downhole and monitoring surface vibration is to immediately stop drilling when potentially troublesome vibrations are perceived. Vibration-reducer tools are now being included in the BHA bottom-hole assembly, the most efficient of which are by using thrusters. These tools can apply a constant weight on the bits in extended reach and horizontal wells, while improvements in well condition are also seen. These improvements lead to decreased occurrences of drillstring component failures. Additionally, for vertical wells using a thruster in the BHA can significantly decrease downtime associated with vibration events (Santos & Galeano, 2002).

2.1.4.6 Computational Fluid Dynamics (CFD)

Fluid mechanics is a category of physics that deals with the mechanics of fluids and the forces acting on them. A subcategory of fluid mechanics, computational fluid dynamics (CFD) employs numerical analysis to investigate and solve fluid flows. Developing CFD models involves a complex combination of geometry and physics, along with other elements and disciplines such as engineering. This chapter presents some model configurations that are typically used in laboratory and field environments, including the meshing technique and chosen boundary conditions. A number of CFD models have been applied in lab simulations.

Chapter 3

3.1 Thruster Design and Simulation

3.1.1 Purpose of Hydraulic Thruster

- A hydraulic thruster is useful for creating a thrust force in a drill bit situated at the bottom end of the drill string.
- A hydraulic thruster is able to transmit drill string torque during the drilling process, enabling the smooth flowing movement of fluid through the relevant components.

3.1.2 Basic Design Parameters for Downhole Thruster BHA

In this section, a simple model to estimate the dynamic properties of thruster assemblies is presented. By using the free body diagram as shown in figure 2, some insight into the dynamic behavior of the inclined thruster BHA can be obtained. First of all, the model considers the buoyancy and corrected weight, F_w , of the BHA, as well as the thruster piston force frictional contact at the bit and at the stabilizers, the bit axial force due to the annulus pressure and the bottom hole reactive force (WOB). Based on the balance of forces in the axial direction WOB could be calculated by using the stationary WOB. Then, based on the WOB from the balance of forces in the axial direction, the stationary WOB can be determined as follows:

$$WOB_0 = P_{thr}A_{thr} - P_{ann}A_{bit} + F_w \cos \alpha - \mu F_w \sin \alpha \quad (2.23)$$

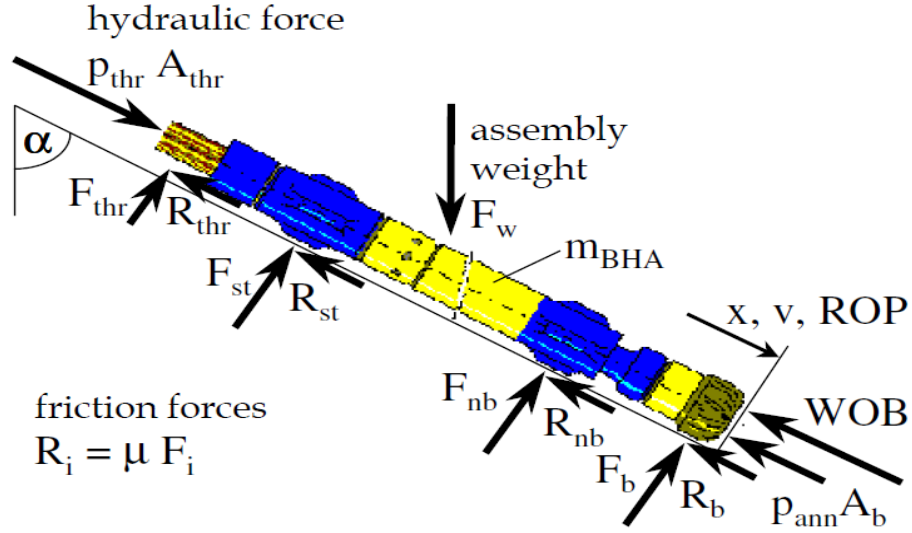


Figure 3.1: Free body diagram of a floating thruster as a part of the BHA

3.1.3 Design of Thrusters

Simply defined, a thruster is a hydraulic cylinder with a piston. It operates through the hydraulic force exerted by the pressure inside the cylinder, which acts on the piston and generates a thrust force. In drilling, a thruster is usually placed in the BHA over the drilling bit. Hence, because a thruster BHA is similar to a hydraulic cylinder, the drill string and the thruster housing make up the cylinder.

The thrust force can be expressed as a function of the cross-sectional area of the piston and the pressure drop between the piston and annulus pressures. In fact, any tool positioned below the thruster piston and generating a pressure drop adds to the WOB. If held in a floating position while drilling, the thruster can serve as an anti-vibration tool. Furthermore, when positioned in this floating state, the thruster is able to move freely between the hard limits.

For available 246.10 mm tool sizes, a thruster can obtain thrusts between 57.75 psi and 1344.319 psi. The maximum benefit from the tool is derived by positioning it as close as possible to the bit. As shown in Figure 3.1, a thruster BHA usually contains a top and string stabilizer to avoid the generation of lateral vibrations and whirl.

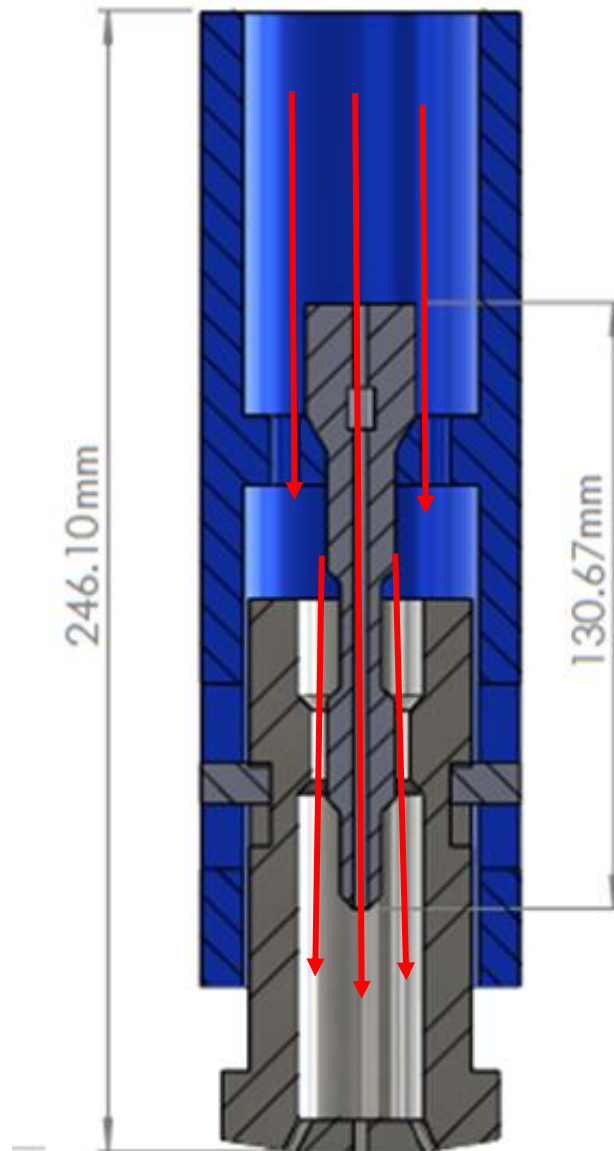


Figure 3.2: 2D drawing of the Thruster



Figure 3.3: 3D Sectional view of the downhole Thruster

This section provides the initial attempt to develop basic tool principle, tool design, and preliminary analysis. By acting like a hydraulic cylinder, a downhole thruster can offer the user WOB that is proportional to the differential pressure.

- The force at which the cylinder will stroke can be calculated as the product of hydraulic pressure TIMES the cylinder's effective area.
- In a thruster, the force (F), which leads the Thruster piston to strike or move forward is the product of the inside-to-outside differential pressure (Pd)

$$F = A_p * Pd \tag{3.1}$$

- A_p is the area which corresponds to the diameter:

$$A_p = DP^2 \pi / 4 \tag{3.2}$$

3.1.3.1 Choke Spear and Sleeve Configuration

On the interior of the thrust cylinder is a choke spear, which features differing areas of outer diameter. The thruster piston features an area of decreased inner diameter which is labelled the ‘sleeve’.

- The pressure drop on thrusters can be either large or small, based on how the sleeve moves towards the choke spear. This can lead to either more or less thrust force and therefore to more or less WOB.
- A bore is positioned along the whole length of the spear, emerging at the mud flow.
- A less complex model enables the estimation of the dynamic properties of thruster assemblies and can help users gain valuable insight into the dynamic behaviour of an inclined thruster BHA.
- The model considers the buoyancy corrected weight, F_w , of the BHA, thruster piston force, frictional contact at the bit, bit axial force due to annulus pressure, and the bottom hole reactive force (WOB). Then, by considering the balance of forces in the axial direction, the stationary WOB can be calculate as follows:

$$WOB_o = P_{thr} A_{thr} - P_{ann} A_{bit} + F_w \cos\theta - F_w \sin\theta \quad (3.3)$$

3.1.3.2 CFD Simulations

The first step in using a CFD simulation is grasping the underlying physics that determines the scope of the problem. A key factor to keep in mind is that the simulations are transient, which

means that the choice of the initial conditions, including boundary conditions, is significant. In fact, the initial conditions will, to a great extent, determine the validity of the study results.

3.1.3.3 CFD Simulation Cases

In the present work, a wide range of representative modeling types, meshes and geometries are investigated and applied. The following section gives a broad overview of the simulations while also providing a summary of the fluid flow in 3D simulations (fluent).

3.1.3.4 Geometries

In order to reduce both the local effects and those effects related to the inlet boundary, the geometries in this work were constructed using ANSYS Fluent R 17.2 (see Figure 3.3).

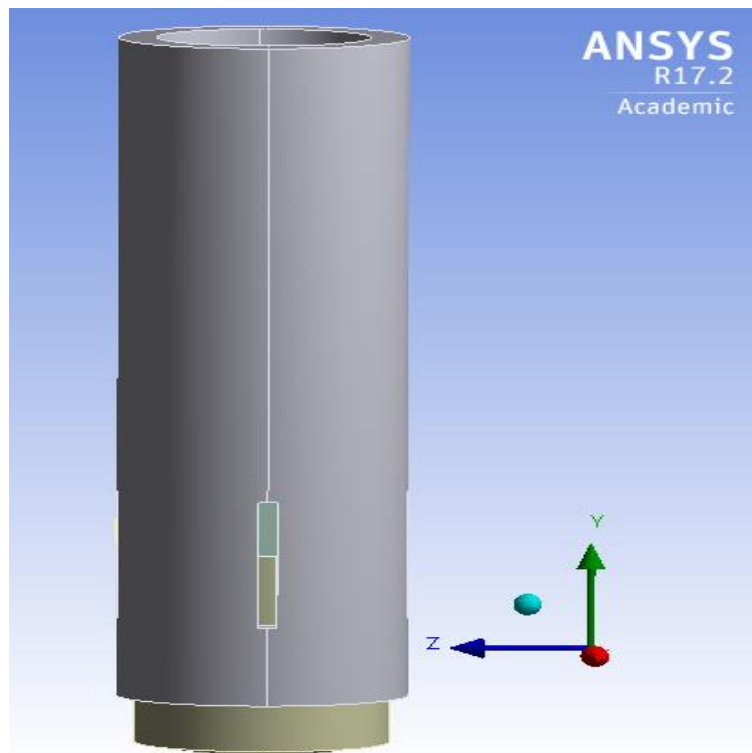


Figure 3.4: Geometry setup fluent

3.1.3.5 Meshing

In CFD simulations, meshing serves as a major factor to obtain viable CFD outcomes. The present study uses meshes that have been created by CFD algorithms (i.e., automatically). In this approach, one mesh per geometry has been developed. Furthermore, a grid chooses the elements or cells where the flow is to be solved, thus forming a discrete representation of the problem's geometry. Because the grid can have a major effect on the convergence rate as well as the viability of the solution, it is crucial for the grid resolution to be small enough to catch and retain ultra-fine flow material. The mesh used in the thruster (i.e., cylinder, spear, and piston) in this study has 223547 elements, along with 45874 nodes. Figure 3.4 shows the best meshing determined for the Thruster design and simulation by ANSYS. The numerical values of the Thruster meshing are shown in Table 3.1. Figure 3.5 shows the graphical plots of data of table 1.

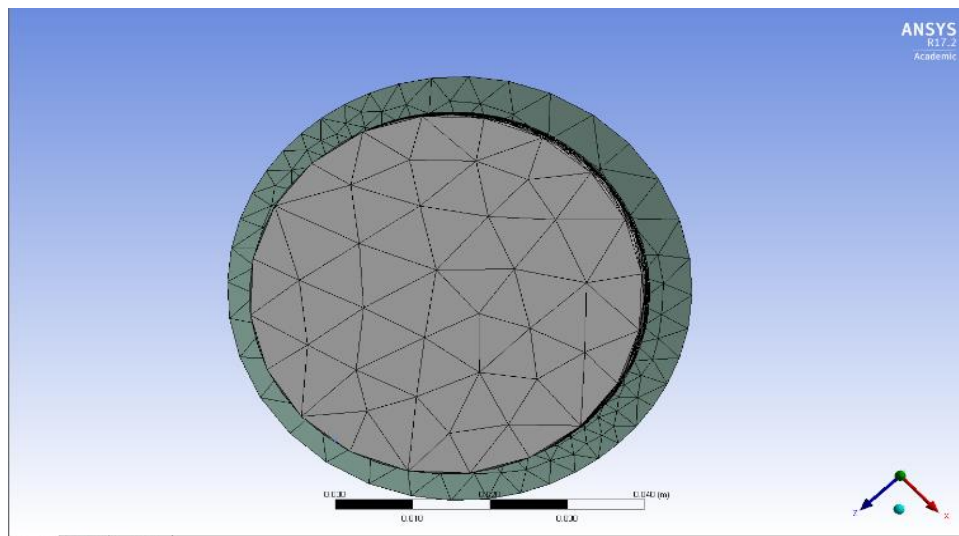


Figure 3.5: Meshing of the Thruster

As depicted in Table 3.1 and Figure 3.5, we can locate the optimal number of elements which is 223547 elements.

Table 3.1: Summary of the numerical values of the Thruster meshing

Ref.	Number of Elements	Pressure (Psi)
1	112691	300
2	140911	745.95
3	167312	1190
4	223547	1136.8
5	467382	1134.7
6	698671	1129.8

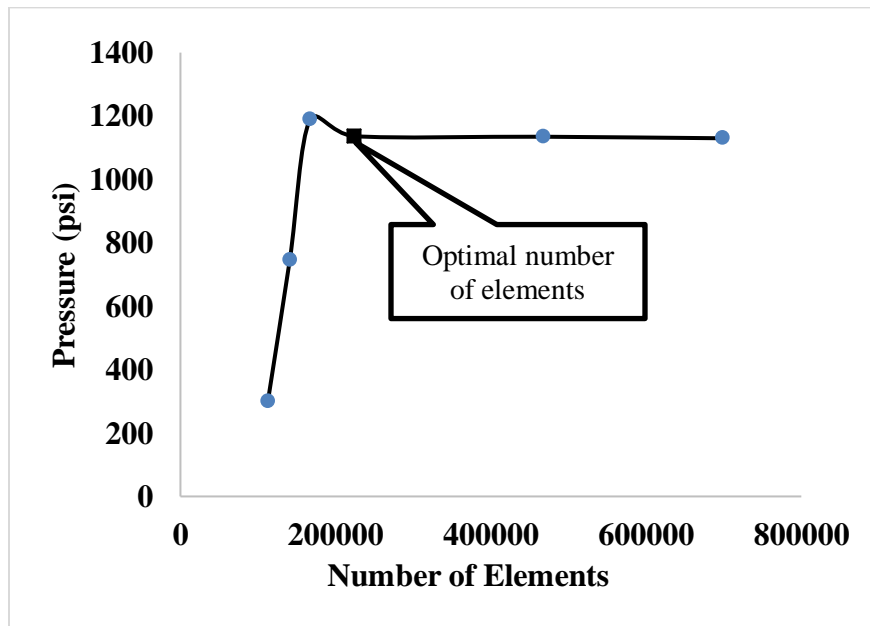


Figure 3.6: Number of elements and the represented pressure for best Thruster meshing

3.1.3.6 Thruster Fluid Flow Simulation

A simulation highlighting how fluid flows in a thruster is carried out in ANSYS as flow assurance. The results of the simulation are depicted in Figure 3.6. The figure also indicates flow

direction. Note that boundary conditions (m/s velocity) for downstream are given in the geometry inlet.

Figure 3.6 also presents the streamline's sequence within the thruster, with the picture to the left indicating the starting point for the simulation. Then, as the simulation proceeds, the results begin the stabilization process, after which the flow moves away from the inlet and in the general direction of the thruster's convergent area.

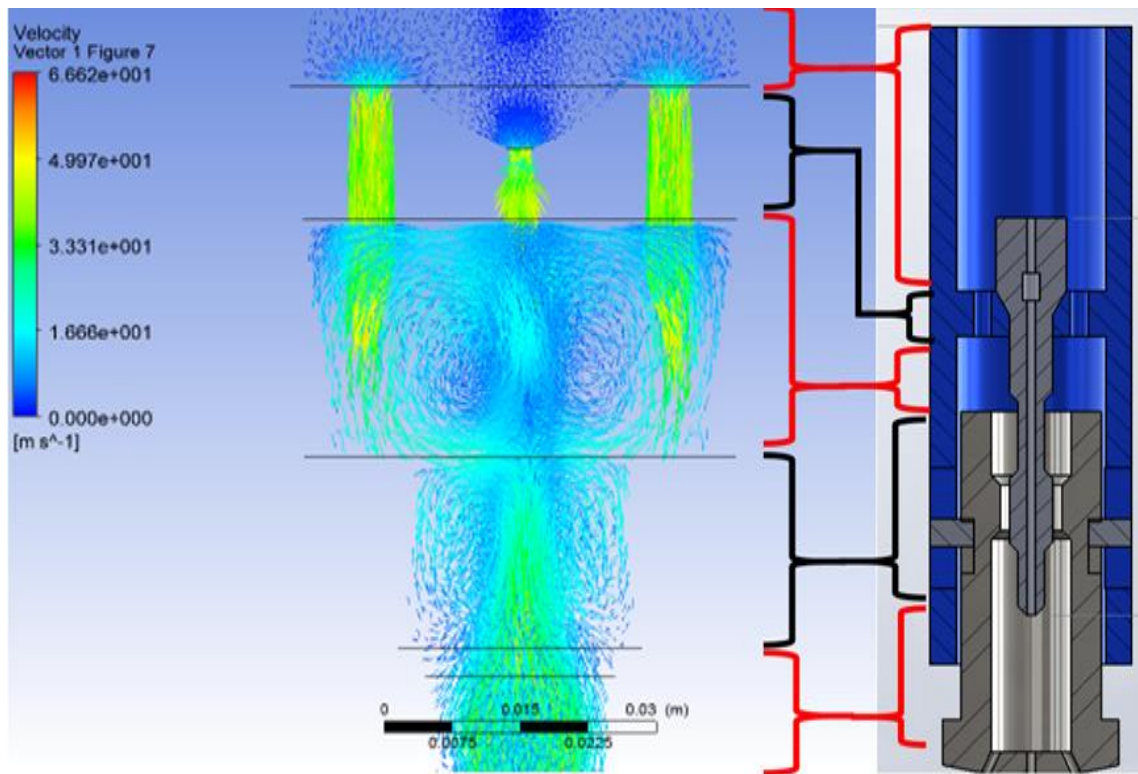


Figure 3.7: ANSYS fluent R 17.2 fluid flow simulation of the Thruster

Some additional parameters which ideally should be included as part of bottomhole thruster design are listed below:

- bit diameter
- choke speak cross-sectional areas

- cylinder volume
- forces
- grip capacity
- material selection
- mud motor speed
- piston area
- pressure
- spline (female and male) diameter
- spline (female and male) length
- torque
- weight-on-bit (WOB)
- wellbore diameter

Chapter 4

4.1 CFD Numerical Simulation for Downhole Thruster Performance Evaluation

This is a paper that was prepared and presented for proceeding of the ASME 2018 37th International Conference on Ocean, Offshore and Arctic Engineering on June 17-22, 2018, Madrid, Spain. The Paper Number: OMAE2018-78101.

Authors: Bashir Mohamed¹, Abdelsalam Aabugarara¹, M.A. Rahman², and Stephen D. Butt¹.

¹ Department of Process Engineering, Faculty of Engineering and Applied Sciences, Memorial University of Newfoundland, St. John's, Newfoundland and Labrador, Canada.

² Petroleum Engineering, Texas A and M University at Qatar, Doha, Qatar.

4.2 Abstract

This study focuses on numerical simulation and evaluation of a hydraulically powered downhole Thruster. This device is numerically simulated and evaluated using ANSYS Fluent 17.2 to show its generation of pressure pulses that can induce downhole forces that magnify the downhole dynamic weight on bit (DWOB) using drilling mud. Such magnification of the DWOB can produce axial motion of the Thruster. Such axial motions, as proved by many publications can improve the drilling rate of penetration (ROP), release stuck pipes, and reduce frictions in non-vertical wells. The special inner design of the Thruster creates pressure pulses that can provide load impact on the drill bit leading to the increase of WOB that can enhance the drilling performance. The current stage of the study of the Thruster involves a mechanical design of the

Thruster by the SolidWorks and an evaluation of the tool function and performance through pressure effect simulation by ANSYS Fluent 17.2. Initially, water is used as the fluid and the main parameters involved in the analysis are pressure and velocity. However, power-law as a non-Newtonian fluid is also used for comparison study in the section of pressure drop analysis.

The results are analyzed based on velocity pressure profiles, pressure drops, pressure effects with applications of various back pressures at several planes using water and power-law fluids.

Keywords: Thruster, CFD, SolidWorks, drilling performance, WOB.

4.3 Introduction

The downhole Thruster is a tool that has been proved to assist in improving drilling performance Schmalhorst, (1999) and Kamatov et al (2015), protect the bottom hole assembly (BHA), reduce friction in non-vertical oil and gas wells, mitigate bucking of drillstring, and reduce lateral and stick/slip vibrations Kamatov et al (2015) and Jones, (2016).

In general, research was investigating positive effect of generating axial vibrations for the purpose of improving ROP by introducing the downhole Thruster, then for intensive research of field and laboratory work showed more benefits of inducing the axial motions which eventually lead to improving the drilling efficiency.

Numerous drilling parameters have direct or indirect impact on drilling ROP either positive or negative influence. Such parameters that increase the drilling ROP when they increase up to the founder point, include rotary speed (RPM), rotary torque, bit hydraulics and drill mud flow rate, and applied weight on bit (WOB) and the associated depth of cut (DOC) of the bit cutters.

As applying drilling parameters that can assist in increasing the drilling ROP at the top of the well (at the surface) may negatively impact the drilling operation and rise the drilling costs more than they could support the drilling performance. Moreover, several downhole parameters effects not controlling the surface WOB such as drill string flexibility and wellbore friction Schmalhorst, (1999)

Numerous reasons are behind adopting applying downhole DWOB at the bit. One of which is a practical approach of implementing the downhole Thruster that allows an axial motion of the drill bit. Other reasons include extending the life of the bottomhole assembly (BHA) and avoiding a pre-mature drillstring and bit change as the axial motion reduces the friction, minimizes stick-slip bit vibration. The axial motion of the Thrusters, also provides better drillstring dynamics, enhances the drilling ROP Reich et al (1995) and Rana et al (2015), assists to facilitate the cutting action of the bit Powell and Ertai (2015), reduces the overall cost of the drilling operation Reich et al (1995) and Powell and Ertai (2015), and mitigates harmful vibrations such as stick-slip in vertical and directional wells Clausen et al (2014).

Downhole axial vibration in unconventional, extended reached, horizontal, and vertical wells has been proven to improve the drilling ROP Wilson and Noynaert (2017) and Gee (2015). Some of methods applied at the drill bit that induce the downhole axial motion (benign vibration), such as pressure pluses generated due to drill mud flow though downhole tools designed to axially move Wilson and Noynaert (2017) and Gee (2015).

This paper uses a downhole Thruster that is mechanically designed by SolidWorks than can provide some dynamic downhole increase in the WOB at the bit. The Thruster performance then simulated and evaluated by ANSYS R-17.2. The data analysis and results are reported below.

4.4 Description of the Thruster

4.4.1 Mechanical Design

The mechanical structure and design of the downhole Thruster used in this paper is shown in Figures. 4.1 and 4.2 as AutoCAD and SolidWorks drawing and design; respectively.

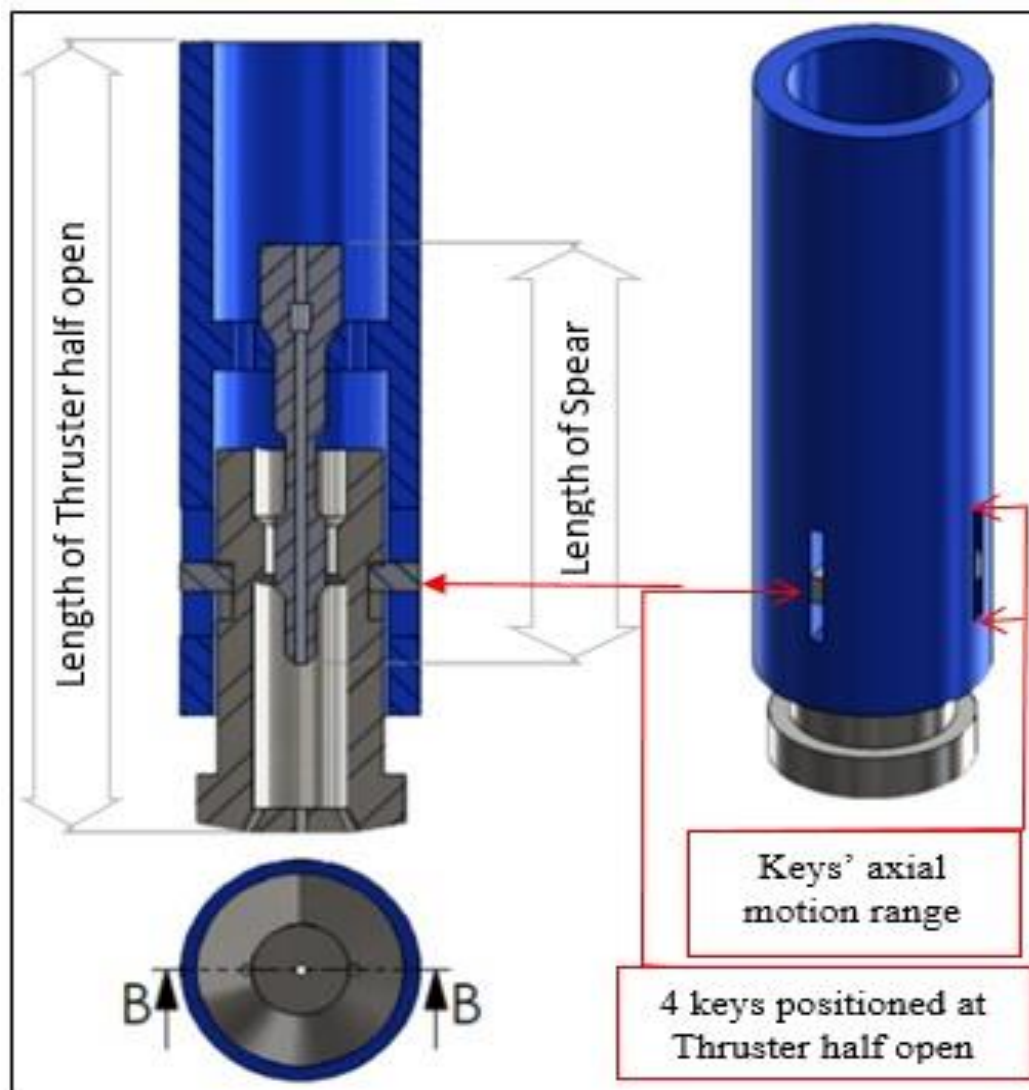


Figure 4.1: Drawing of the Thruster

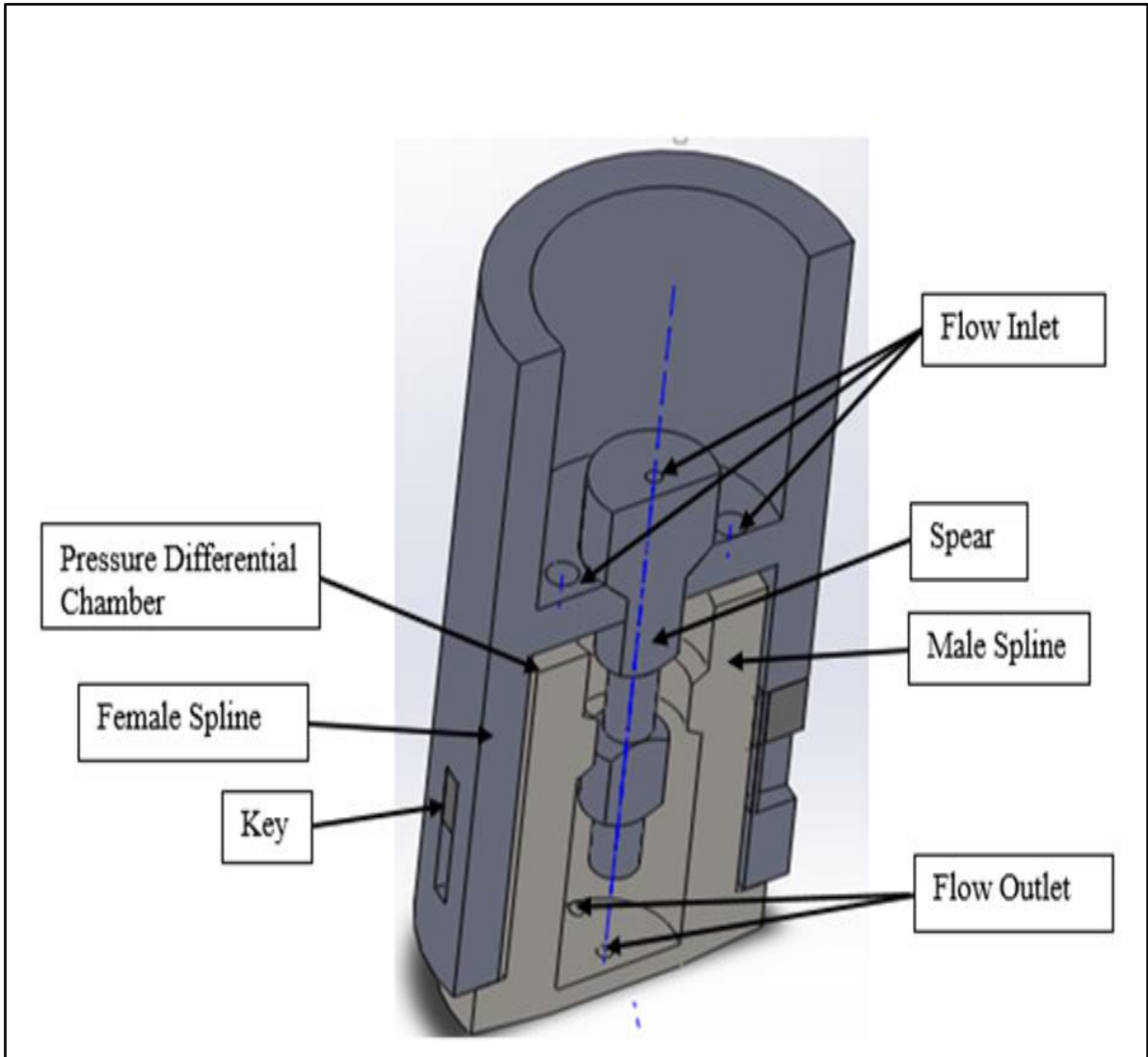


Figure 4.2: Thruster mechanical design

4.4.2 Thruster Geometry

Figure 4.3 shows the Thruster geometry simulated by ANSYS.

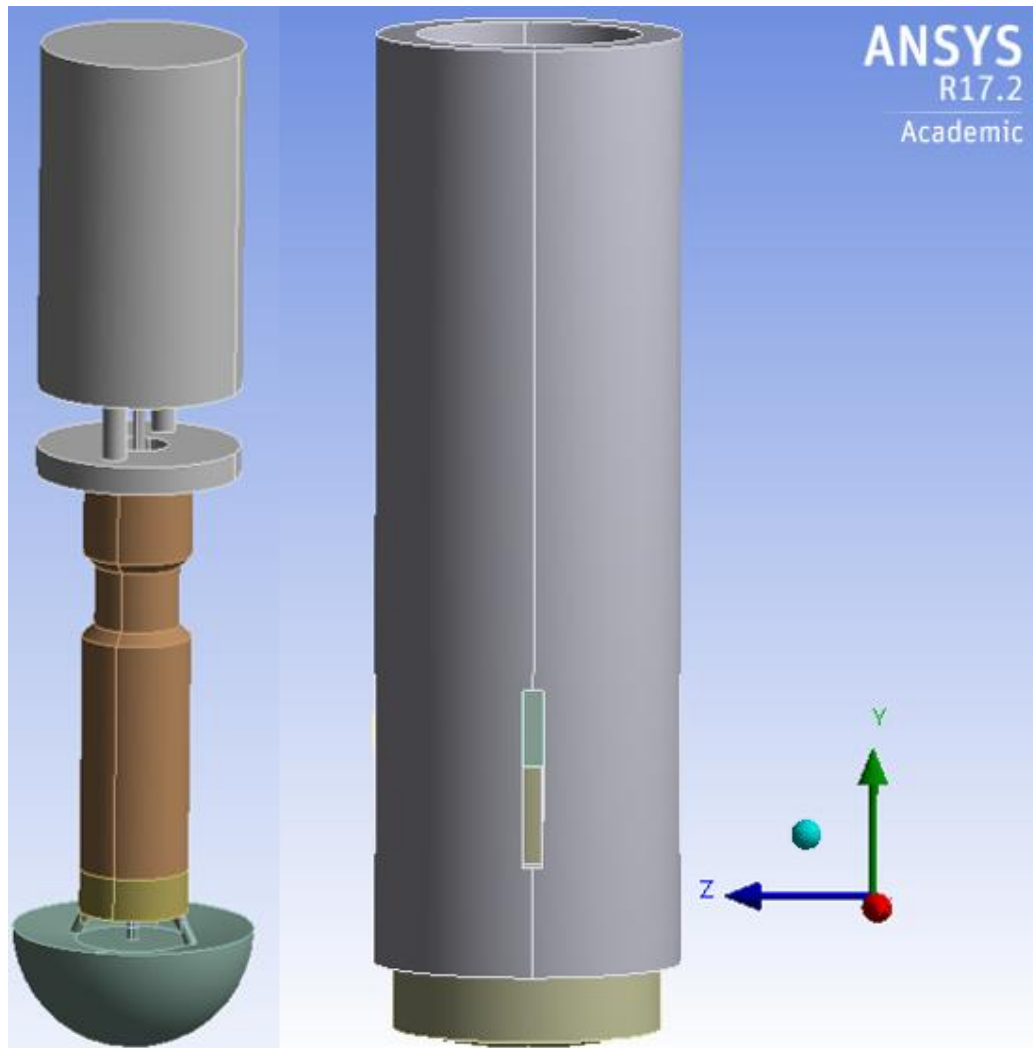


Figure 4.3: Thruster geometry simulated by ANSYS

4.4.3 Thruster Meshing

Figure 4.4 shows the best meshing determined for the Thruster design and simulation by ANSYS. The numerical values of the Thruster meshing are shown in Table 4.1. Figure 4.5 shows the graphical plots of the data presented in table 4.1.

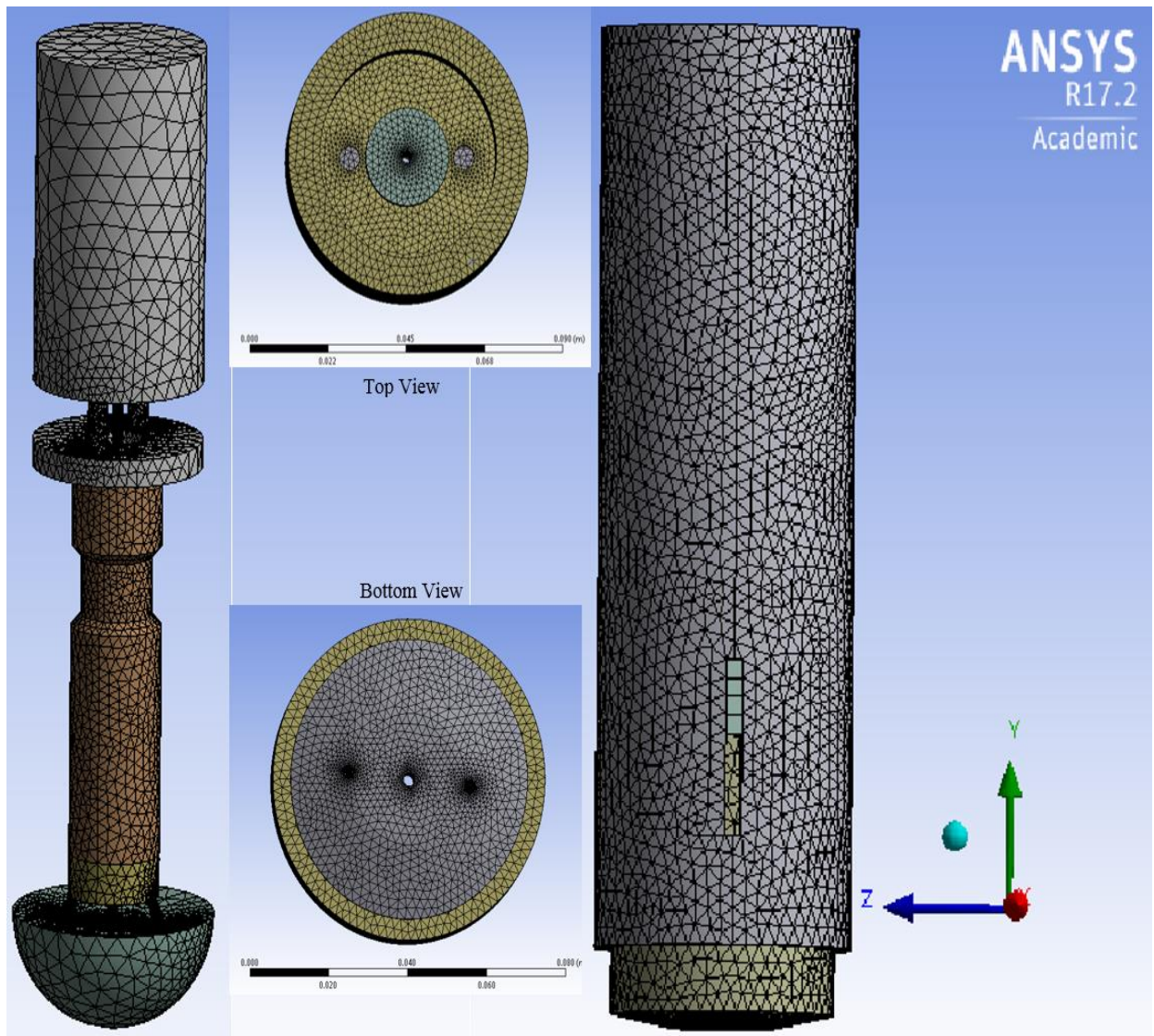


Figure 4.4: Thruster meshing

Table 4.1: Summary of the numerical values of the Thruster meshing

Ref.	Number of Elements	Pressure (Psi)
1	112691	300
2	140911	745.95
3	167312	1190
4	223547	1136.8
5	467382	1134.7
6	698671	1129.8

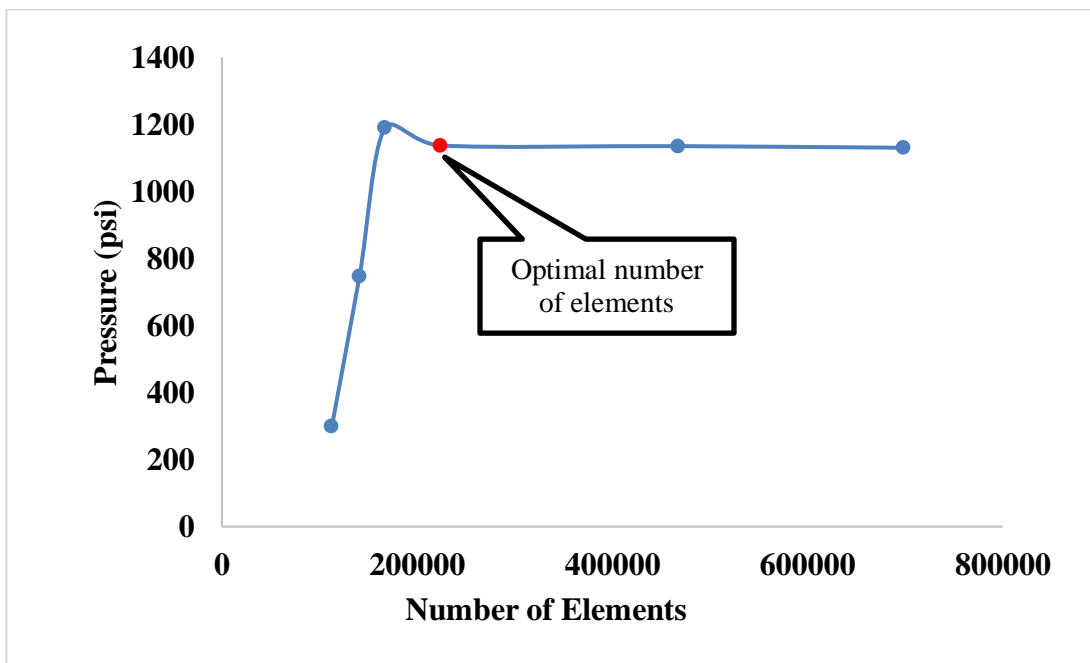


Figure 4.5: Number of elements and the representative pressure for best Thruster meshing

4.4.4 Thruster Fluid Flow Simulation

The simulation of the fluid flow through the Thruster was performed by ANSYS for fluid flow assurance. The simulation was, also intended to evaluate the mechanical design of the Thruster for optimal pressure pulse generation. The simulation result is shown in Figure 4.6.

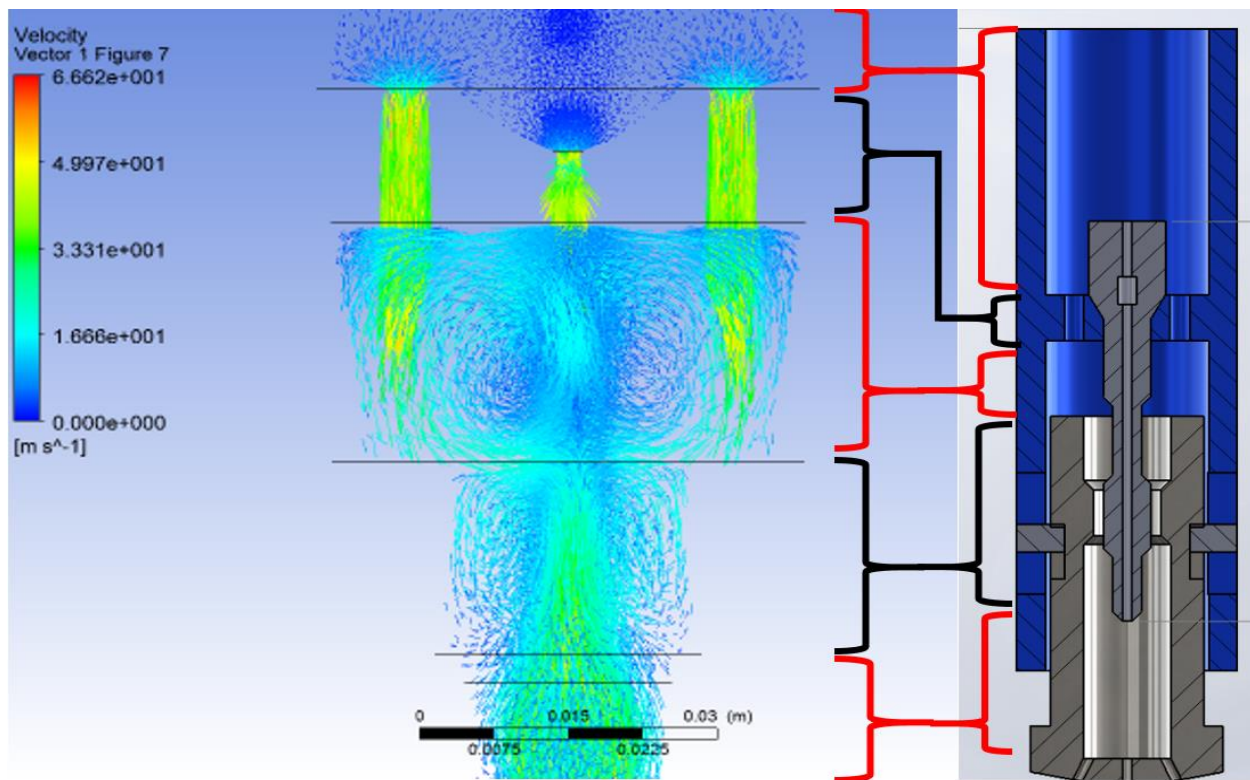


Figure 4.6: ANSYS Fluent 17.2 fluid flow simulation of the Thruster

4.4.5 Data Analysis

In this section the description of data analysis, data included in the analysis and their effect on drilling ROP is presented. The two main parameters included in the ANSYS simulation of the downhole Thruster performance evaluations are fluid velocities and their pressure effectiveness. Two applications were implemented in the analysis involving “with Thruster” vs. “without

Thruster”. The difference between the two applications is the chocking path that exists in the “with Thruster” that allows the spear of the tool to axially move and then generate “Pressure Pulses”. Such produced pulses provide loading impact on the piston of the Thruster. This chocking path is not existed in the “without Thruster” applications.

4.5 Results

4.5.1 Thruster Downhole Force Generation

As the fluid flow rate was the input parameter in ANSYS, subsequently the change in fluid velocity and the associated pressure effect of this change were analyzed. Table 4.2 contains the numerical data of various values of pressure effect and the corresponding ROP for both applications. Figure 4.7 shows the result of the mean values of the pressure effect in generating downhole forces. Figure 4.8 shows the compared result of the influence of the generated downhole forces on the drilling ROP using Maurer model.

Table 4.2: Summary of the Pressure effect, forces, and ROP for with/without Thruster

Density Kg/m ³	Thruster Pressure effect (psi)			Generated Force (N), with Thruster	Estimated ROP (m/hr), with Thruster
	Min (psi)	Max (psi)	Mean (psi)		
1000	100	100	100	943	0.03
	200	200	200	1887	0.11
	39	383	255	3613	0.39
	39	383	255	3613	0.39
	50	506	339	4773	0.67
	76	782	523	7381	1.61
	16	902	609	8505	2.14
	140	903	689	8521	2.15
	74	1001	756	9440	2.64
	28	1137	850	10725	3.40
	"No-Thruster" Pressure effect (psi)			Generated Force (N), without Thruster	Estimated ROP (m/hr), without Thruster
Kg/m ³	Min	Max	Mean		
1000	42	100	100	551	0.01
	138	200	200	1101	0.02
	239	300	300	1652	0.05
	337	400	400	2202	0.10
	443	500	500	2753	0.15
	540	600	600	3304	0.22
	637	700	699	3854	0.29
	738	800	800	4405	0.38
	844	900	900	4955	0.48
	943	1000	1000	5506	0.60

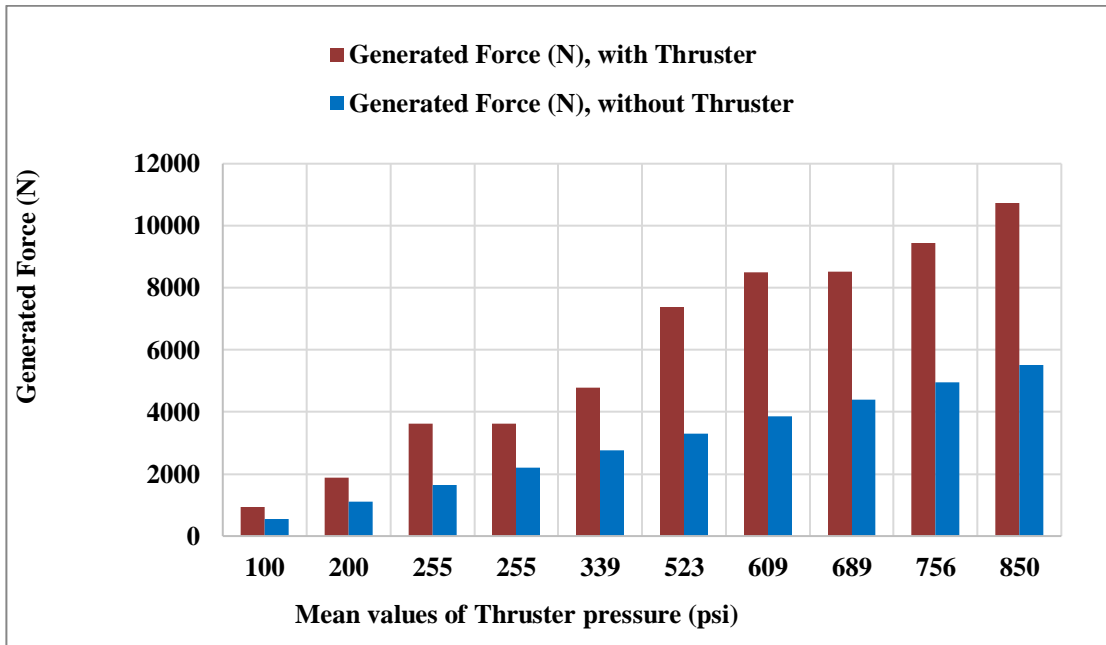


Figure 4.7: The generated force due to the measured mean pressure effects in both applications of with and without Thruster

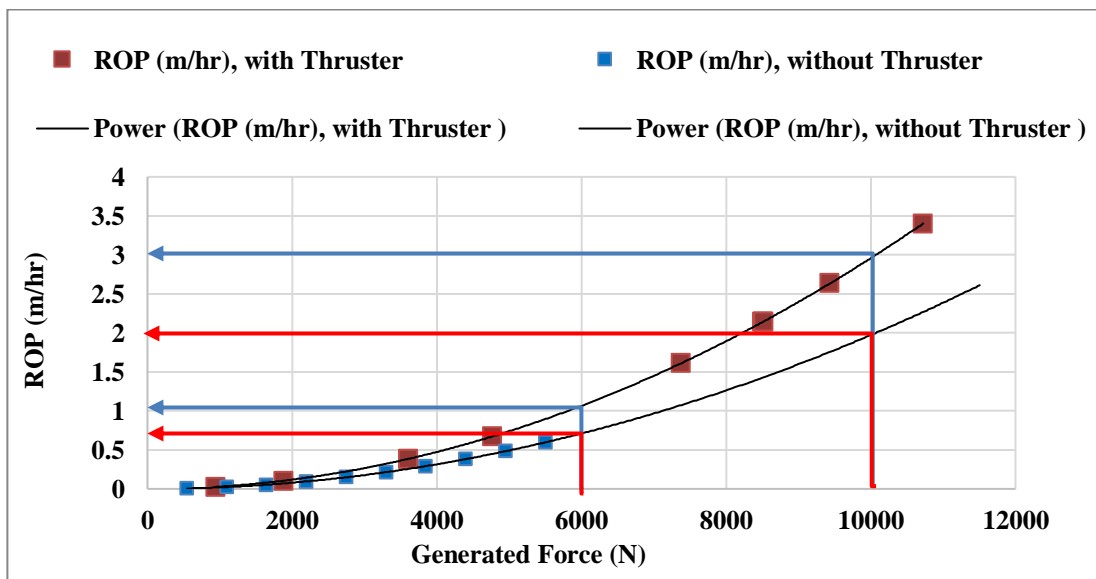


Figure 4.8: The resultant ROP in both applications based on Maurer Model for with and with no Thruster

4.5.2 Thruster Velocity and Pressure Analysis

Once the Thruster performance was identified based on the calculated ROP implementing Maurer model as shown in Figures 4.7 and 4.8 versus “without Thruster”, performance was using the maximum generated pressure values in both cases, then the study of the Thruster proceeded for more data analysis using the pressure effect. The pressure effect analysis includes introducing back pressure at the bottom of the Thruster, based on which the Thruster performance was further analyzed. Figure 4.9 shows the influence of the increase of the back pressure as percentage of the effect pressure at three selected fluid velocities.

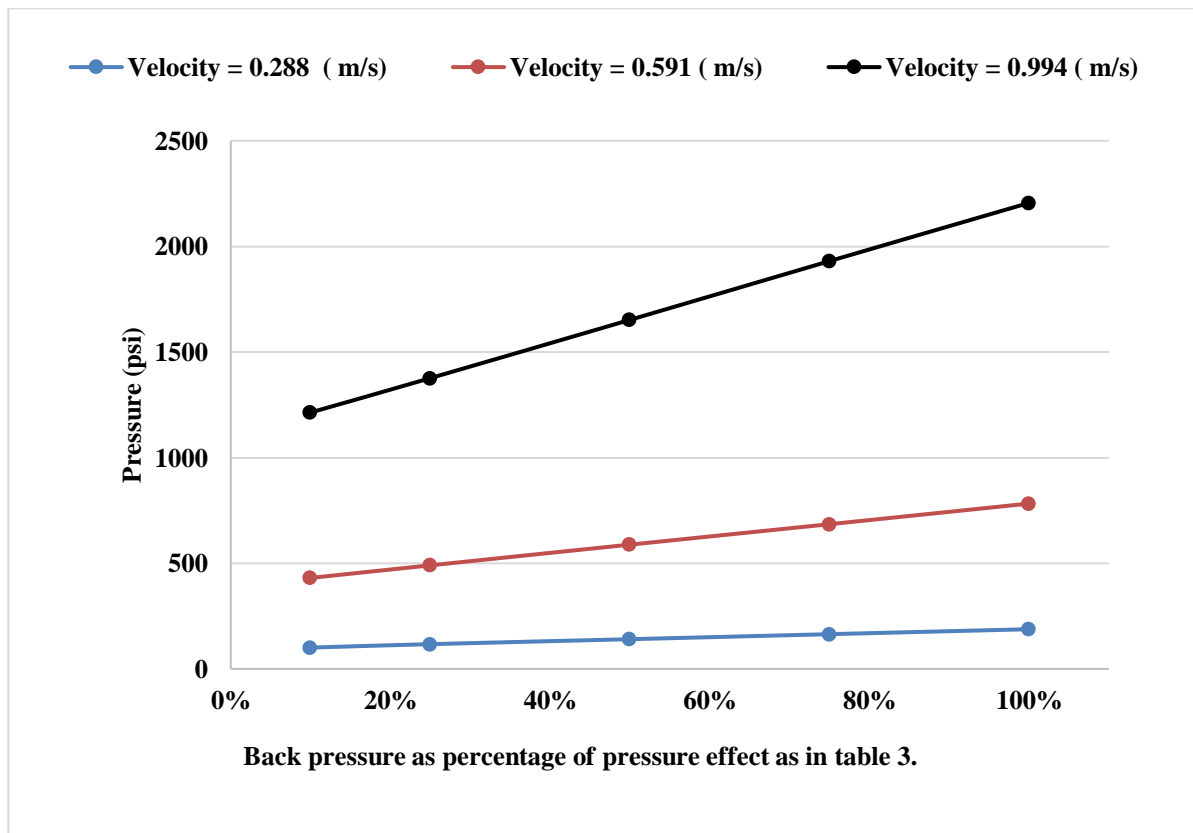


Figure 4.9: Thruster generated pressure as percentage back pressure of the pressure affect

Table 4.3: Numerical data plotted in Figure 9

Back pressure (bp) as %	Pressure effect (psi)		
of the pressure effect	@ V= 0.288 (m/s)	@ V= 0.591 (m/s)	@ V= 0.995 (m/s)
10%	100.892	430.789	1214.008
25%	117.198	490.419	1376.597
50%	140.644	588.386	1652.400
75%	164.443	685.046	1930.698
100%	187.881	782.788	2206.198

Table 4.3 shows the effect of the back pressure as a percentage of the pressure effect at 3 various velocities. Table 4.4 shows the relationship between the fluid velocity as inlet to the thruster and the corresponding pressures. The inlet velocities provided in table 4.4 are based on the available laboratory pump capability with the measured corresponding pressure values.

Table 4.4: Various inlet fluid velocities and the resultant pressure effect

Ref.	Inlet Fluid Velocity (m/s)	Pressure (Psi)
1	0.225	57.757
2	0.288	94.164
3	0.396	176.523
4	0.496	275.299
5	0.591	391.672
6	0.682	520.339
7	0.901	906.332
8	0.994	1102.607
9	1.099	1344.319
10	1.201	1610.180

Figures 4.10 to 4.13 show Thruster pressure pulses' generation. Figures 4.10 and 4.11 show the pressure pulse and the lowest applied fluid velocity, respectively. Figure 4.12 shows combination of Figures 4.10 and 4.11 confirming the exact correspondence and reactions of both, the pressure and the velocity by the defined by the recorded signals. Each signal of the pressure and the velocity can be divided to main regions, including the choked and the un-choked as shown in Figure 4.13.

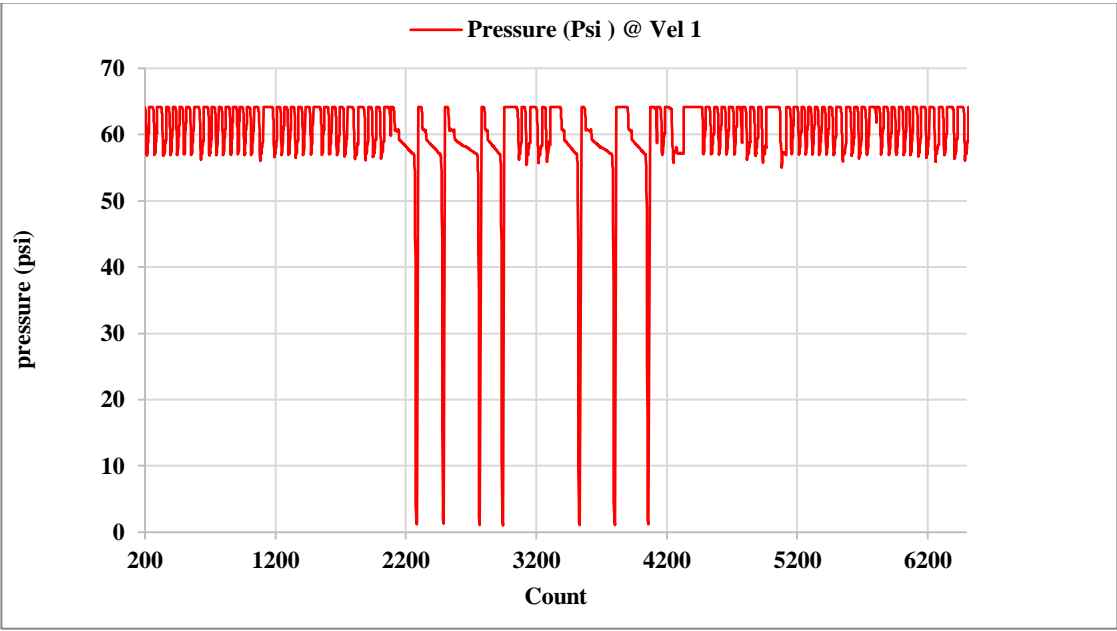


Figure 4.10: Generated Thruster pressure pulse at the input velocity 1

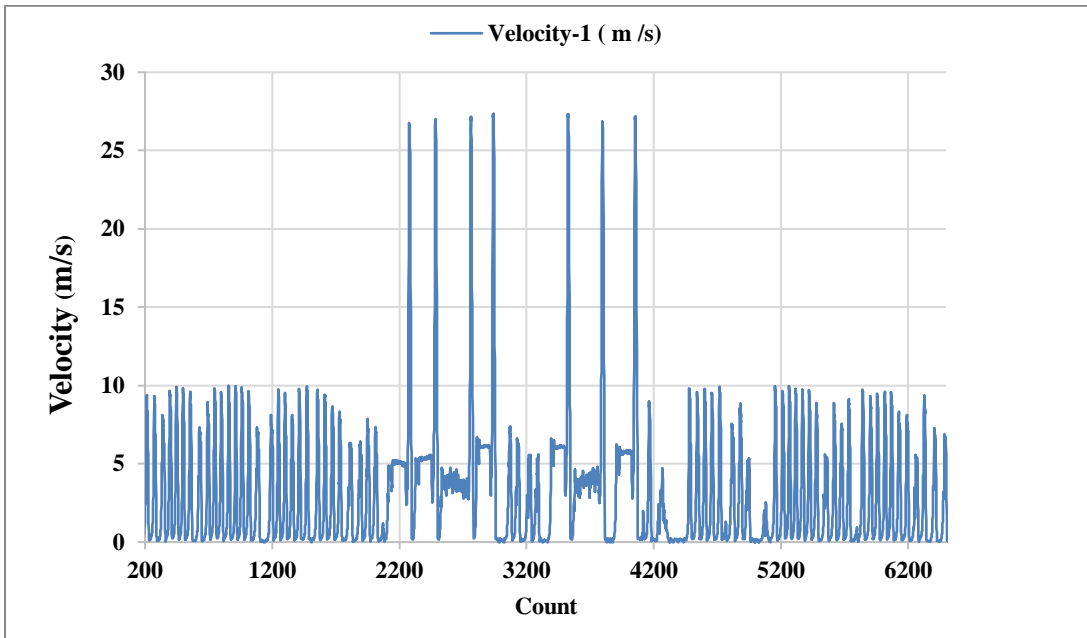


Figure 4.11: Input velocity 1 corresponding to pressure pulse in Figure 10

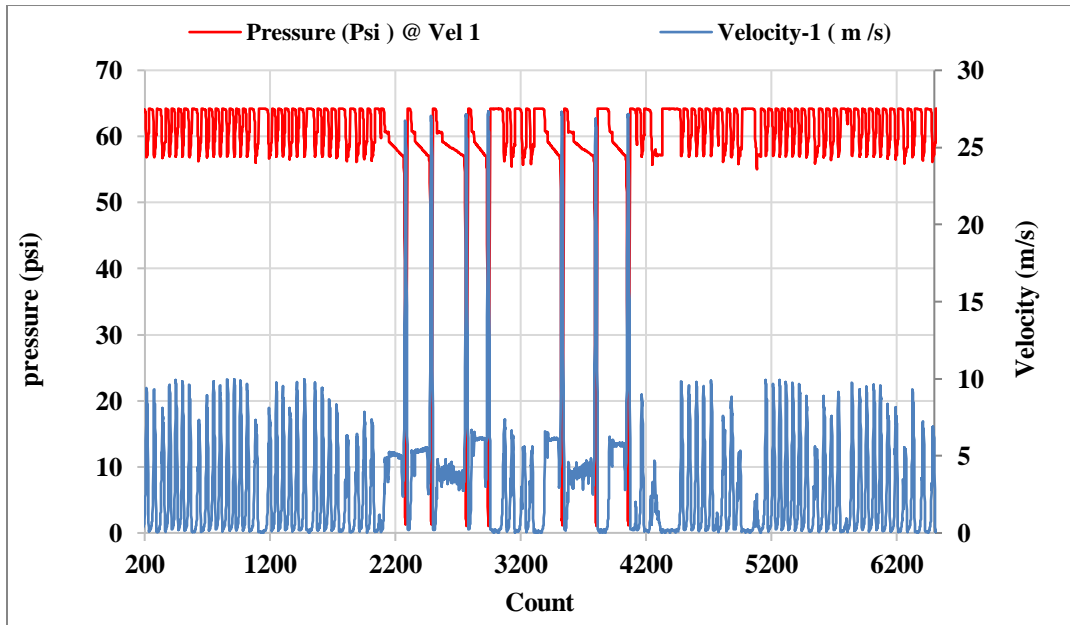


Figure 4.12: Combined pressure pulse at the input velocity 1 as a result of the Thruster operation under this condition

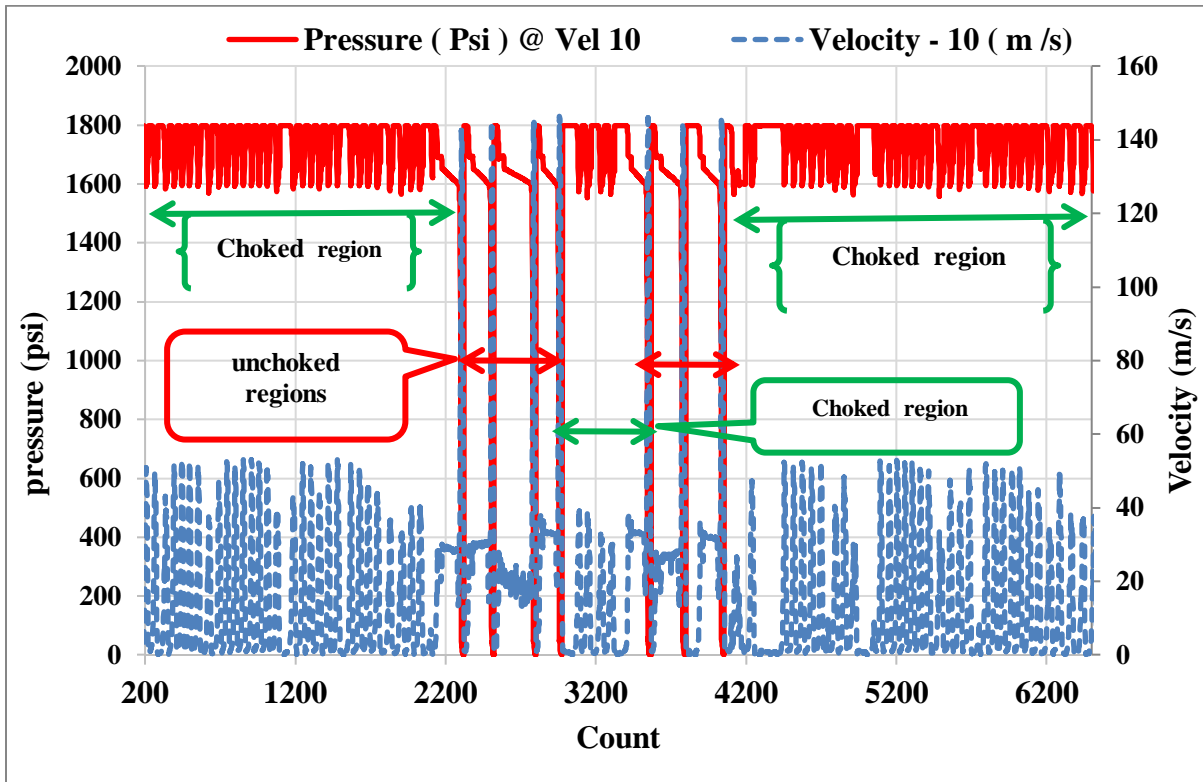


Figure 4.13: Thruster pressure pulse at velocity 10 with Choked and unchoked regions

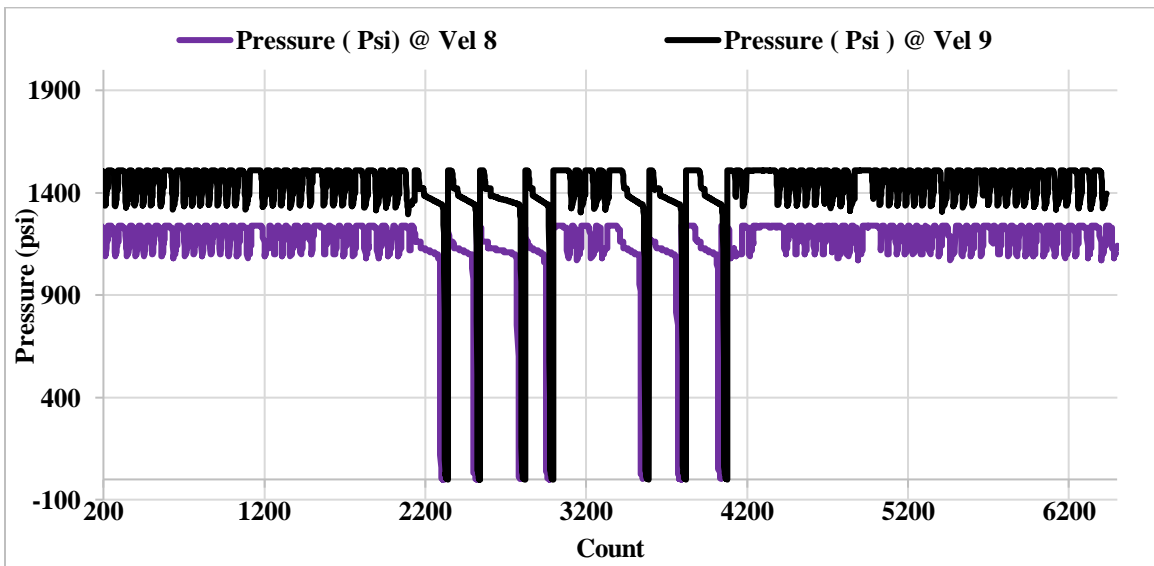


Figure 4.14: The relationship between various inlet fluid velocities and the resultant pressure effect

4.5.3 Thruster Positional Velocity and Pressure Drop

Analysis

This section contains an investigation of the Thruster performance based on the analysis of various fluid velocities and their corresponding pressure drops. Such analysis is conducted at various locations throughout the length of the Thruster. These locations are represented by planes as described in Figure 4.14 are selected to show the influence of the Thruster design on the pressure increase or decrease at various fluid velocities. This analysis also involved Thruster positional velocity and pressure variations with applying many different back pressures (bp). Figure 4.15 shows full recorded signals of pressure pulses at velocities 7 to 10. This figure, also shows the consistency of pressure and velocity variation as a response of the Thruster operation.

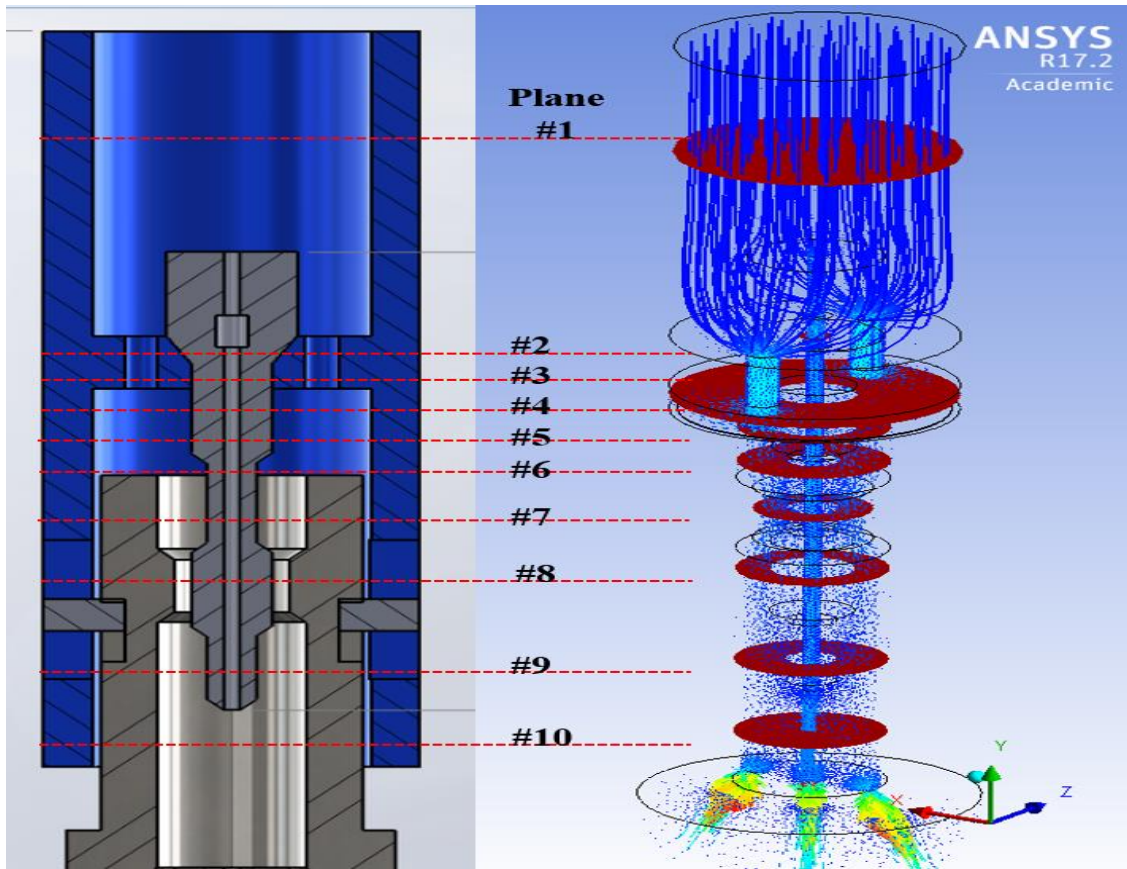


Figure 4. 15: Planes at various locations throughout the Thruster for velocity and pressure drop analysis

Figures 4.16 to 4.19 show the pressure drops at various velocities at different plane positions. Figure 4.16 shows the relationship between the fluid velocities and the corresponding pressure drops at plane 1, the most top and plane 10, the lowest as shown in Figure 4.14. The analysis was performed at 0 back pressure. Figures 4.17, 4.18, and 4.19 show velocity and pressure drops relationship at planes #1, # 8, and # 10, corresponding to different applying back pressures of 0 and 110 psi, respectively.

Figure 4.20 shows the velocity and pressure drops at planes 1 and 10 at 0 psi back pressure using water versus a Non-Newtonian Power-law fluid. The curves of the plotted result show an

increase in pressure drop that generally occurs with the increase of length and with the decrease of the diameter due to the increase of friction, which is mainly influenced by fluid viscosity. The pressure drop is further analyzed in Figures 4.21 and 4.22.

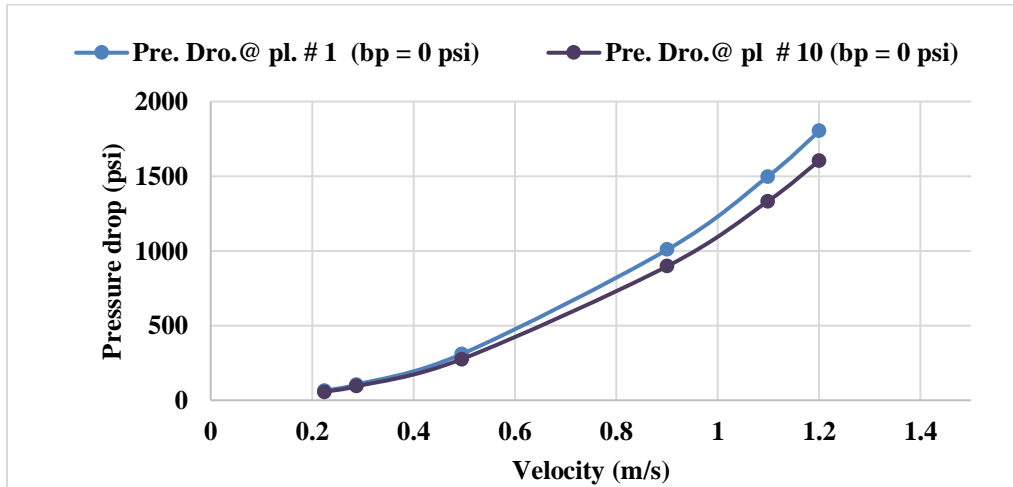


Figure 4.16: Relationships between fluid (water) velocities and pressure drops at plane #1 at back pressure = 0 psi

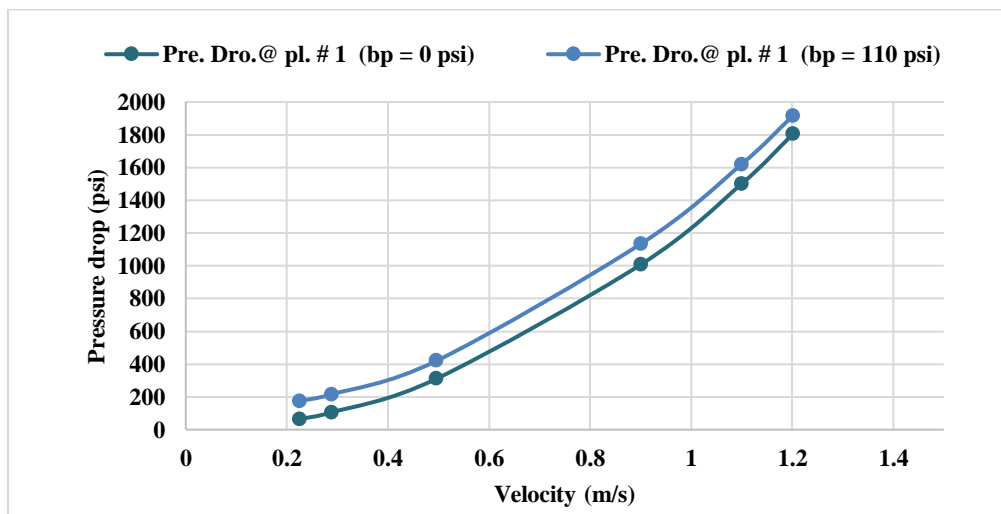


Figure 4. 17: Relationships between fluid (water) velocities and pressure drops at plane #1, which is located at the entrance of the Thruster at 2 different back pressures including 0 psi and 110 psi, as the lowest and the highest, respectively

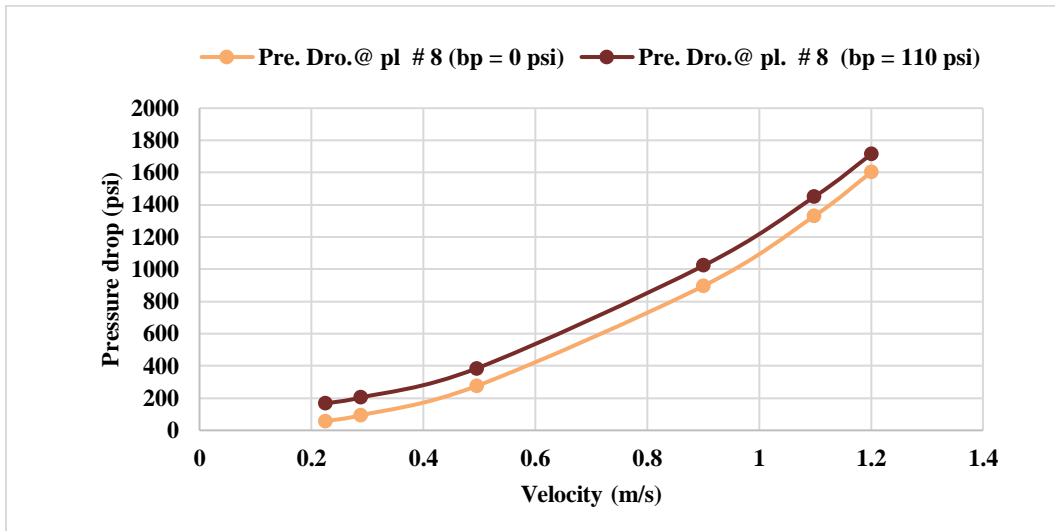


Figure 4.18: Relationships between fluid velocities and pressure drops at plane # 8, which is located at the choking region of the Thruster at 2 different back pressures including 0 psi and 110 psi

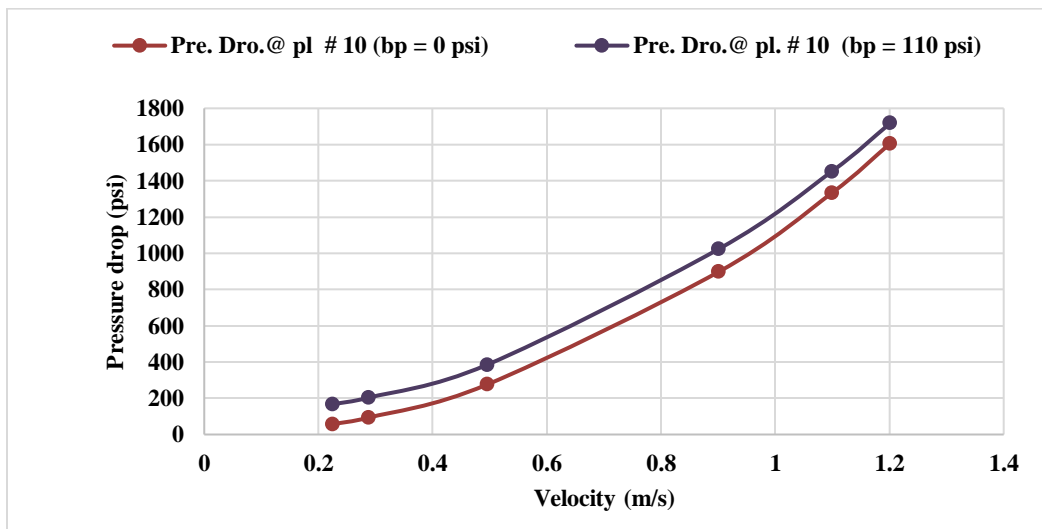


Figure 4. 19: Relationships between fluid velocities and pressure drops at plane #10, which is located prior to fluid exit from the Thruster at 2 different back pressures including 0 psi and 110 psi

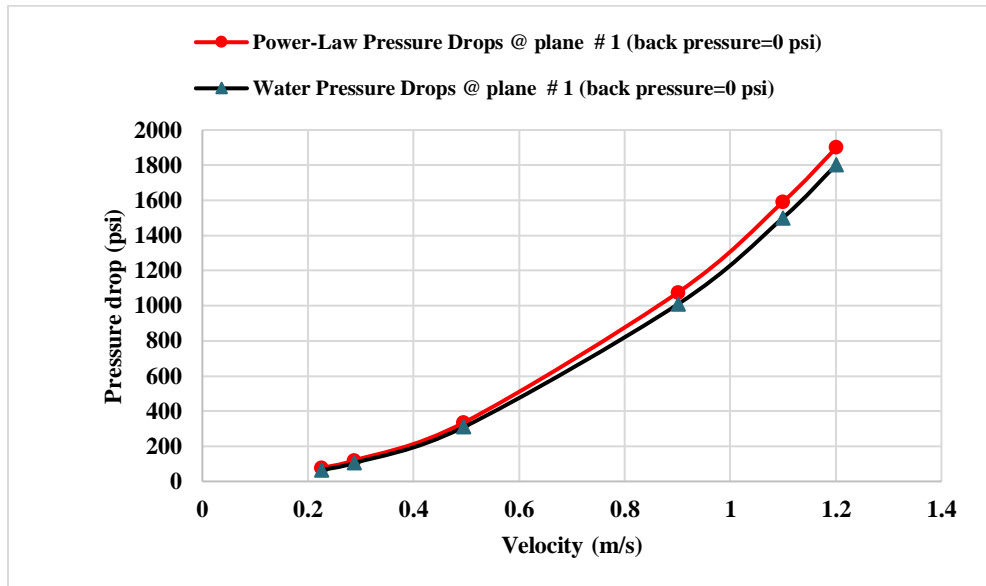


Figure 4. 20: Velocity and pressure drop relationship at back pressure 0 psi at plane #1 using water vs. Power Law

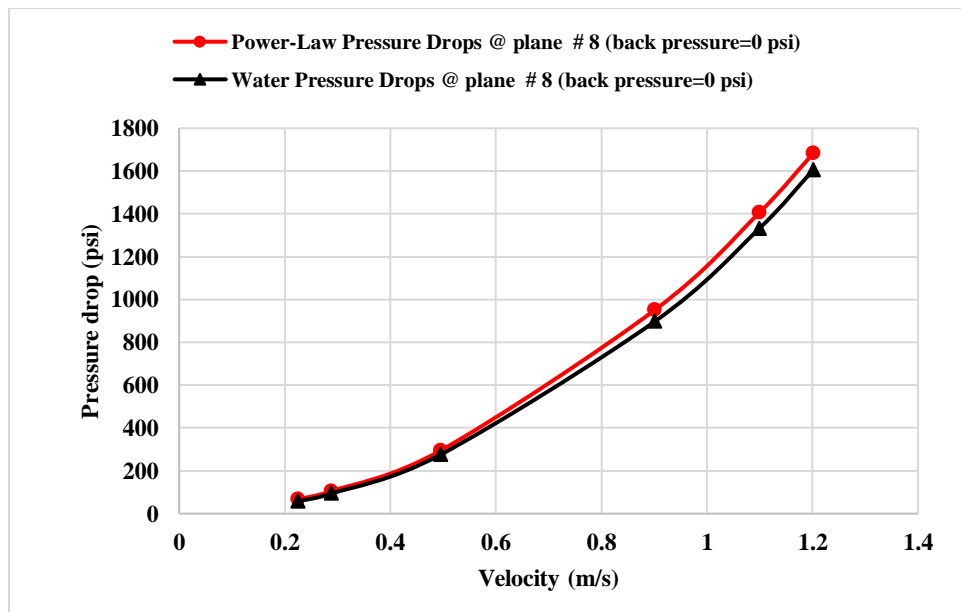


Figure 4.21: Velocity and pressure drop relationship at back pressure 0 psi at plane #8 using water vs. Power Law fluids

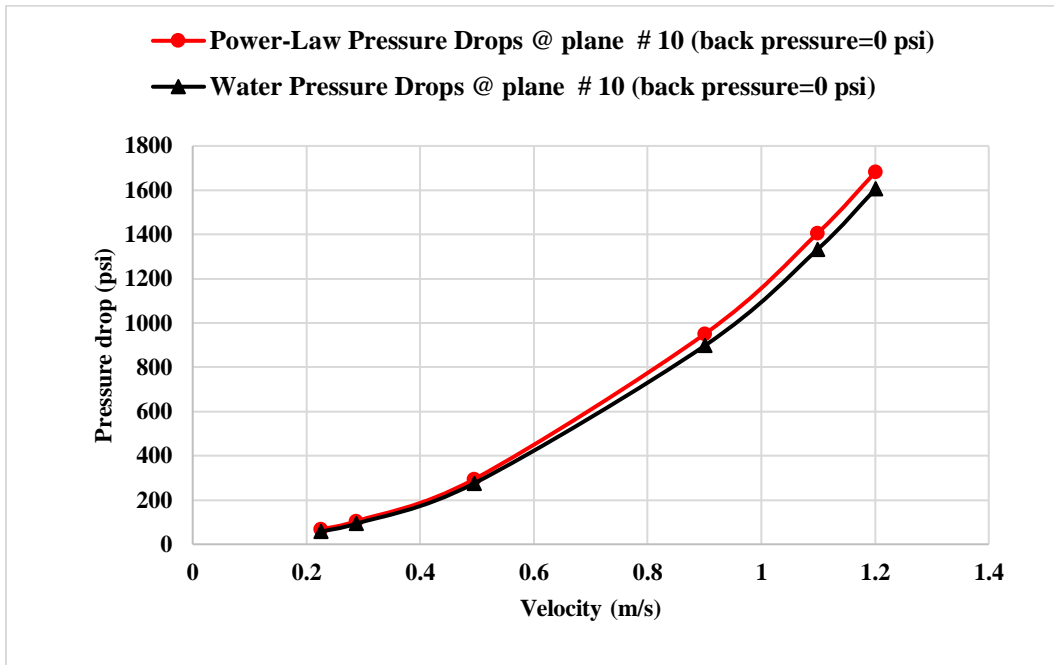


Figure 4. 22: Velocity and pressure drop relationship at back pressure 0 psi at plane #10 using water vs. Power Law fluids

4.6 Discussions

The Thruster working mechanism is providing an axial motion due to fluid impact on the piston, which is located at plane #6 (resulting the Thruster to be either in chocked or in un-chocked position). The axial motion that is influenced by the fluid chocking process is causing the fluid velocity and pressure to fluctuate. Such fluctuation generates the Thruster movement axially. The range of the axial motion of the Thruster is limited by the locking key movement range shown in Figure 4.1. The axial motion of the Thruster is induced by the Thruster inner design and the generated pressure pulses with the corresponding velocities. The magnitude of the pressure pulse increases with the increase of velocity. Two examples of lowest and highest-pressure pulse generated by the Thruster are shown in Figures 4.12 and 4.13. The Thruster operation and its axial motion regions can be classified to 2 main regions for all pressure and velocity profiles; including chocking, and un-chocking regions. These regions can be seen in the profiles of all pressure and fluid velocity classified in Figure 4.13.

This work, also analyzed the Thruster based on the pressure drop profiles that correspond to various fluid velocity inputs at different plane locations. The purpose of this analysis was to further investigate the Thruster function and performance. Moreover, two different fluid types were used for the in-depth Thruster performance analysis, including water (as Newtonian fluid) and Power Law (as a Non-Newtonian fluid). The result of the pressure drops using these two fluids with the corresponding velocities are shown in Figures 4.20 to 4.22.

The study of Thruster showed the generated downhole pressure pulses, which generate downhole load and can overcome numerous drilling problems that can be encountered in drilling operations such as damaging BHA tools as well as enhancing ROP are shown in Figure 4.8.

4.7 Summary

- The downhole Thruster was mechanically designed and structurally tested by SolidWorks.
- The fluid flow through the Thruster was simulated by ANSYS Fluent 17.2.
- Two fluid rheologies were used for Thruster evaluation including water and Power-Law.
- The Thruster operation performance was also evaluated by fluid velocity and pressure pulse generation.
- Detailed analysis of velocity and pressure pulses was involving back pressure applications.
- Pressure drop corresponding to various velocities at different planes was observed in a higher magnitude using the Power-Law versus water.
- The ANSYS simulation provided some positive reposes of the Thruster that can be uses to enhance drilling performance.

4.8 Future work

The Thruster studied in this paper was analyzed and tested only numerically. This numerical work used ANSYS 17.2. It can be further analyzed for more applications and scenarios such as different fluid viscosities and densities other than Non-Newtonian fluids. The Thruster also can be redesigned or modified for the purpose of generating more downhole pressure pulses that can lead to more increase in the downhole dynamic WOB as well as to generate more axial motions that can assist in various drilling applications such as releasing stuck pipes, reducing friction in non-vertical oil and gas wells, and extending the life by protecting the BHA, and eventually reduce the overall cost.

4.9 Acknowledgement

This work was conducted at the Drilling Technology Laboratory (DTL) at Memorial University of Newfoundland, St. John's, Canada. The project is financially funded by Atlantic Canada Opportunity Agency (AIF contract number: 781-2636-1920044), involving Husky Energy, Suncor Energy and Research and Development Corporation (RDC) of Newfoundland and Labrador. The financial support is also provided by the Ministry of Higher Education and Scientific Research, Libya through Canadian Bureau for International Education (CBIE).

4.10 Nomenclature

BHP	Bottom Hole Assembly.
bp	back pressure.
CBIE	Canadian Bureau for International Education.
DOC	Depth Of Cut.
DTL	Drilling Technology Laboratory.
DWOB	Dynamic Weight On Bit
RDC	Research Development Cooperation
ROP	Rate of Penetration
WOB	Weight On Bit

4.11 References

- Schmalhorst, B. (1999, January 1). Dynamic Behaviour of a Bit-Motor-Thruster Assembly. Society of Petroleum Engineers. The 1999 SPE/IADC Drilling Conference and Exhibition held in Amsterdam, Holland, 9-11 March 1999. doi:10.2118/52823-MS.
- Reich, M., Hoving, P. G., & Makohl, F. (1995, January 1). Drilling Performance Improvements Using Downhole Thrusters. Society of Petroleum Engineers. The IADC/SPE Drilling Conference and Exhibition held in Amsterdam, The Netherlands, 28 February – 2 March 1995. Texas, USA, 1-3 March 2016. doi:10.2118/29420-MS.
- Powell, S. W., & Ertai, H. (2015, January 26). Hydraulic Percussion Drilling System with PDC Bit Increases ROP and Lowers Drilling Cost. Society of Petroleum Engineers. The SPE Middle East Unconventional Resources Conference and Exhibition held in Muscat, Oman, 26 – 28 January 2015. doi:10.2118/172935-MS.
- Clausen, J. R., Schen, A. E., Forster, I., Prill, J., & Gee, R. (2014, March 4). Drilling with Induced Vibrations Improves ROP and Mitigates Stick/Slip in Vertical and Directional Wells. Society of Petroleum Engineers. The IADC/SPE Drilling Conference and Exhibition held in Fort Worth, Texas, USA, 4-6 March 2014. doi:10.2118/168034-MS.
- Abtahi, A., Butt, S., Molgaard, J., & Arvani, F. (2011, January 1). Wear Analysis and Optimization on Impregnated Diamond Bits in Vibration Assisted Rotary Drilling (VARD). American Rock Mechanics Association. The 45th US Rock Mechanics / Geomechanics Symposium held in San Francisco, CA, June 26–29, 2011.
- Rana, P.S, A.N. Abugharara, S.D. Butt and J. Molgaard. Experimental and Field Application

of Passive-Vibration Assisted Rotary Drilling (p-VARD) Tool to Enhance Drilling Performance. The 49th US Rock Mechanics / Geomechanics symposium held in San Francisco, CA, USA, 28 June- 1 July 2015.

Wilson, J. K., & Noynaert, S. F. (2017, March 14). Inducing Axial Vibrations in Unconventional Wells: New Insights through Comprehensive Modeling. Society of Petroleum Engineers. The SPE/IADC Drilling Conference and Exhibition held in The Hague, The Netherlands, 14-16 March 2017. doi:10.2118/184635-MS.

Jones, S., Feddema, C., Sugiura, J., & Lightey, J. (2016, March 1). A New Friction Reduction Tool with Axial Oscillation Increases Drilling Performance: Field-Testing with Multiple Vibration Sensors in One Drill String. Society of Petroleum Engineers. The SPE/IADC Drilling Conference and Exhibition held in in Fort Worth, Texas, USA, 1-3 March 2016. doi:10.2118/178792-MS.

Gee, R., Hanley, C., Hussain, R., Canuel, L., & Martinez, J. (2015, March 17). Axial Oscillation Tools vs. Lateral Vibration Tools for Friction Reduction- What's the Best Way to Shake the Pipe? Society of Petroleum Engineers. The SPE/IADC Drilling Conference and Exhibition held in London, United Kingdom, 17-19 March 2015. doi:10.2118/173024-MS.

Jones, S., Feddema, C., & Sugiura, J. (2016, March 1). A New Steady Weight-on-Bit Tool Reduces Torque and RPM Variations and Enhances Drilling Efficiency and Bit/BHA Life. Society of Petroleum Engineers. The IADC/SPE Drilling Conference and Exhibition held in Fort Worth, Texas, USA, 1-3 March 2016. doi:10.2118/178818-MS.

Barton, S. P., Baez, F., & Alali, A. (2011, January 1). Drilling Performance Improvements in

Gas Shale Plays using a Novel Drilling Agitator Device. Society of Petroleum Engineers. The SPE North America Unconventional Gas Conference and Exhibition held in the Woodlands, Texas, USA, 14-16 June 2011. doi:10.2118/144416-MS.

Khorshidian, H., Mozaffari, M., & Butt, S. D. (2012, January 1). The Role of Natural Vibrations In Penetration Mechanism of a Single PDC Cutter. The 46th US Rock Mechanics / Geomechanics Symposium held in Chicag, IL, USA, 24-27 June 2012.

Kamatov, K. A., & Buslaev, G. V. (2015, October 26). Solutions for Drilling Efficiency Improvement in Extreme Geological Conditions of Timano-Pechora Region. Society of Petroleum Engineers. The SPE Russian Petroleum Technology Conference held in Moscow, Russia, 26-28 October 2015. doi:10.2118/176530-MS .

Chapter 5

5.1 Conclusion

This work was focusing on studying a mechanical device “Thruster” as a proposed mechanical tool that can be installed right above the drill bit for the purpose of enhancing drilling in oil and gas wells. One encouraging point for studying the Thruster was the accumulate studies and research conducted by the Drilling Technology Laboratory (DTL) members, which have been showing a positive effect of inducing a controlled downhole vibration on drilling performance.

For conducting a complete study of the effect of the Thruster on drilling performance, a numerical simulation of the performance of the devise was conducted first by using CFD. The numerical study included fluid flow simulation and fluid pressure and fluid velocity analysis. The SolidWork and AutoCAD softwares were, also initially used for an optimal mechanical design of Thruster.

For fluid flow simulation, 10 planes were selected across the body of the Thruster, which each the fluid pressure and the fluid velocity was recorded and plotted in separated charts. This 10-plain simulation included 10 input fluid velocities at atmospheric outlet pressure as main boundary conditions. Then, some plains from the 10-plains were selected for further study of the Thruster performance. At these selected 3 to 5 plains, more parameters were implemented, including different fluid viscosity at multiple backpressure sets. In all above scenarios of fluid velocity and back pressures, the pressure drops and fluid velocity was analysed at all plains.

By implementing and adopting the Thruster as main part of the BHA, an axial motion (desirable vibration) can be generated and a Dynamic WOB can be magnified.

The production of the axial motion results in:

- Minimizing drillstring damage
- Minimizing well formation damage
- Minimizing inputs energy
- Minimizing the overall drilling operation cost
- The increase of the DWOB leads to:
 1. Maximizing the drilling rate of penetration
 2. Enhancing the overall drilling performance

This research provides, only an initial, but an encouraging and solid-start towards studying the downhole Thruster. Further research on investigating the influence of the Thruster on drilling performance is highly recommended. The future research should implement more boundary conditions and various fluid properties of viscosities and densities. The research should also include analysis of the magnitude of the axial oscillations of the Thruster and their amplitudes at each applied boundary condition. for their invaluable guidance, and constant support throughout this research.

References

- Aadnoy, B. S. Transversal vibrations in stabilized drilling assemblies. *Energy sources*, **1986**, 8(4), 305-329.
- Al Dushaishi, M. F. Investigation of drillstring vibration reduction tools, **2012**.
- AlsUPIe, H. Vibration of Periodic Drillstrings with Local Sources of Resonance (Doctoral dissertation), **2016**.
- Azizov, A., Lemesany, L., Augustine, N., & Loesel, C. The Latest Generation of Steerable Motor Overcomes Drilling Challenges in the Niobrara Shale Unconventional Play. In IADC/SPE Drilling Conference and Exhibition. Society of Petroleum Engineers, **2014**, March.
- Bailey, J. R., Elsborg, C. C., James, R. W., Pastusek, P., Prim, M. T., & Watson, W. W. Design Evolution of Drilling Tools to Mitigate Vibrations. *SPE Drilling & Completion*, **2013**, 28(04), 350-369.
- Buslaev, G. V., & Belkin, A. S. Development and Field Testing of the Downhole Multi-Purpose Thrusting Device for Drilling of Deep Vertical and Directional Wells (Russian). In SPE Russian Petroleum Technology Conference. Society of Petroleum Engineers, **2015**, October.
- Clausen, J. R., Schen, A. E., Forster, I., Prill, J., & Gee, R. Drilling with induced vibrations improves ROP and mitigates stick/slip in vertical and directional wells. In IADC/SPE Drilling Conference and Exhibition. Society of Petroleum Engineers, **2014**, March.
- Cooper, I., Miska, S. Z., Mitchell, R. F., & Payne, M. L. Advanced drilling and well technology (pp. 301-440). B. S. Aadnoy (Ed.). SPE, **2009**.

Drilling Design and Implementation for Extended Reach and Complex Well, K & M Technology,

3rd Edition, **2003**, Pg 133.

Dupriest, F. E., Witt, J. W., & Remmert, S. M. Maximizing ROP with real-time analysis of digital

data and MSE. In International petroleum technology conference. International Petroleum

Technology Conference, **2005**, January.

Dykstra, M. W., Chen, D. K., Warren, T. M., & Azar, J. J. Drillstring component mass

imbalance: a major source of downhole vibrations. SPE drilling & completion, **1996**,

11(04), 234-241.

Ernst, S., Pastusek, P. E., & Lutes, P. J. Effects of RPM and ROP on PDC Bit Steerability.

In SPE/IADC Drilling Conference. Society of Petroleum Engineers, **2007**, January.

Geldof, W., Merrall, E., Kent, D., & Dautel, M. World record horizontal bit runs in Oman.

In SPE/IADC Middle East Drilling Technology Conference. Society of Petroleum

Engineers, **1999**, January.

Gidh, Y. K., Ibrahim, H., & Purwanto, A. Real-time drilling parameter optimization system

increases ROP by predicting/managing bit wear. In SPE Digital Energy conference and

Exhibition. Society of Petroleum Engineers, **2011**, January.

Giles, C. A., Seesahai, T., Brooks, J. W., & Johnatty, W. Hydraulic thrusting devices improve

drilling efficiencies. World Oil, **2001**, 222(9), 59-66.

Irgens, F., & SpringerLink. Rheology and Non-Newtonian Fluids, **2014**.

- Larsen, L. Tools and techniques to minimize shock and vibration to the bottom hole assembly (Master's thesis, University of Stavanger, Norway), **2014**.
- Li, H., Butt, S., Munaswamy, K., & Arvani, F. Experimental investigation of bit vibration on rotary drilling penetration rate. In 44th US Rock Mechanics Symposium and 5th US-Canada Rock Mechanics Symposium. American Rock Mechanics Association, **2010**, January.
- Mensa-Wilmot, G., Benet, P., Ramchune, D., & Maddoux, B. Little Things, Big Effects- I In SPE/IADC Drilling Conference. Society of Petroleum Engineers, **2013**, March
identifying Causes and Addressing Vibrations Issues in Challenging Deepwater Applications.
- Meyer-heyne, B., Reckmann, H., & Ostermeyer, G. P. Underreamer dynamics. In SPE/IADC Drilling Conference and Exhibition. Society of Petroleum Engineers, **2011**, January.
- Mikalsen, A. Analysis of drilled wells on the Norwegian Continental Shelf (NCS) (Master's thesis, University of Stavanger, Norway), **2013**.
- Osnes, S. M., Amundsen, P. A., Weltzin, T., Nyrnes, E., & Grindhaug, G. Vibration Measurements: A Time for Standardisation. In SPE/IADC Drilling Conference and Exhibition. Society of Petroleum Engineers, **2009**, January.
- Radford, S. R., Jenkins, M. A., & Li, T. Novel concentric expandable stabilizer results in increased penetration rates and drilling efficiency with reduced vibration. In SPE/IADC drilling conference and exhibition. Society of Petroleum Engineers, **2009**, January.
- Reich, M., Hoving, P. G., & Makohl, F. Drilling performance improvements using downhole

- thrusters. In SPE/IADC Drilling Conference. Society of Petroleum Engineers, **1995**, January.
- Rahimov, E. (2009). Through tubing rotary managed pressure drilling (Master's thesis, University of Stavanger, Norway).
- Reimers, N. Antistall tool reduces risk in drilling difficult formations. *Journal of Petroleum Technology*, **2012**, 64(01), 26-29.
- Santos, H., Placido, J. C. R., & Wolter, C. Consequences and relevance of drillstring vibration on wellbore stability. In SPE/IADC drilling conference, **1999**.
- Schmalhorst, B. Dynamic behaviour of a bit-motor-thruster assembly. In SPE/IADC drilling conference, **1999**.
- Schmalhorst, B., Brommundt, E., Baumgart, A., & Richter, U. Drilling dynamics in the presence of mud flow. In IADC/SPE Drilling Conference. Society of Petroleum Engineers, **2000**, January.
- Selnes, K. S., Clemmensen, C. C., & Reimers, N. Drilling difficult formations efficiently with the use of an antistall tool. *SPE drilling & completion*, **2009**, 24(04), 531-536.
- Sowers, S. F., Dupriest, F. E., Bailey, J. R., & Wang, L. Use of roller reamers improves drilling performance in wells limited by bit and bottomhole assembly vibrations. In SPE/IADC Drilling Conference and Exhibition. Society of Petroleum Engineers, **2009**, January.
- Thomson, I. J., Radford, S. R., Powers, J. R., Shale, L. T., & Jenkins, M. A systematic approach to a better understanding of the concentric hole-opening process utilizing drilling mechanics and drilling dynamics measurements recorded above and below the reamer.

In IADC/SPE Drilling Conference. Society of Petroleum Engineers, **2008**, January.

Ubaru, C. C., Thomson, I. J., & Radford, S. R. Drilling and Under-Reaming in the GOM Deepwater Ultradeep Lower Tertiary: History of a Record Run in the World. In SPE Annual Technical Conference and Exhibition. Society of Petroleum Engineers, **2011**, January

Ugochukwu, O. Optimizing Hydraulics For Drilling Operations. In SPE Nigeria Annual International Conference and Exhibition. Society of Petroleum Engineers, **2015**, August.

Appendix. A

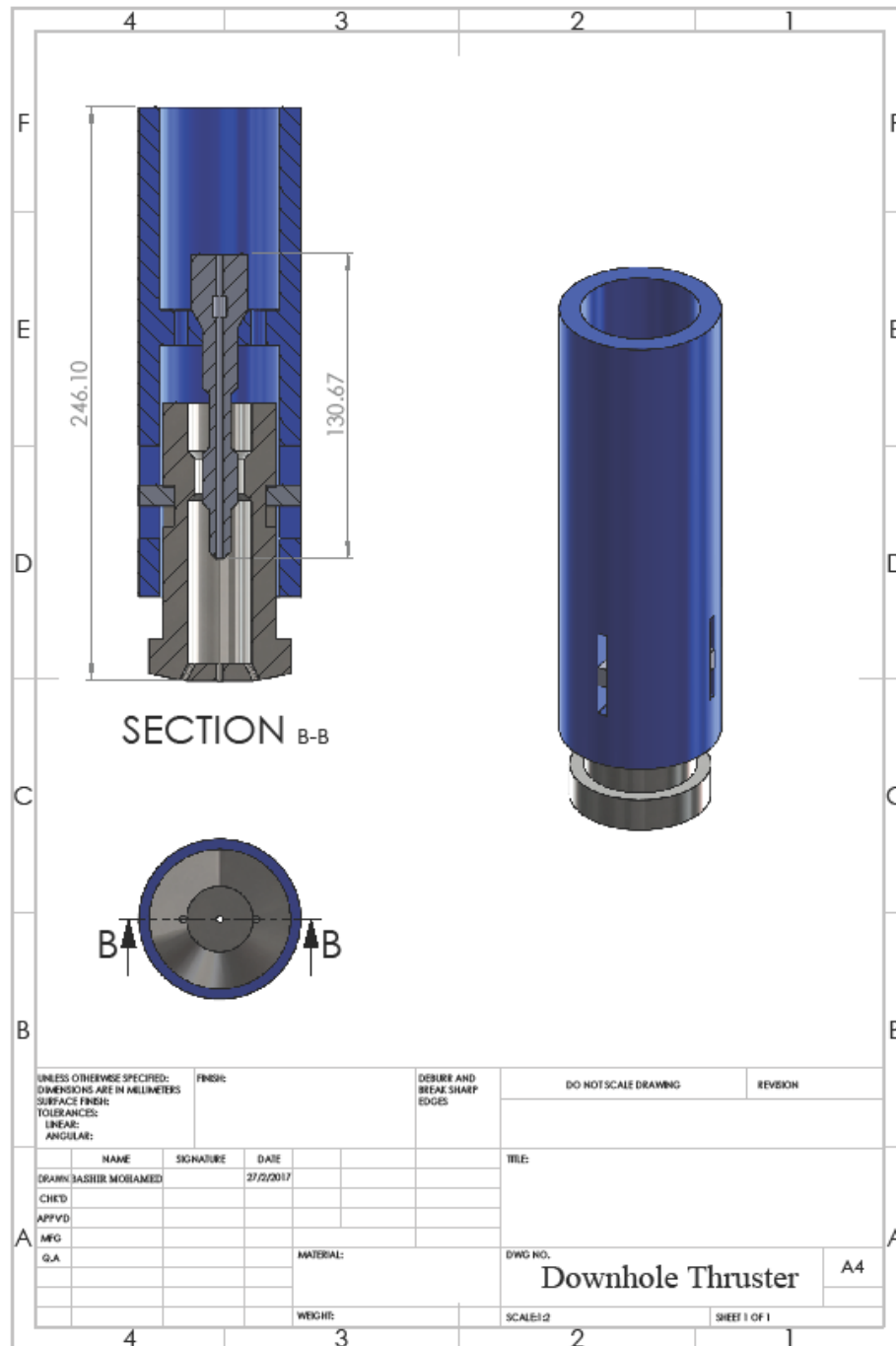


Figure A.1: AutoCAD drawing of the Thruster

Table A.1: Summary of the pressure effect, generated forces and ROP for both applications of with Thruster and without Thruster

	Flowrate Q (m ³ /s)	Velocity (m/s) inlet	Pressure effect	
			Pressure (Pascal)	Pressure (Psi)
1	0.000458	0.22537286	398223	57.75736314
2	0.000586	0.288359161	649237	94.16386591
3	0.000805	0.396124787	1217080	176.5225302
4	0.001007	0.495525044	1898120	275.2990313
5	0.0012015	0.591234697	2700480	391.6715107
6	0.0013863	0.68217117	3587610	520.3388392
7	0.001599	0.90099936	6248940	906.3321225
8	0.001831	0.99400257	7602210	1102.607342
9	0.00202	1.099307793	9268750	1344.318534
10	0.002234	1.201119245	11101800	1610.17996

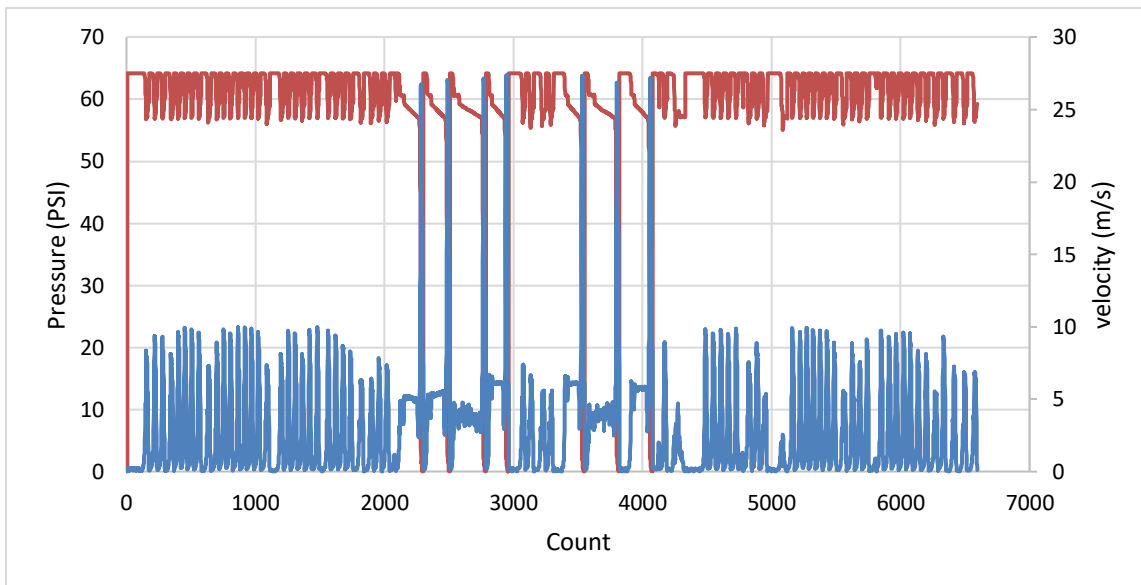


Figure A.2: Pressure vs First Velocity Value

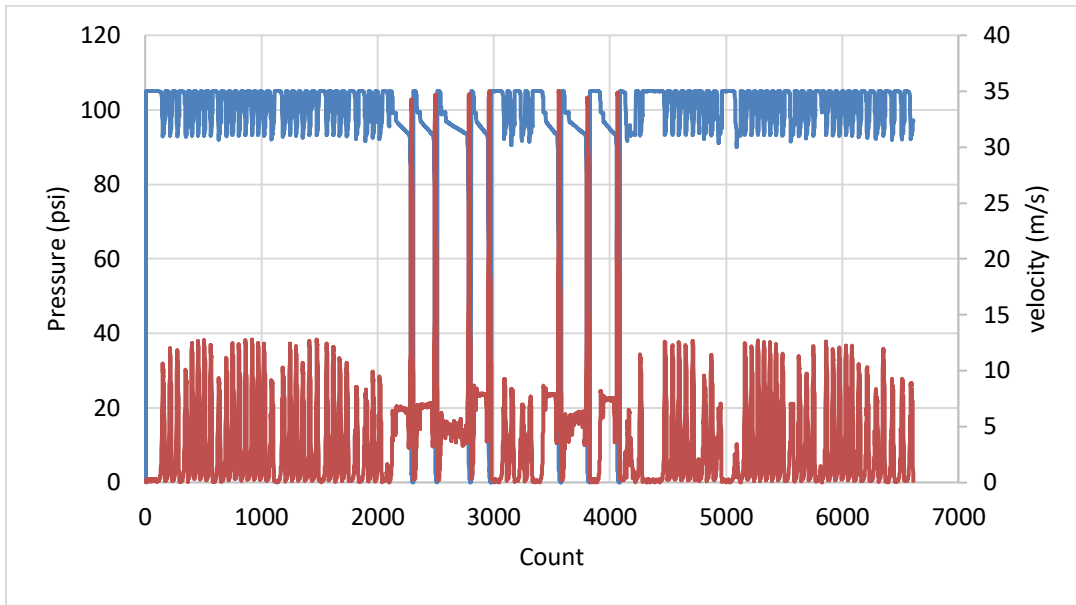


Figure A.3: Pressure vs Second Velocity Value

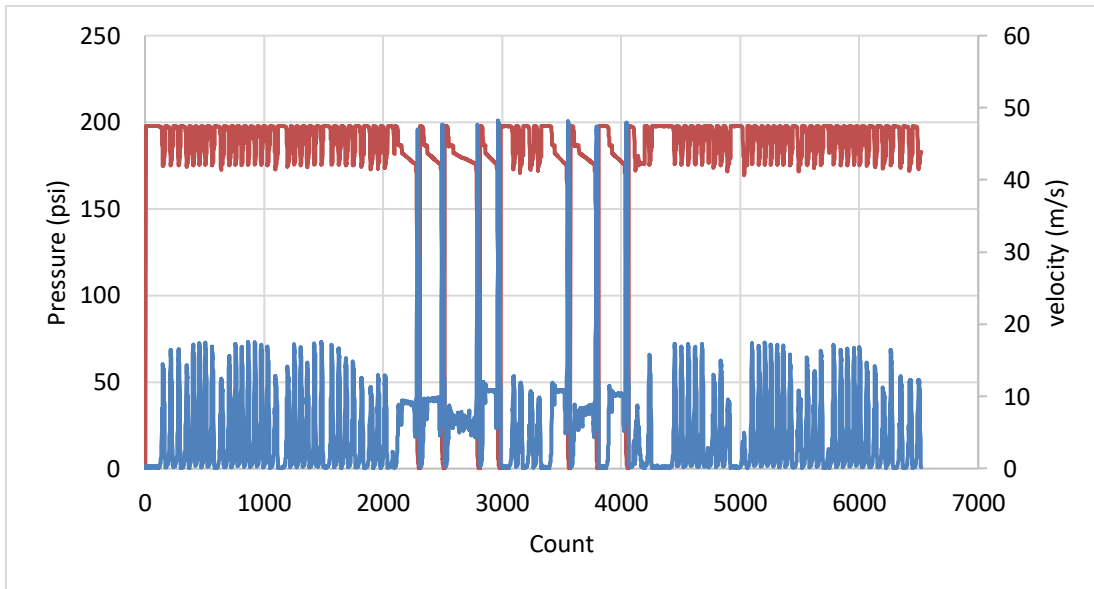


Figure A.4: Pressure vs Third Velocity Value

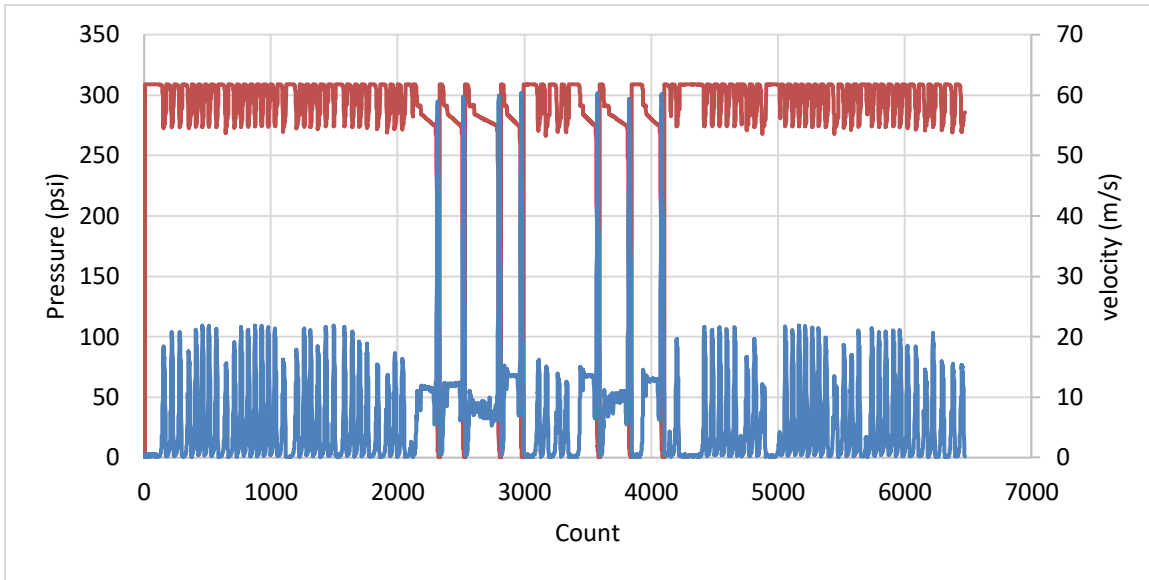


Figure A.5: Pressure vs Forth Velocity Value

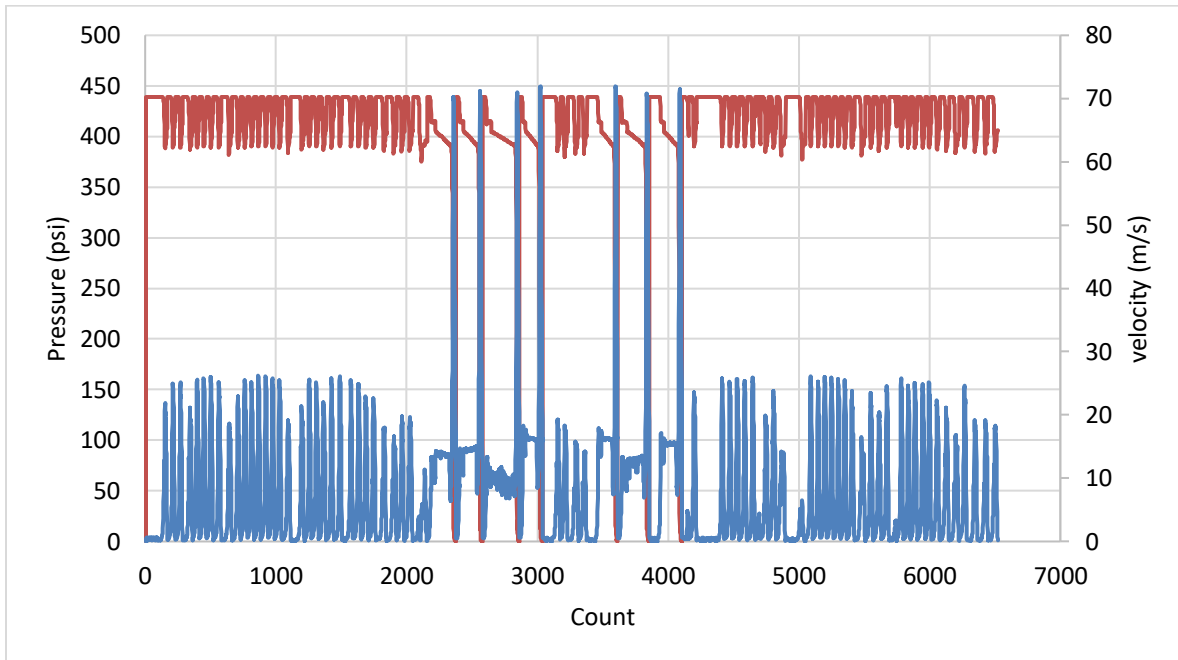


Figure A.6: Pressure vs Fifth Velocity Value

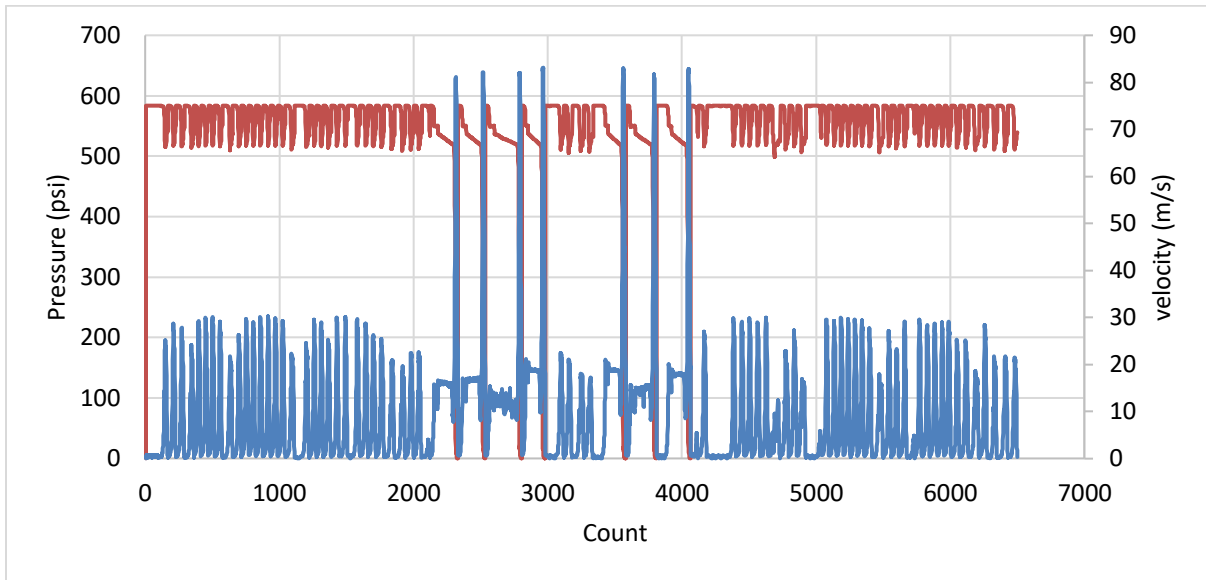


Figure A.7: Pressure vs Sixth Velocity Value

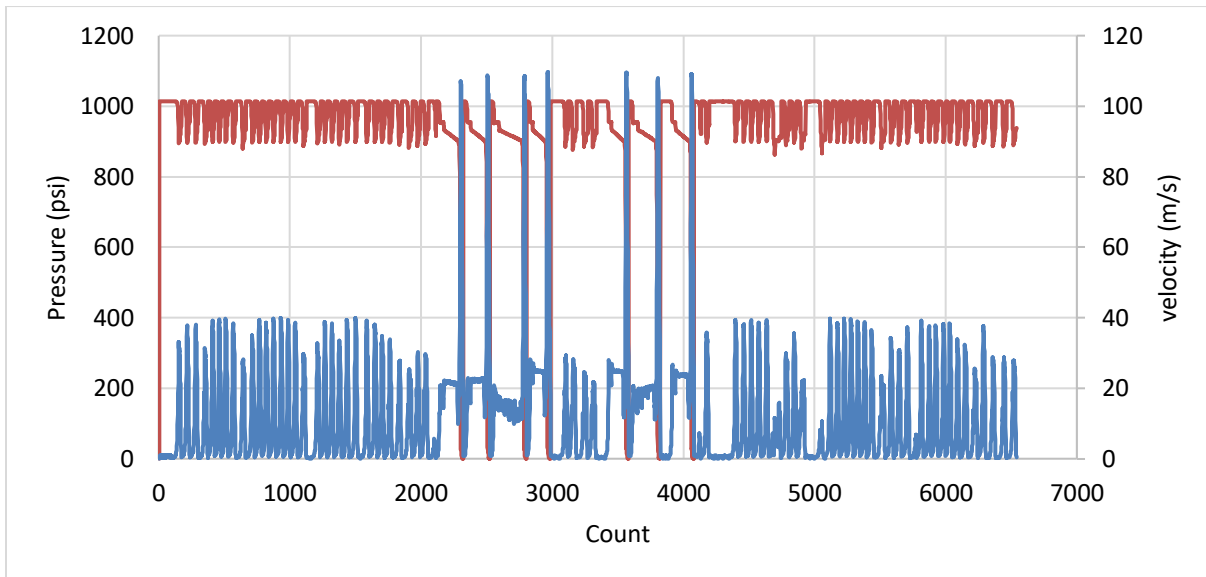


Figure A.8: Pressure vs Seventh Velocity Value

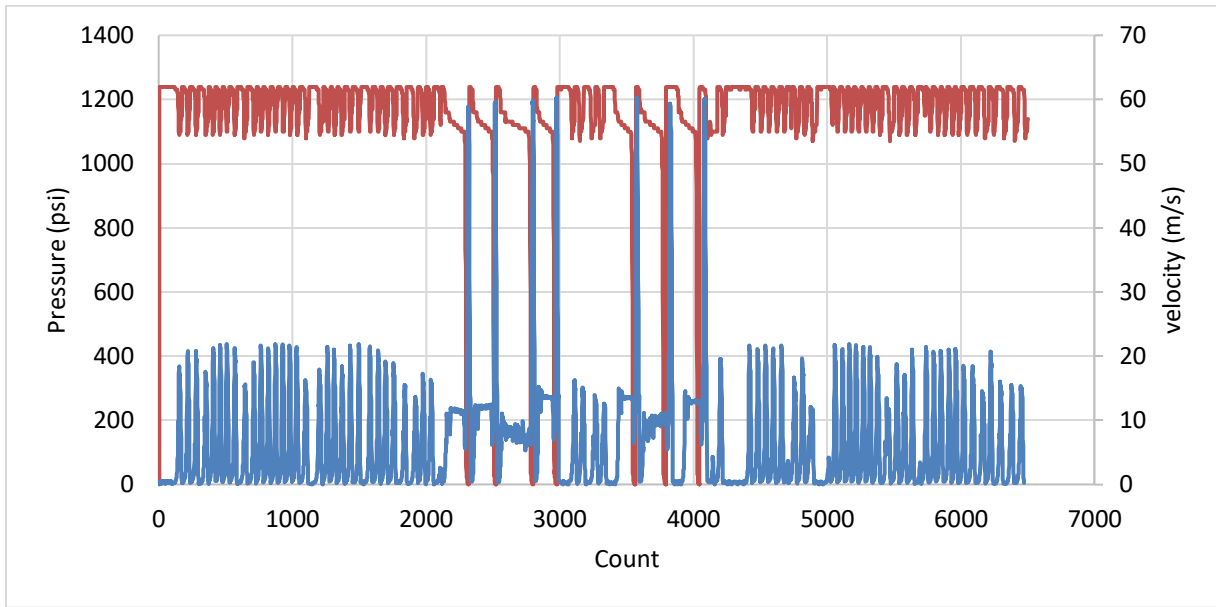


Figure A.9: Pressure vs Eighth Velocity Value

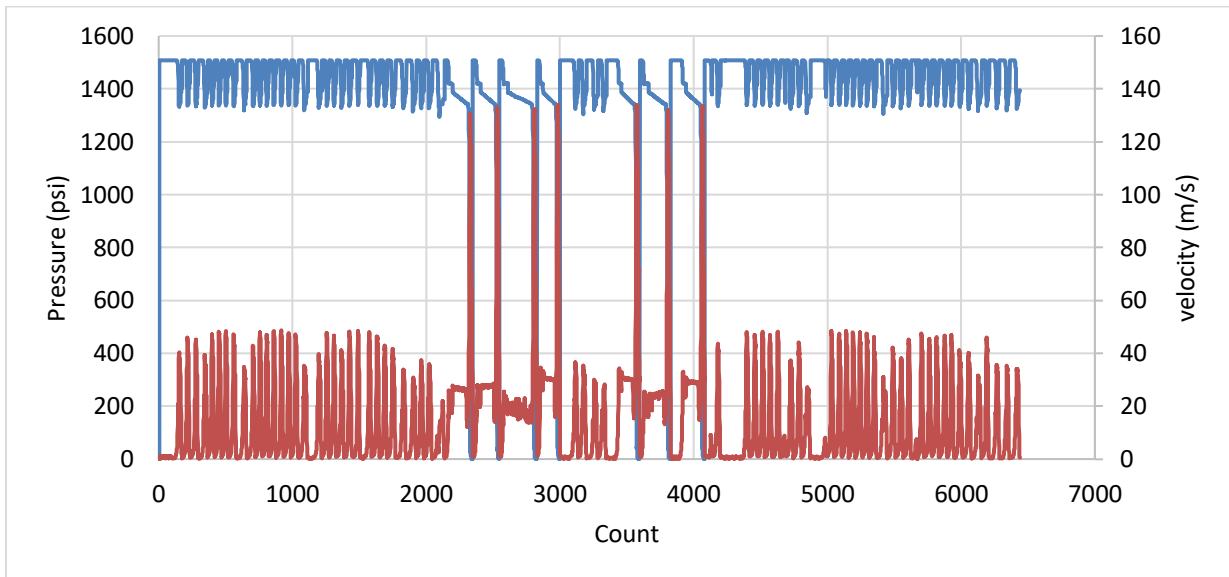


Figure A.10: Pressure vs Ninth Velocity Value

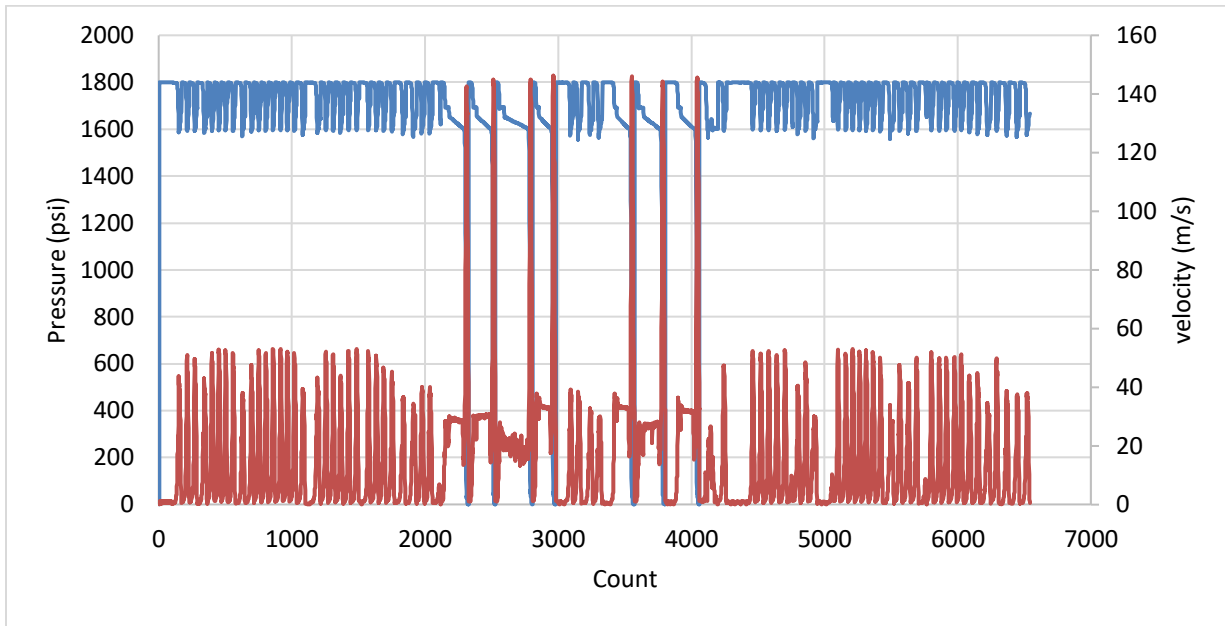


Figure A. 11: Pressure vs Tenth Velocity Value

Table A.2: Back pressure

	pressure effect		
percentage of Pressure	94.163 psi	391.67 psi	1102.60 psi
10%	100.892	430.789	1214.0079
25%	117.198	490.419	1376.5966
50%	140.644	588.386	1652.4004
75%	164.443	685.046	1930.698
100%	187.881	782.788	2206.198

Table A.3: Percentage back pressure of the pressure effect

Flowrate Q (m ³ /s)	Velocity (m/s) inlet	Pressure effect					
		0	10	25	50	75	100
0.000586	Velocity low= 0.288359161496121	94.163 psi	100.892	117.198	140.644	164.443	187.881
0.0012015	Velocity medium= 0.591234697163122	391.67 psi	430.789	490.419	588.386	685.046	782.788
0.001831	Velocity high= 0.994002570344991	1102.60 psi	1214.0079	1376.5966	1652.4004	1930.698	2206.198

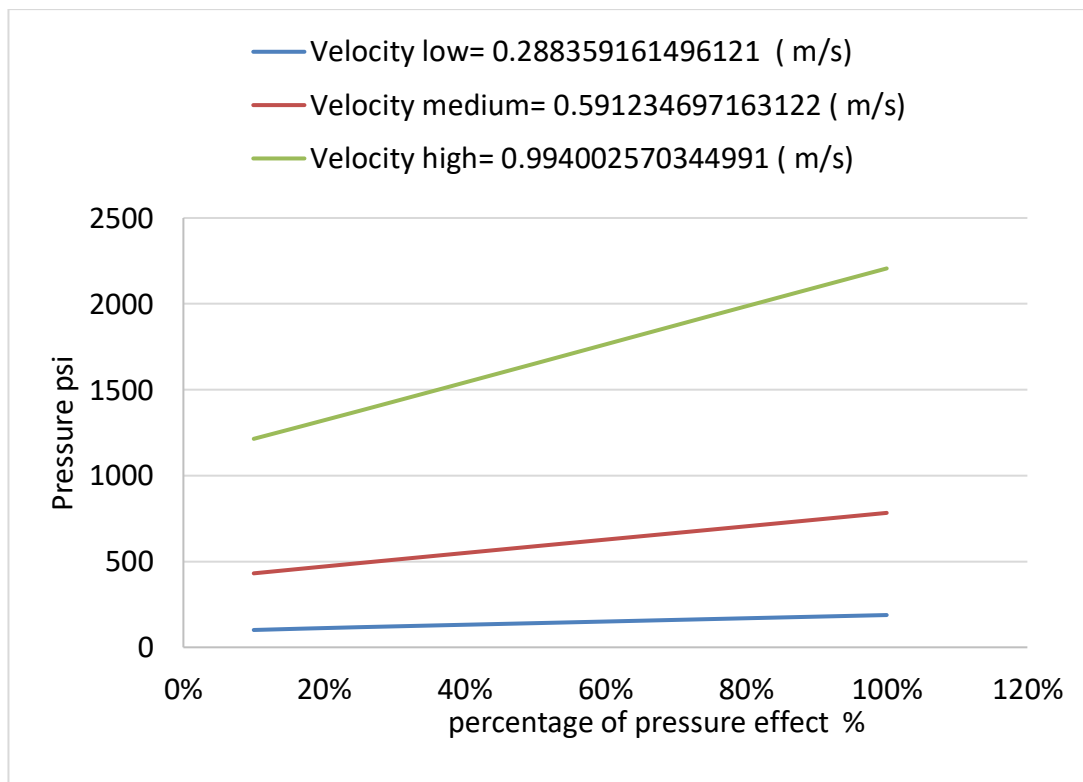


Figure A. 12: Percentage back pressure of the pressure effect

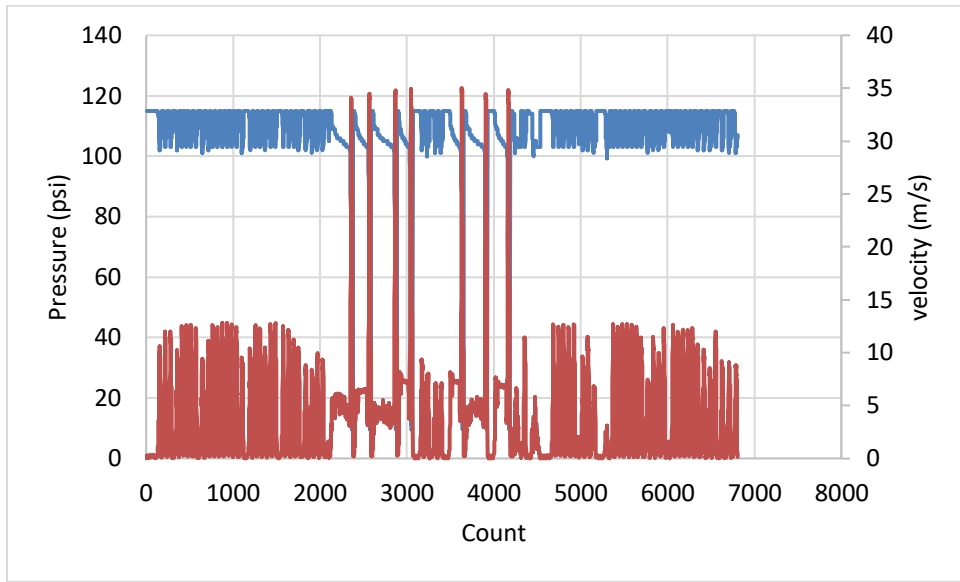


Figure A. 13: Back pressure 10%

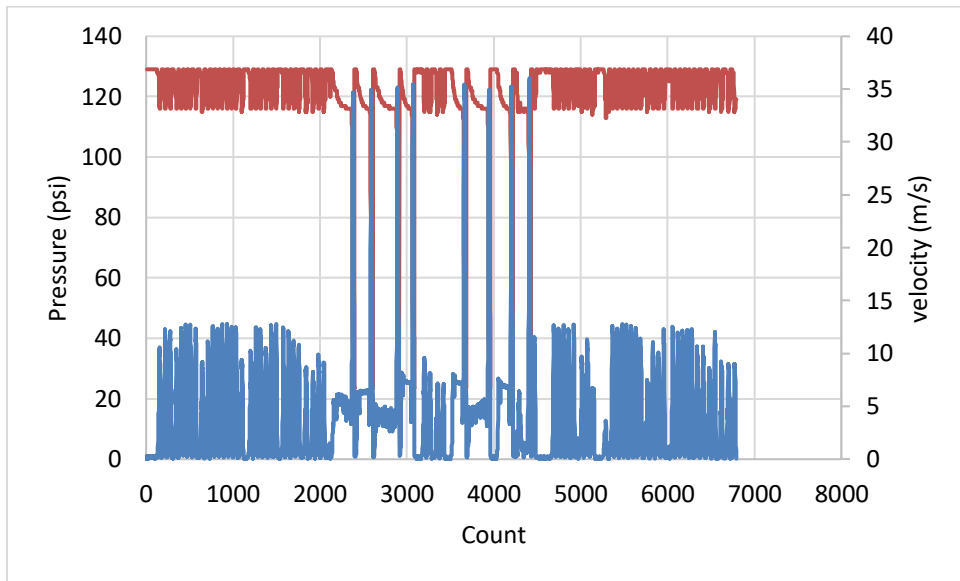


Figure A.14: Back pressure 25%

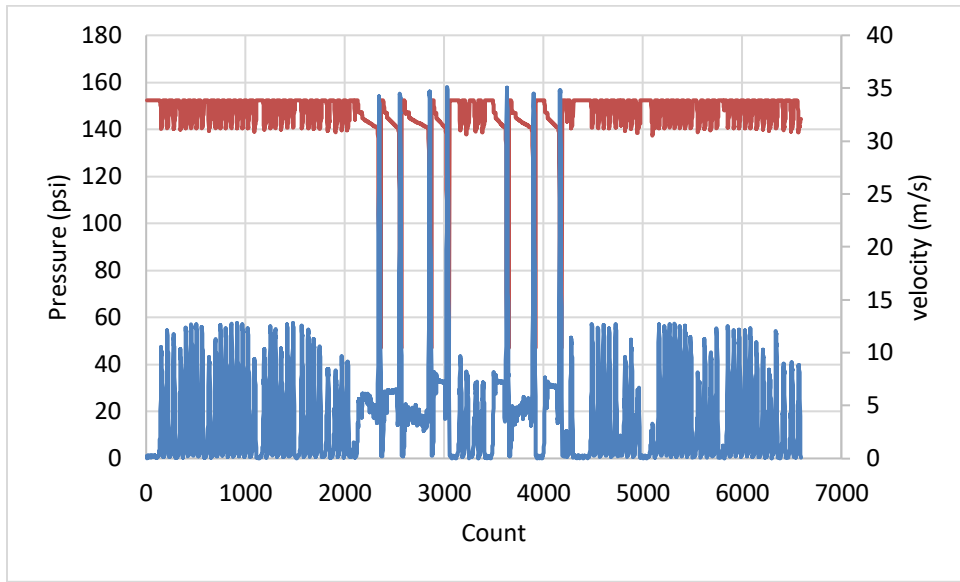


Figure A. 15: Back pressure 50%

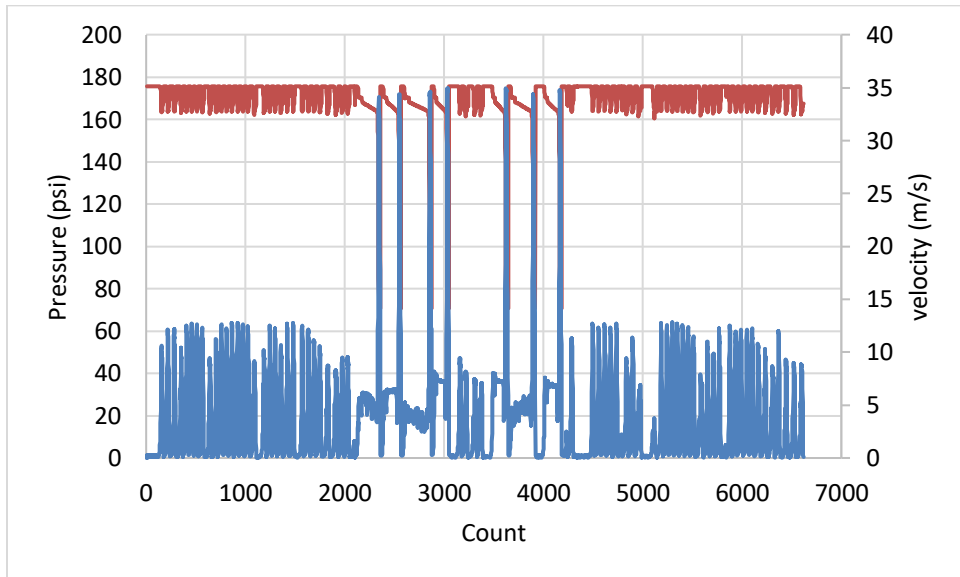


Figure A. 16: Back pressure 75%

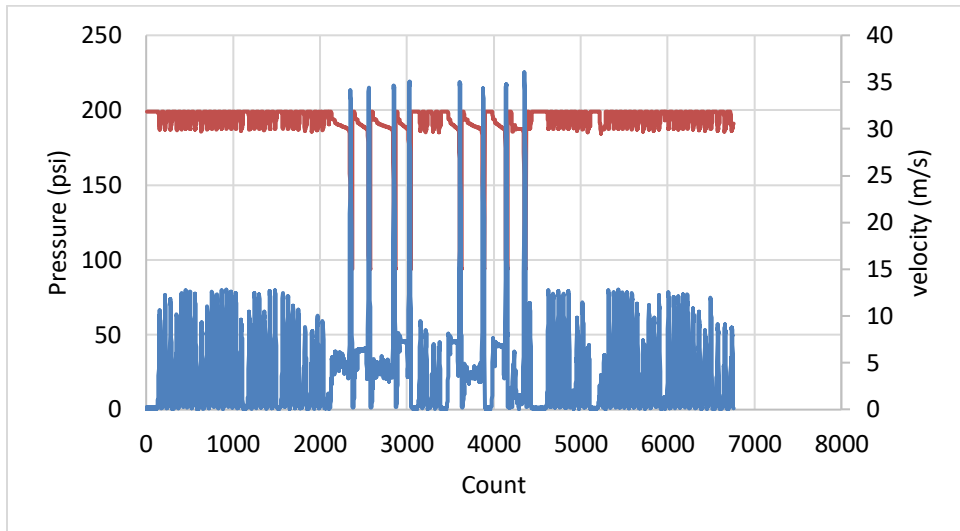


Figure A.17: Back pressure 100%

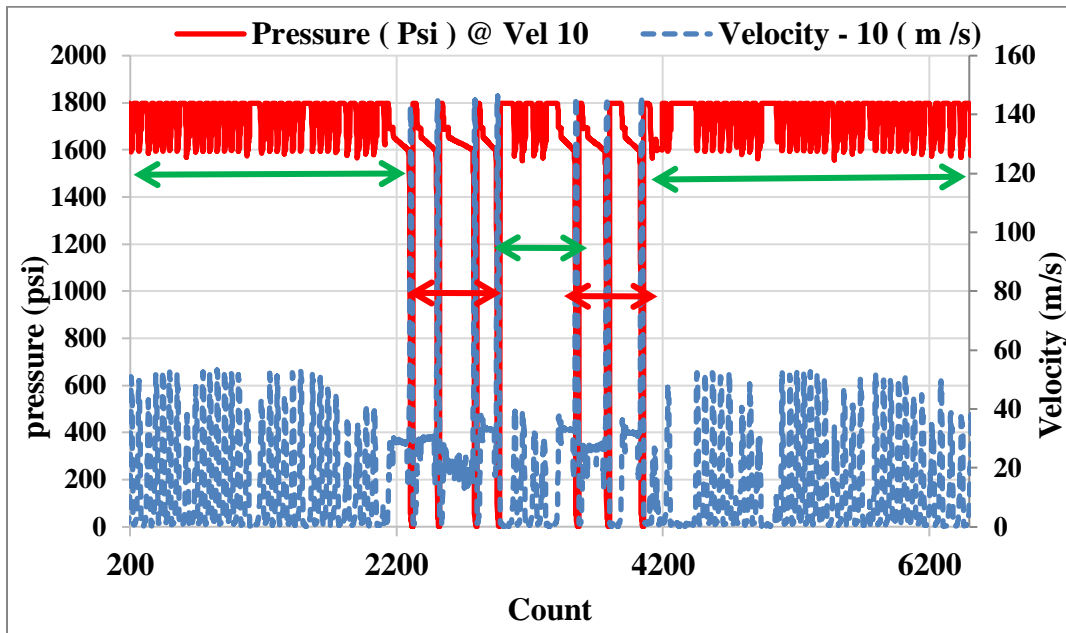


Figure A.18: Combined pressure and velocity profiles for full length of Thruster. Green: Pre and Post choked regions, Red: Unchoked region

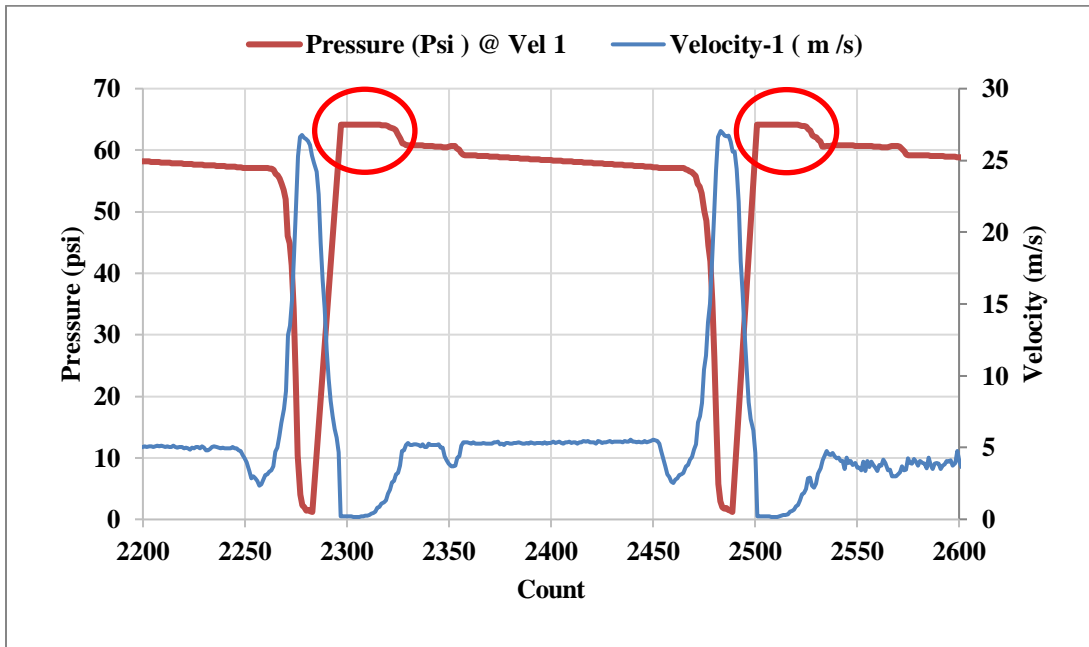


Figure A.19: Pressure and velocity fluctuation inducing axial motion of the Thruster. After the drop, the pressure gains some increase compared to the pre-drop stage pressure

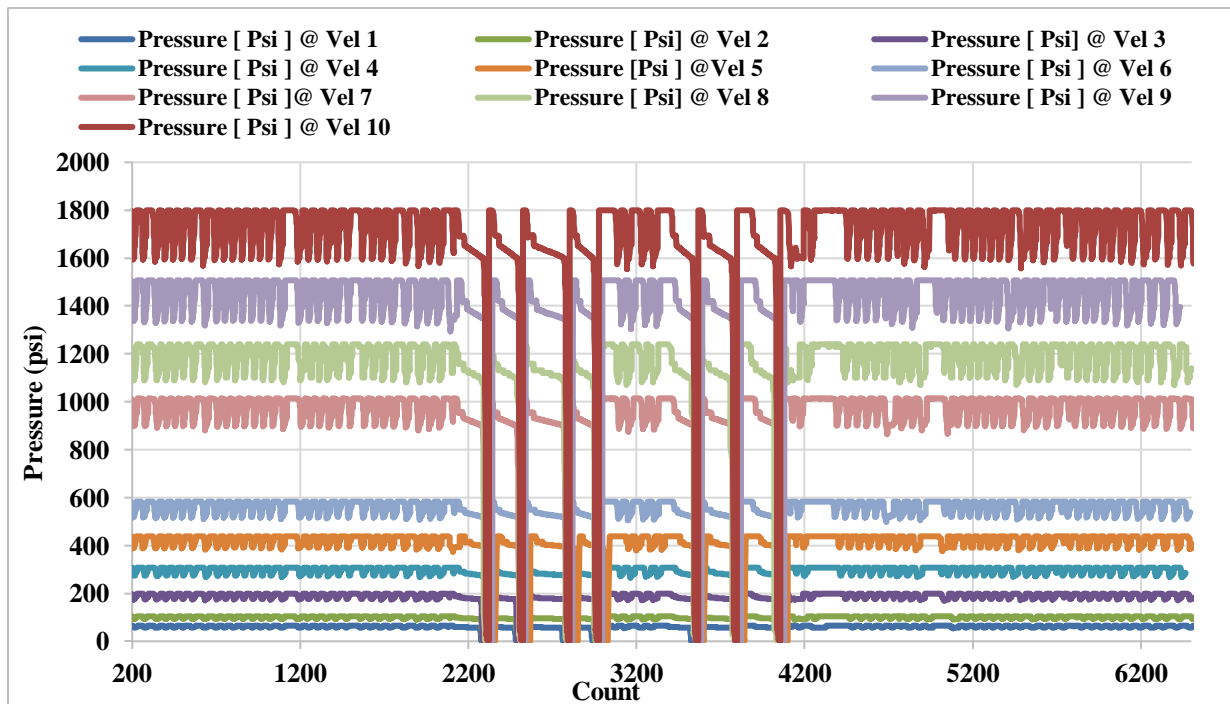


Figure A.20: Relationship between 10 pressure profiles and 10 corresponding flow rates

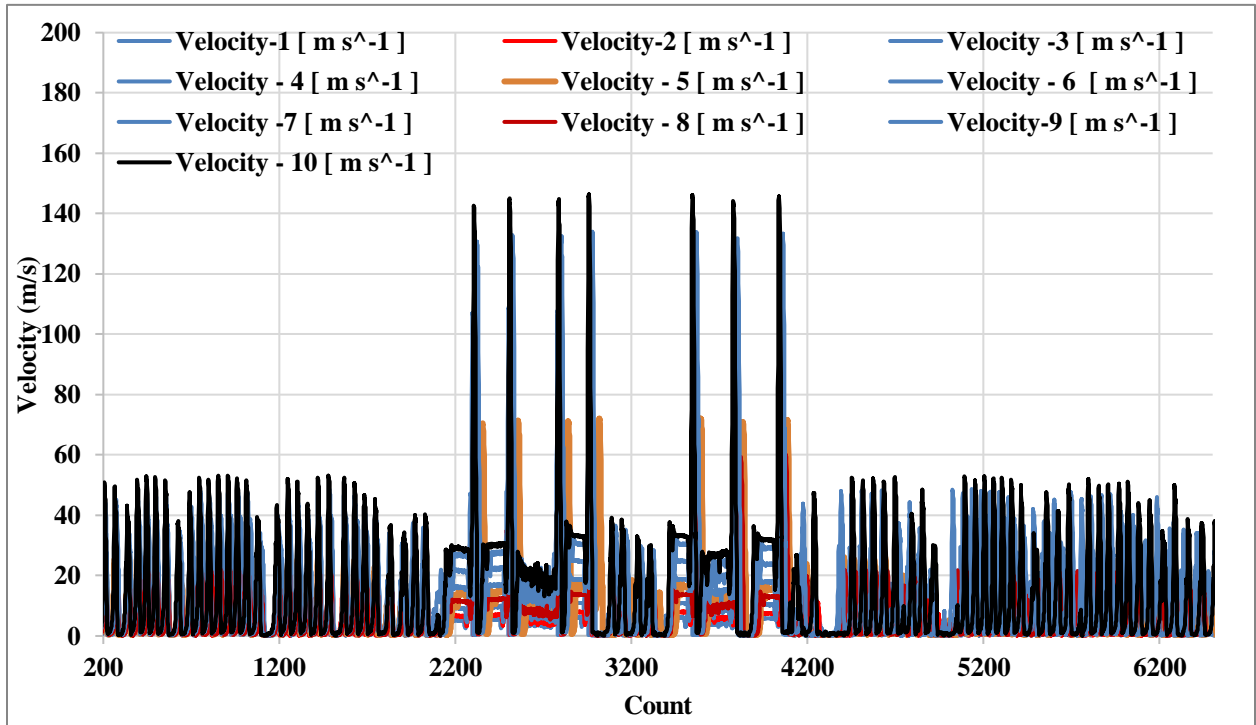


Figure A.21: Full 10 velocities profiles of ANSYS evaluating Thruster performance induced by 10 inlet flow rates

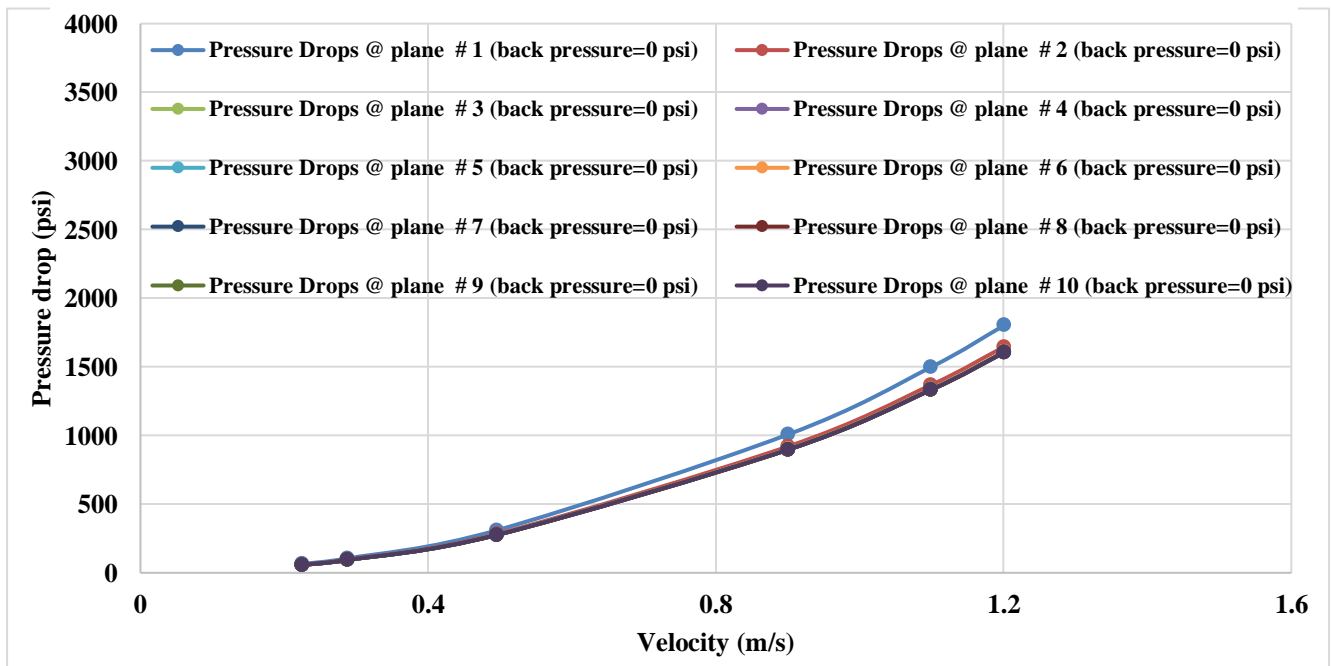


Figure A.22: Relationships between fluid velocities and pressure drops at back pressure = 0 psi

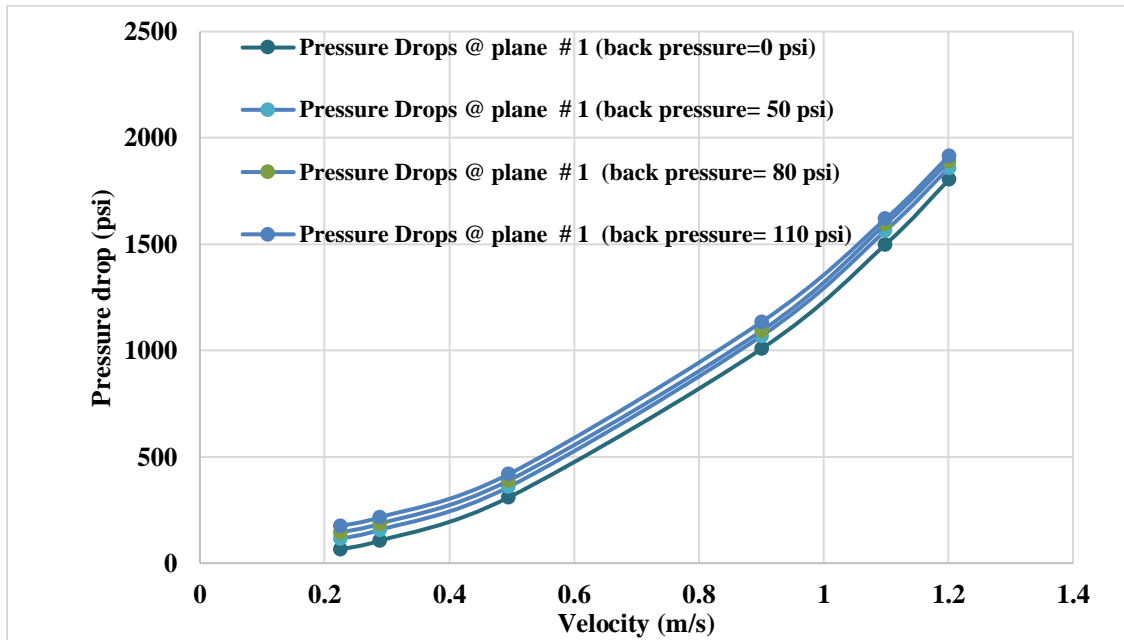
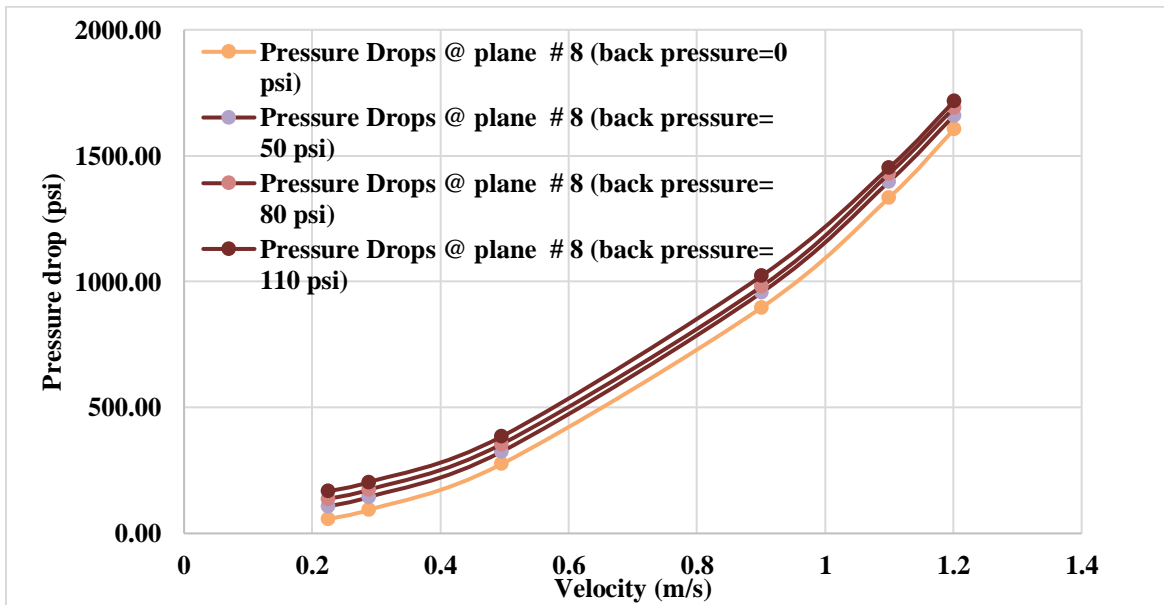


Figure A. 23: Relationships between fluid velocities and pressure drops at plane #1



FigureA.24: Relationships between fluid velocities and pressure drops at plane #8

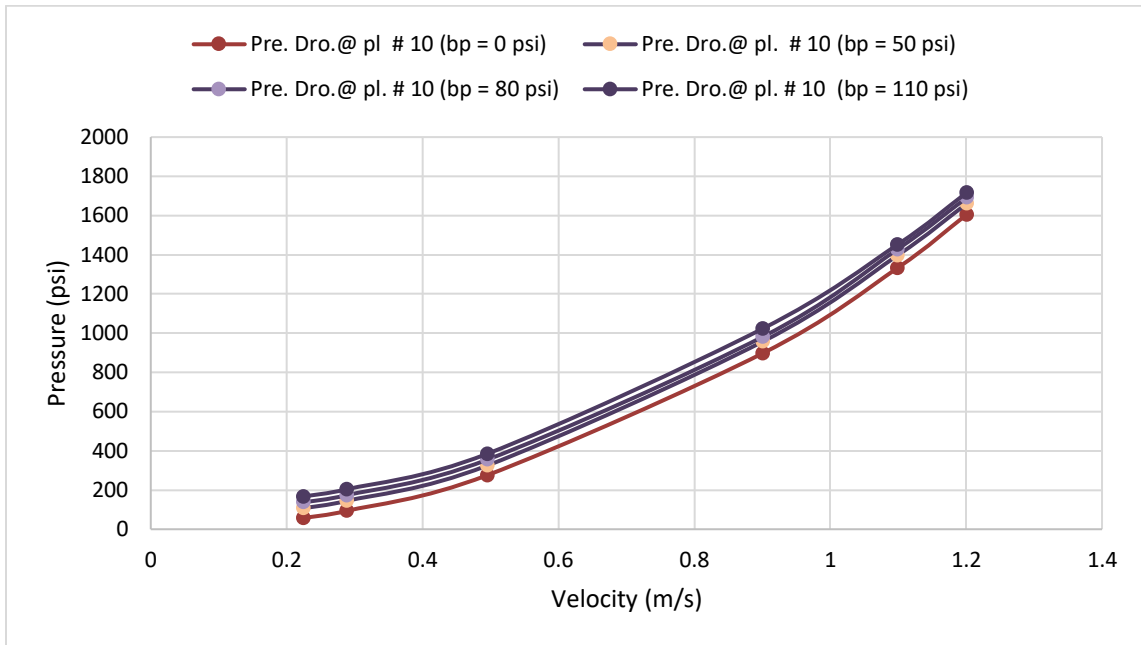


Figure A.25: Relationships between fluid velocities and pressure drops at plane #10